AN EXPERIMENTALLY DETERMINED MODEL FOR THE PERIODIC CHARACTER OF WINDS FROM 85 TO 135 KM

By E. Manring, J. Bedinger, H. Knaflich, and D. Layzer

Prepared under Contract No. NASw-712 by
GEOPHYSICS CORPORATION OF AMERICA
Bedford, Massachusetts

NATIONAL AERONAUTICS AND SPACE ADMINISTRATION

For sale by the Office of Technical Services, Department of Commerce,
Washington, D.C. 20230 -- Price $2.50

ABSTRACT

25119

Since 1959, measurements of upper atmosphere winds have been made from Wallops Island, Virginia, utilizing the sodium vapor technique. To date, measurements from 22 different vapor trails have been analyzed. In the height range 85 to 135 km, the measurements show that the winds have large quasi-periodic components. Analysis shows that the 8-hour component is dominant over the entire range. A new picture of the wind structure at these altitudes is proposed.

Author

TABLE OF CONTENTS

SECTION 1

INTRODUCTION

During the past four years, the sodium vapor technique has been used to measure upper atmospheric winds from Wallops Island, Virginia. The method has been completely described elsewhere.[1-4] Briefly, winds are derived from the rate of motion of a trail of sodium vapor ejected from a rocket during twilight. Resonance scattering of sunlight in the sodium D-line provides sufficient brightness for the trail to be photographed during twilight. Triangulation techniques are used to determine exact trail positions from simultaneous photographs taken at widely separated known locations. The data are reduced by an analog method which allows very precise wind determinations at height intervals as small as desired.

Results from a total of 22 different trails are reported here. About half of these have previously been published.[5,6] The remainder have had only limited distribution in contractual reports.[2,7,8] The altitude range of the data varies from trail to trail, the upper limit being determined by rocket performance. Three types of rockets have been used: Nike-Cajuns which reach about 140 km, Nike-Apaches which usually reach about 180 km, and Nike-Asps which have reached 220 km. The lower limit is often determined by atmospheric conditions and partial cloud cover.

Below about 80 km chemical recombination of the atomic sodium is rapid, and the trail is white rather than the characteristic orange or red of sodium

or lithium vapor. The white trail is more affected by atmospheric attenuation at low elevation angles from distant locations and generally persists for only a short time. Photography of this portion is generally possible from close-in sites, but often there is so much overlapping of the trail in the viewing direction that accurate winds cannot be determined in the observing time available. Thus, although measurements have been made from 50 km to 200 km, the largest number of measurements is in the range 85 to 135 km. All the wind profiles that have been obtained up until now are included in Appendix A.

SECTION 2

WIND DATA

2.1 CLASSIFICATION OF WIND PROFILES

The wind profiles and trails may be grouped into three classes, illustrated in Figure 1, where the wind speed and wind direction (direction toward which the wind is blowing) are plotted separately against height. Photographs of the corresponding trails, taken from the launch site, are shown in Figure 2.

Class I. The direction varies rapidly with height but does not change by more than 90^{o}. Wind speed fluctuations with height are numerous, but usually do not amount to more than 40 m/sec.

Class II. The defining feature of these trails is a single high-shear region, usually between 100 and 110 km, in which a large directional change, usually 180^{o}, occurs and in which the wind speed attains values as high as 150 m/sec. Above and below this region, the wind speed is small.

Class III. These trails are characterized by a continuous, spiraling change of direction with height, the wind speed gradually increasing with height until a maximum of 120 to 150 m/sec is reached close to 110 km. Above this level the wind speed decreases to about 80 m/sec and then, in most cases, remains relatively constant at greater heights. The direction of rotation of

the spiral motion is clockwise, i.e., N-E-S-W, with height.

Of the 22 trails discussed here, 7 belong to Class I, 6 to Class II, and 8 to Class III. No seasonal preference is shown by any group. There are nearly equal numbers of morning and evening measurements in Class I; Class II has more morning than evening measurements; and Class III has more evening than morning measurements.

2.2 COMPARISON WITH OTHER MEASUREMENTS

Wind measurements have been made by other methods below 100 km.

On several occasions grenade and sodium-vapor experiments have been made within a few minutes of one another. The measured winds usually agree well except in regions of high shear. Here the grenade data give values averaged over the height interval between successive grenades and do not show the fine structure of the sodium trails.

Measurements up to about 60 km with small meteorological rockets have been obtained on a routine basis from many locations.[9] These measurements are consistent with the sodium trail measurements.

Most of the reported data on winds above 90 km come from radar observations of ionized meteor trails. These observations give valuable information about the periodic wind components and their seasonal variations, but their height resolution is much less than that of the sodium trail measurements. The radar data complement, rather than overlap, the sodium-trail data.

2.3 PERIODIC AND QUASI-PERIODIC VARIATIONS

The present data are not well suited to the determination of seasonal variations, for two reasons. The total number of observations is too small for an analysis of seasonal variations; and almost one third of the data were obtained during March and April.

The data are somewhat better suited to a study of diurnal and semi-diurnal variations, since about equal numbers of measurements have been made during morning and evening twilight and the local times of sunrise and sunset vary by nearly three hours through the year. However, the number of measurements proved to be too small to allow the periodic components to be separated from the non-periodic components. Radar measurements of ionized meteor trails at Jodrell Bank[10] and Adelaide[11] have established that at these latitudes the amplitudes of the periodic components are much less than the amplitude of the non-periodic components.

The prevalence of the non-periodic component leads one to expect that if the wind vectors derived from different flights for a given height are plotted on the same polar diagram the points will tend to be distributed in a more or less random way over a certain area. The observed distributions of data points are conspicuously non-random, however. They tend to form well-defined chains consisting of from three to eight points. In every case the chains may be connected to form a closed curve consisting of three loops; see Figures 3-31 and Table 1, where dates, times, and height ranges are given for the flights designated in the figures by the numerals 2 through 27, 7S, and 8S.

TABLE 1

No.	Date	Twilight	Range of Height in km
	(1959)		
1	17 August	AM	140-220
2	18 November	PM	94-163
	(1960)		
3	24 May	PM	84-169
4	9 December	AM	90-138
	(1961)		
5	19 April	AM	92-154
6	19 April	PM Sardinia	83-183
7	20 April	AM Sardinia	108-189
8	20 April	PM	81-165
9	21 April	AM	82-162
7S	7 September	PM Sardinia	90-200
8S	8 September	AM Sardinia	100-200
10	16 September	PM	78-146
11	17 September	AM	96-172
	(1962)		
12	1 March	PM	71-126
13	2 March	AM	65-127
14	23 March	PM	59-140
15	27 March	PM	80-118
16	17 April	AM	76-191
17	6 June	PM	56-137
18	7 November	AM	68-152
19	30 November	AM	77-157
20	5 December	PM	83-138
	(1963)		
21	20 February	PM	58-151
22	21 February	PM	83-164
25	20 May	PM Sardinia	94-195
26	21 May	AM Sardinia	98-200
27	21 May	PM Sardinia	84-205
23	23 May	PM	81-205
24	24 May	PM	84-170

That a closed curve of some kind can be drawn through twenty-eight data points is in itself without significance. What is significant is that the same, relatively simple, type of curve can be drawn through twenty-nine distinct sets of data points and that the characteristics of the curve change smoothly with height. The fact that the wind vectors for a given flight form a continuous sequence with height does not explain this result, as one can readily see by inspecting the figures. Compare, for example, Figure 3 (85 km) with Figure 31 (135 km). In Figure 3, data points 6, 10, 14, 18, and 20 fall on the innermost loop; in Figure 31, data point 6 has moved to the middle loop, data points 10, 14, and 20 have moved to the outermost loop, and only data point 18 has returned to the inner loop.

The fact that the wind vectors at a given height trace out -- or at least stay close to -- closed curves indicates that the winds have a quasi-periodic character. Because the strictly periodic components are known to be small, the rate at which the wind vector sweeps out its pattern at a given height must show appreciable departures from the rate that would be appropriate to strictly periodic motion. This point will be discussed at greater length in the next section.

The data are insufficient to establish the wind patterns above 135 km and below 85 km. Above 135 km, the wind vector has a large prevailing component directed toward the south. The region below 85 km has been studied by other techniques[14-19].

SECTION 3

MATHEMATICAL REPRESENTATION OF THE WIND DATA

It is convenient to represent the horizontal wind at a given height as a vector in the complex plane. If u,v denote the components of the wind in the north and west directions respectively, we may represent the wind vector in complex notation by

$$W = u + iv \ . \tag{1}$$

That is, u and v are, respectively, the real and imaginary parts of W. In quasi-periodic motion u and v depend on a common phase angle $\varphi(t)$. The dependence may be expressed by the equation

$$u(t) = a \cos[\varphi(t) + c_1] \quad , \quad v(t) = b \cos[\varphi(t) + c_2] \ . \tag{2}$$

The function $\varphi(t)$ is arbitrary. As φ varies between 0 and 2π, W traces out an ellipse whose size, shape, and orientation are determined by the three parameters a, b, and $(c_1 - c_2)$.

In strictly periodic motion $\varphi(t)$ is given by

$$\varphi(t) = \omega t = 2\pi/T \ , \tag{3}$$

where T denotes the period. In quasi-periodic motion $\varphi(t)$ is a non-linear function of t.

If a = b, the ellipse degenerates into a circle. We have found that the quasi-periodic components into which the wind pattern between 85 and

135 km can be resolved may be represented reasonably well in a first approximation by circles. This considerably reduces the number of parameters needed for the representation. A more refined representation, based on ellipses, would require more data than we have as yet accumulated.

The formula

$$W = W_0 e^{i\alpha_0} + W_1 e^{i(\varphi+\alpha_1)} + W_2 e^{i(2\varphi+\alpha_2)} + W_3 e^{i(3\varphi+\alpha_3)} , \qquad (4)$$

where W_0, W_1, W_2, and W_3 are real numbers, represents a superposition of a prevailing component (amplitude W_0, phase α_0), a "fundamental" (amplitude W_1, phase α_1), and its first two overtones. The prevailing component merely displaces the center of the figure. Figures 32-36 are plots of W for various values of the amplitudes W_i and phases α_i. In all the figures, $W_3 > W_2 > W_1$; the third overtone has the highest amplitude. Note, for example, the resemblance between the experimental Figure 21 and the theoretical Figure 35.

For the analysis of the data figures, it is convenient to introduce two auxiliary quantities, δ_2 and δ_1. These are defined as follows. Suppose that $W_0 = W_1 = 0$, so that only the second and third components are present. The axis of the resultant figure (which passes through the two nodes) makes an angle δ_2 with the direction of north. The angle δ_2 may also be defined as the direction in which W is a maximum when $W_0 = W_1 = 0$. This occurs when the phases of the second and third components are equal, i.e., when

$$2\varphi + \alpha_2 = 3\varphi + \alpha_3 \quad , \quad \varphi = \alpha_2 - \alpha_3 . \qquad (5)$$

Thus

$$\delta_2 = 3\alpha_2 - 2\alpha_3 \cdot \tag{6}$$

The angle δ_1 is defined as the phase of the first component reckoned (clockwise) from the direction north, then

$$\delta_1 - \delta_2 = \alpha_1 - 2\alpha_2 + \alpha_3 \, , \tag{7}$$

and

$$\delta_1 = \alpha_1 + \alpha_2 - \alpha_3$$

If $\delta_1 = 0$ the pattern will possess bilateral symmetry. A line drawn through the two nodes will divide the pattern into two parts that are mirror images of one another. The angle between this line and the direction of north is then δ_2. When $\delta_1 \neq 0$ the pattern is asymmetrical. The direction of the outer node is particularly sensitive to the value of δ_1. Figure 37 shows δ_1 plotted against the direction of the outer node (measured from the center of the figure) for a typical set of values of W_1, W_2, and W_3.

The magnitude and direction of the prevailing component determine the position of the center of the pattern. Since the position of the center cannot be determined with great precision, the values of W_0 and α_0 ($= \delta_0$) are rather uncertain, especially when W_0 is small. Given approximate values of the W_i for i = 1,2,3, one can determine the parameters δ_1 and δ_2 by comparing the observed pattern with theoretical patterns in a graduated series. It turns out that the ratios of the W_i do not vary much over the observed

height range. Moreover, the shape of the pattern is not very sensitive to small variations in these ratios. Because of this, δ_1 and δ_2 can be evaluated with fair accuracy when the W_i are known only roughly. Having determined δ_1 and δ_2, one obtains the W_i by solving sets of simultaneous equations that express the distances between selected pairs of points in terms of the W_i. The best-determined parts of the data patterns were used for this purpose.

The values of the W_i and δ_i that emerge from the analysis are indicated on the individual Figures 3-31. In Figures 38-43 these parameters are plotted against height. In view of the small number of data points used to determine the individual data patterns and of the rather rough method of analysis, all these figures, with the possible exception of the one for δ_0, show remarkably smooth and systematic variation of the plotted quantity with height. The systematic character of these variations would seem to leave little doubt that the mathematical representation here employed has a sound physical basis.

Up until now we have not discussed the information contained in the local times of the wind measurements. If the winds were strictly periodic instead of quasi-periodic, the position of a point on its data pattern would be determined by its local time. In the theoretical Figures 33-36 the local times are indicated. Roughly speaking, equal time intervals correspond to equal angular displacements as seen from the center of the figure. The zero of local time has arbitrarily been made to coincide with the direction of the figure axis when $W_1 = 0$.

During April 1961, there was a series of closely spaced firings at Wallops Island and at Sardinia. The times of observation are shown in Table 2. At almost every height, the five points 5, 6, 7, 8, 9 occur in correct sequence. However, the "theoretical" time intervals -- that is, the time intervals appropriate to strictly periodic motion -- often differ substantially from the observed time intervals. Table 3 gives all the information pertaining to time intervals for sequential observations included in our data. In some instances, large discrepancies between actual time interval and the "theoretical" interval probably result from the assignment of a data point to the wrong loop in its pattern, but there is no doubt that the rate at which the wind vector at a given height traces out its pattern departs substantially from the rate appropriate to strictly periodic motion.

TABLE 2

TIME OF OBSERVATION FOR THE APRIL 1961 SERIES

Number	Site	Approximate LMT	Approximate EST	Time Difference
5	Wallops	19 April 04.6 hours	19 April 04.6 hours	
6	Sardinia	19 April 19.2	19 April 13.5	8.9 hours
7	Sardinia	20 April 04.6	19 April 22.9	9.4
8	Wallops	20 April 19.2	20 April 19.2	20.3
9	Wallops	21 April 04.6	21 April 04.6	9.4

SECTION 4

DISCUSSION

The preceding analysis leads to the following general conclusions.

(1) At each height, the observed wind vectors define a pattern which is accurately reproduced by a theoretical figure composed of prevailing diurnal, semi-diurnal, and 8-hour components.

(2) The parameters that define the pattern vary smoothly with height as shown in Figures 38 through 42. The magnitudes of all components increase to a maximum between 100 and 110 km, and the phase angles change rapidly in this region. This is also the region where the large shears occur most frequently.

(3) The 8-hour component is dominant at all heights. Sometimes its magnitude is twice that of the semi-diurnal component. The diurnal component is small below about 95 km, but increases above this height. The prevailing component varies from near zero to a maximum of 40 m/sec at 105 km. The direction is generally toward the east below 120 km and toward the west above.

(4) The motion of the wind vector at a given height is not accurately periodic; that is, it is not true in general that

$$W(t + 24\text{-hr}) = W(t); \quad \delta(t + 24\text{-hr}) = \delta(t)$$

This fact shows up when time differences of the successive measurements in Table 2 are compared with "predicted" time differences obtained from the corresponding computed model. The time differences for the sequential firings as indicated by the model figures are shown in Table 3. The rate of rotation of the tip of the wind vector fluctuates by as much as a factor of three at specific heights. However, average values for a range of heights at a given time, as well as time averages for a given height, are close to the predicted values. It follows that at a given instant of time, there is no unique pattern for the height variation of W or δ. Thus a large variation of the altitude profiles of the wind is to be expected and is observed.

Previous quantitative information about winds in the height range under consideration comes mainly from the work of Greenhow[10,20] and his co-workers based on a radio-echo technique devised by Greenhow. This technique enables one to measure the velocities of one or more short sections of a suitably oriented ionization trail, such as are produced in large quantities in the height range 85-100 km by meteors. The accompanying absolute height determinations have an uncertainty of ± 2 km; however, Greenhow extended his technique to permit direct measurements of vertical gradients of horizontal winds (wind-shear). From a very extensive set of observations, Greenhow and his co-workers determined, for every month of the year, the height-averaged amplitudes and phases of the prevailing, diurnal, semi-diurnal, and terdiurnal components of the horizontal wind in the height range 90-94 km. They also determined the vertical gradients of these quantities in the height range 90-100 km. Finally they determined the frequency distribution of the

TABLE 3

TIME INTERVAL IN HOURS OF SEQUENTIAL OBSERVATIONS AS OBTAINED FROM MODEL FIGURES. (Occasionally two time intervals were possible)

Height km	Flight Number						
	5-6	6-7	8-9	25-26	7S-8S	12-13	10-11
85						10	
86.25						11	
88.75						3	
90			10			6	
91.25			3			4	
92.5	3		3			9	
93.75	4		9			9	
95	5		10			9	20
96.25	5		5			10	20
97.5	13		5	1		9	20
98.75	11		20	0		0	6
100	5		8	17	17	8	12
101.25	9		7	7	18	12	8
102.5	12		10	7	19	19	9
103.75	11		3(17)	3	10	18	10
105	5		9	10	13	11	6
106.25	11		11	5	13	8	4
107.5	7	13	4	14	13	8	5
108.75	7	10	10	19	14	14	5(12)
110	8	8	3	19	16	7	13
111.25	8	3	19(3)	17	17	11	16
112.5	6	3	19	9	10	0	15
113.75	7	3	1	10	10	0	10
115	7	3	2	11	11	23	14
116.25	7	4	1	10	10	23	23
120	6	4	0	23	10		10
125	5	3	10	2	10		17
130	5	4(9)	2	9	10		5
135	5	9	0	19	10		19
Actual time interval in hours	8.9	9.4	9.4	8.5	10	11.5	10.4

amplitude of the horizontal wind and the frequency distribution of the wind shear in the same height range.

The experimental results obtained by the radio-echo method indicate that the non-periodic component of the horizontal wind is much larger, in the height range under consideration, than the prevailing and periodic components. However, owing to their limited height resolution, they contain little information about the nature of the non-periodic component. This is precisely the kind of information that the data presented here supply. On the other hand, these data supply little information about strictly periodic variations. The two experimental approaches are thus largely complementary.

On the basis of the radar data, the winds in the region 85-105 km have been envisioned as made up of three contributions: a prevailing component, similar to those that occur at lesser heights; a small tidal or thermally driven component which, like the tidal winds at lesser heights, can be analyzed into a diurnal, a semi-diurnal and a terdiurnal component, and a non-periodic component, much larger than the other two and characterized by steep vertical gradients, sometimes exceeding 0.1 sec^{-1} (= 100 m sec^{-1} km^{-1}). The radio-echo observations, as well as earlier optical observations of persistent meteor trails[21] showed that the non-periodic winds had a very narrow energy spectrum, Fourier components with a vertical wavelength of less than 1 km being essentially absent. The non-periodic winds could therefore not be described as turbulent in the technical hydrodynamic sense. The wavelike forms of persistent meteor trails led Hines[22] to attribute the non-periodic winds to upward-propagating waves generated near the surface of the earth and

combining the properties of sound waves and internal gravity waves. This interpretation has been widely accepted.

Although the picture just sketched seems to rest on a solid observational basis, it is by no means the only picture that is consistent with the radio-echo data, which afford a very incomplete, statistical description of what is, at least numerically, the major component of the horizontal winds. In addition, Hines's interpretation of the non-periodic winds raises certain theoretical questions that have not yet been adequately answered. For example: How are the travelling waves excited? Hines's hypothesis requires a non-periodic driving mechanism considerably more effective than the processes responsible for the periodic winds - presumably[23] the absorption of insolation by water vapor and by ozone. What is the nature of this mechanism?

The data from the sodium trails suggest a strikingly different picture. The resultant wind at any height in the height range 85 to 135 km may be represented by a prevailing component and cyclic components with periods of 24 hours, 12 hours, and 8 hours. The magnitudes of the cyclic components vary smoothly with height, but there is a "phase anomaly". That is, the phase ϕ is a non-linear function of the time. The lack of correlation between the phase anomaly at different heights gives rise to the variability of the wind profiles.

On the present picture, virtually the entire amplitude of the wind at a given height can be attributed to periodic, thermal driving forces. There

is no room in this picture for traveling waves produced by non-periodic driving forces. The dominance of the 8-hr component should find a quantitative explanation in the resonance characteristics of the atmosphere in this height range. In this connection, we recall that Butler and Small[24] have recently shown that the amplitude of the 24-hr component is greatly reduced, in comparison with the 12-hr component, because of the structure of the atmosphere below 80 km.

The origin of the phase anomaly remains to be explained. We tentatively attribute it to magnetohydrodynamic effects which enhance the effective viscous coupling between adjacent layers and to variability in the reflection properties of the atmosphere above 135 km. This question will be discussed at greater length in a forthcoming publication.

It is perhaps significant that data from two trails at Wallops Island are not contained in the closed loop figures. The observations of 17 August 1959 are not shown on the plots since the wind speeds were greater than the scale of the graph. Some of the data from 24 May 1960, although plotted, are not contained in the figures. These observations were made during times of very great solar activity and the upper winds were noticeably different from the usually observed structure.

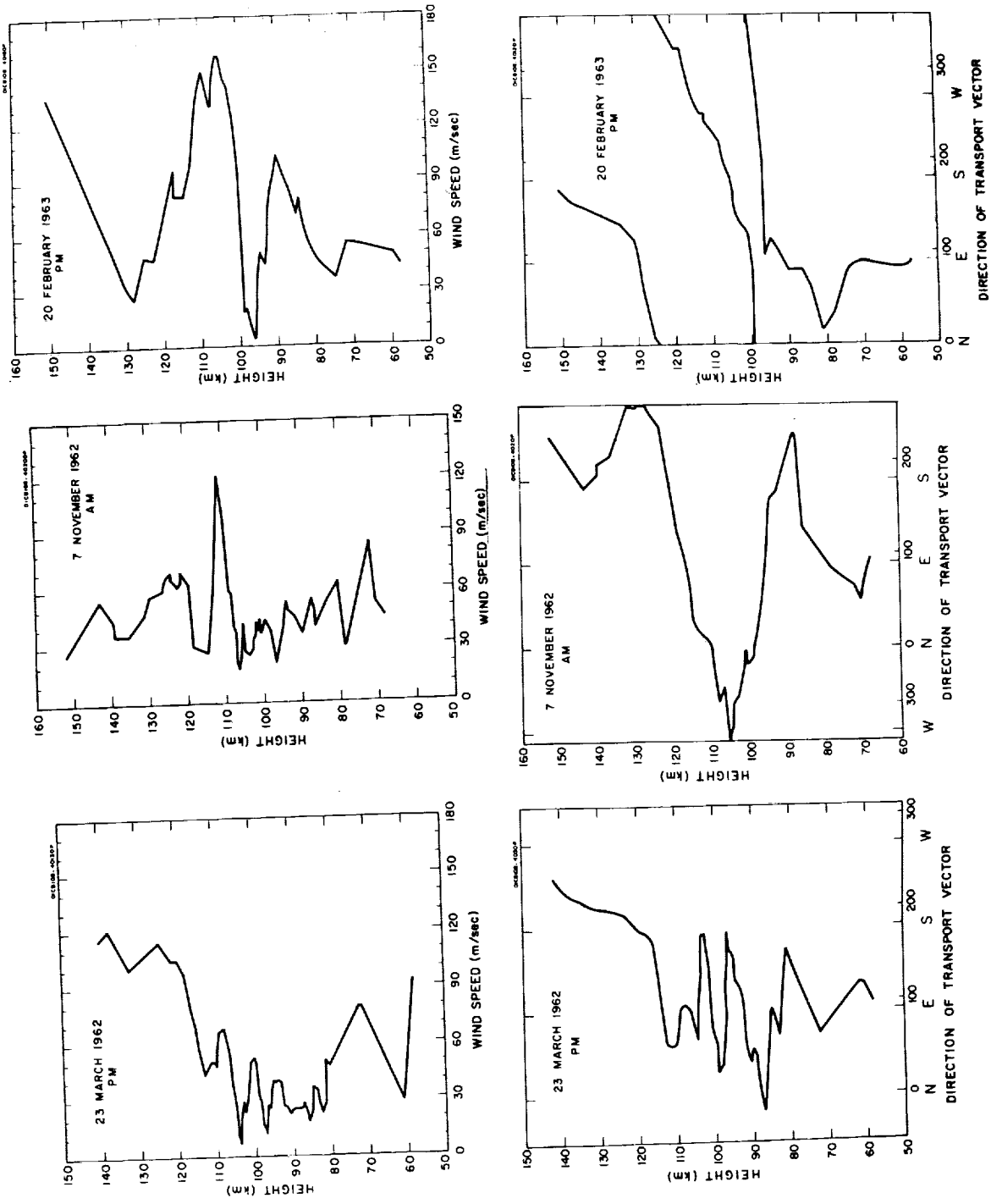

Figure 1. Change of wind speed and direction of transport vector with height for 23 March 1962, 7 November 1962, and 20 February 1963 to illustrate classes I, II, and III respectively.

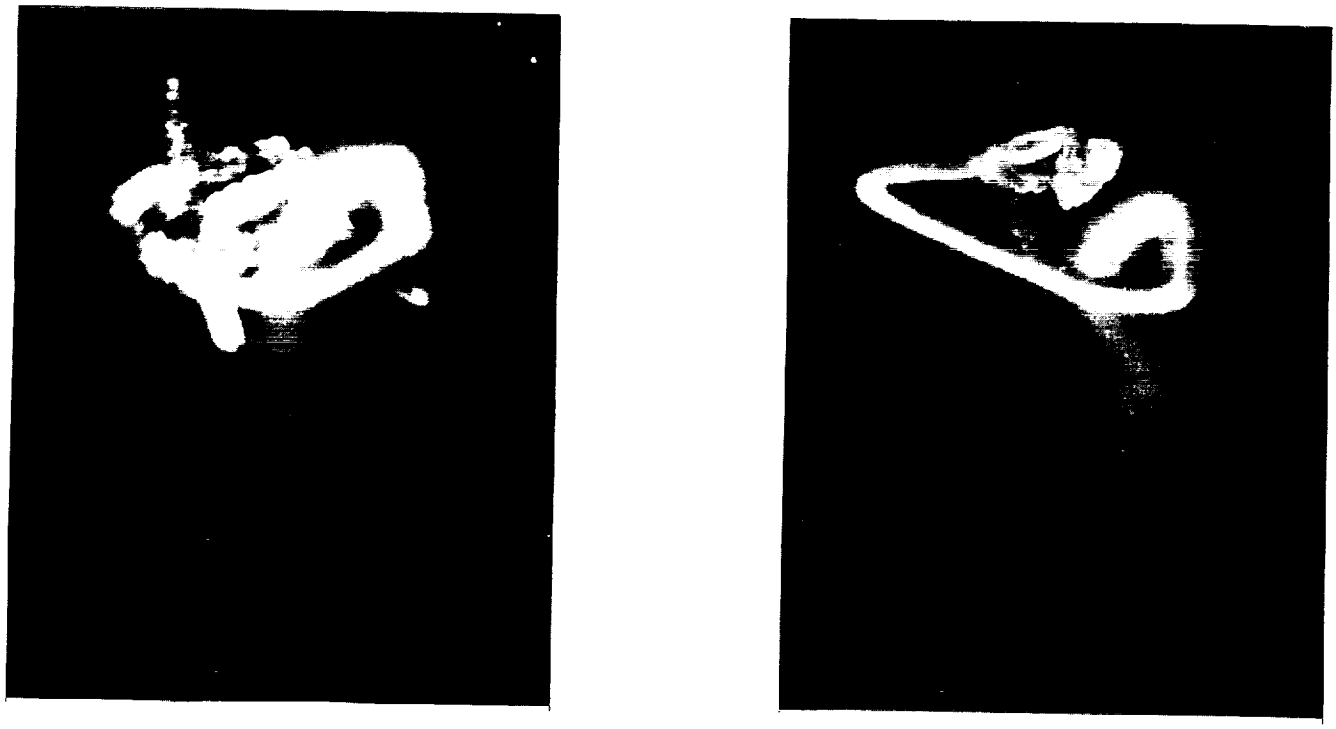

(a) (b)

(c)

Figure 2. Photographs of the sodium trail taken 200 sec after launch, from the launch site, on (a) 23 March 1962, (b) 7 November 1962, and (c) 20 February 1963. Note the obvious difference in appearance.

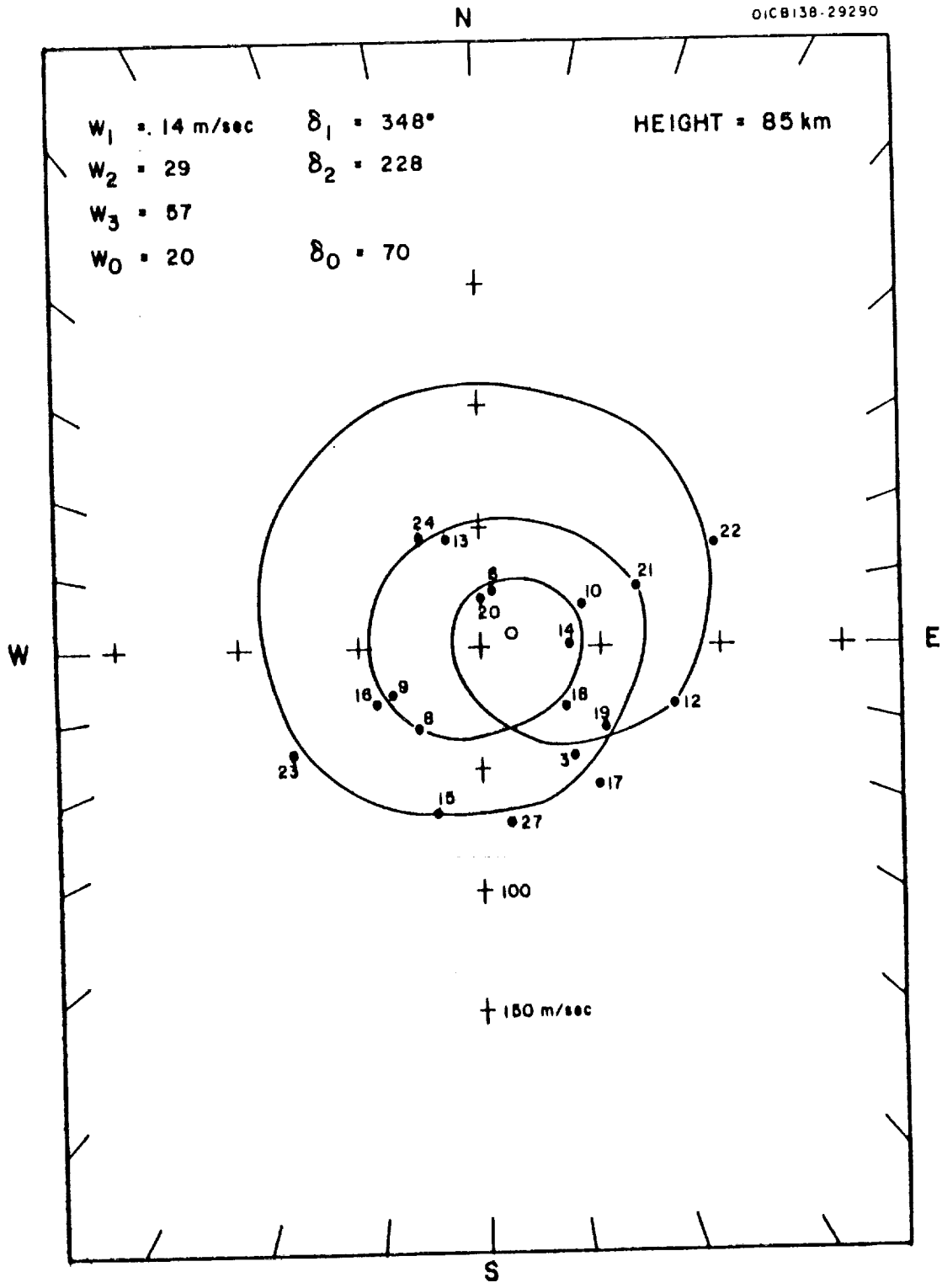

Figure 3. The pattern of wind structure as observed for a height of 85 km. The numbers refer to the dates listed in Table 2. The geometric center of the figure is an open circle. W_1 = 24-hour, W_2 = 12-hour, W_3 = 8-hour, and W_o = prevailing components with accompanying phase angles, δ.

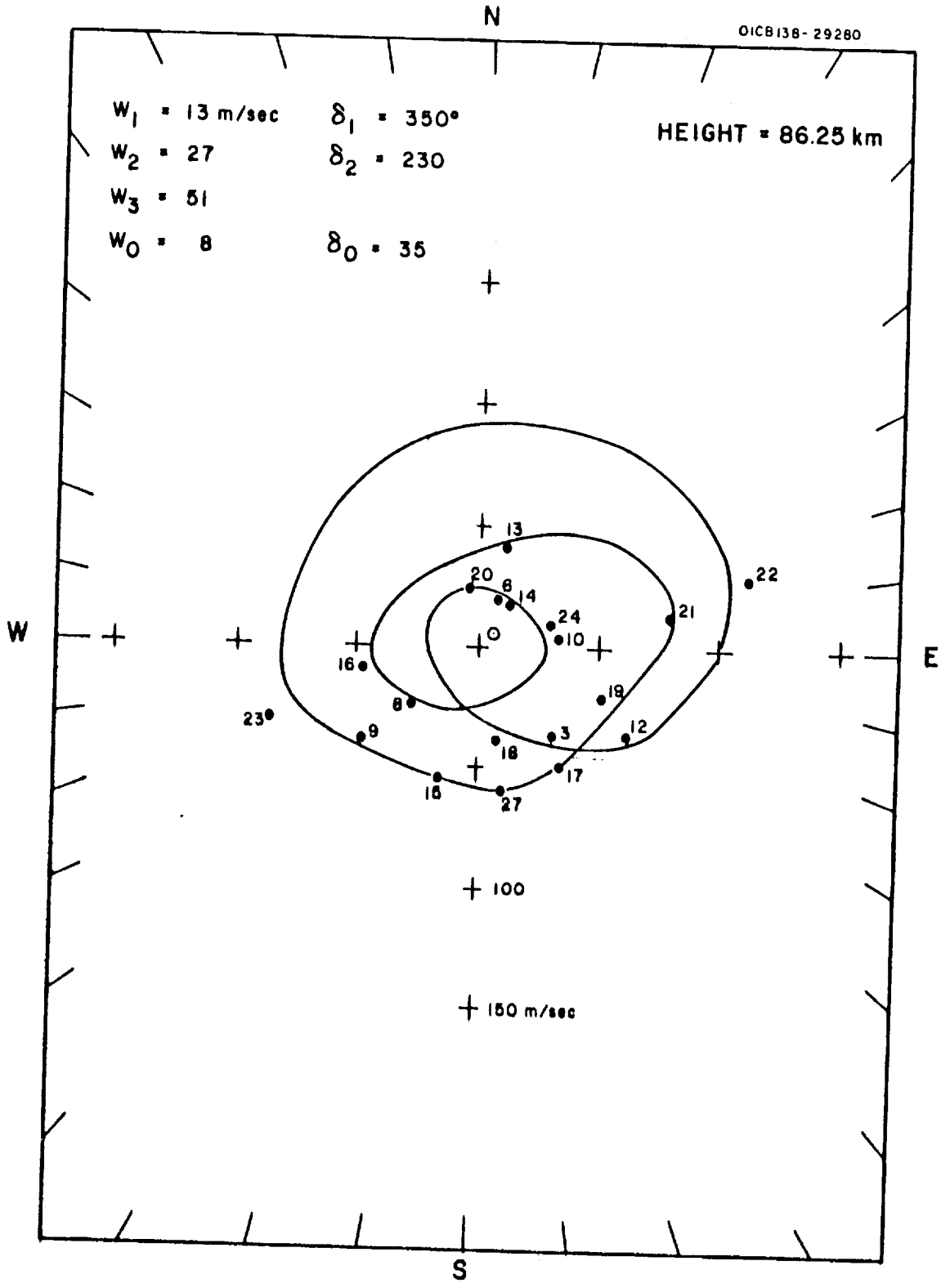

Figure 4. The pattern of wind structure as observed for a height of 86.25 km.

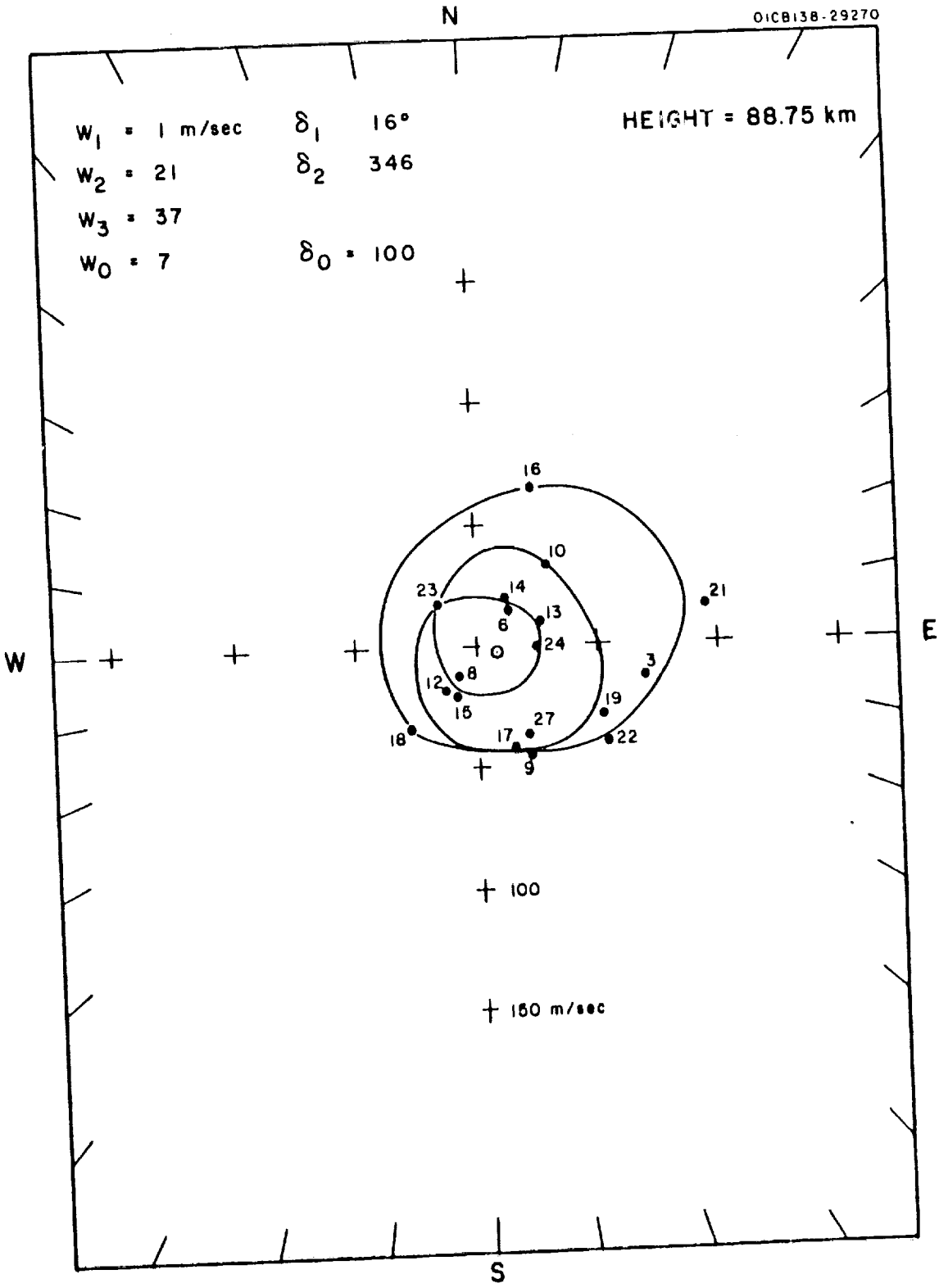

Figure 5. The pattern of wind structure as observed for a height of 88.75 km.

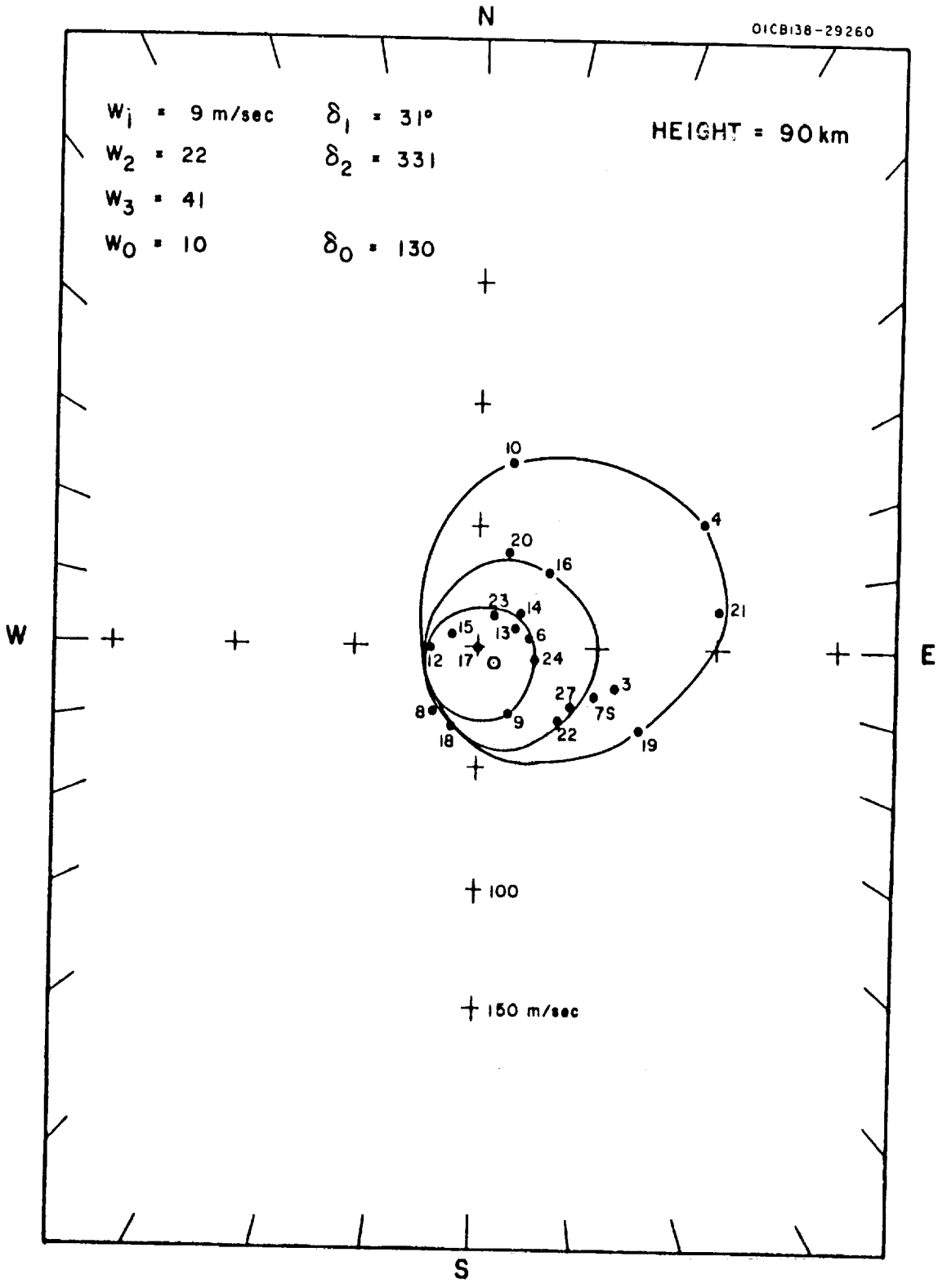

Figure 6. The pattern of wind structure as observed for a height of 90 km.

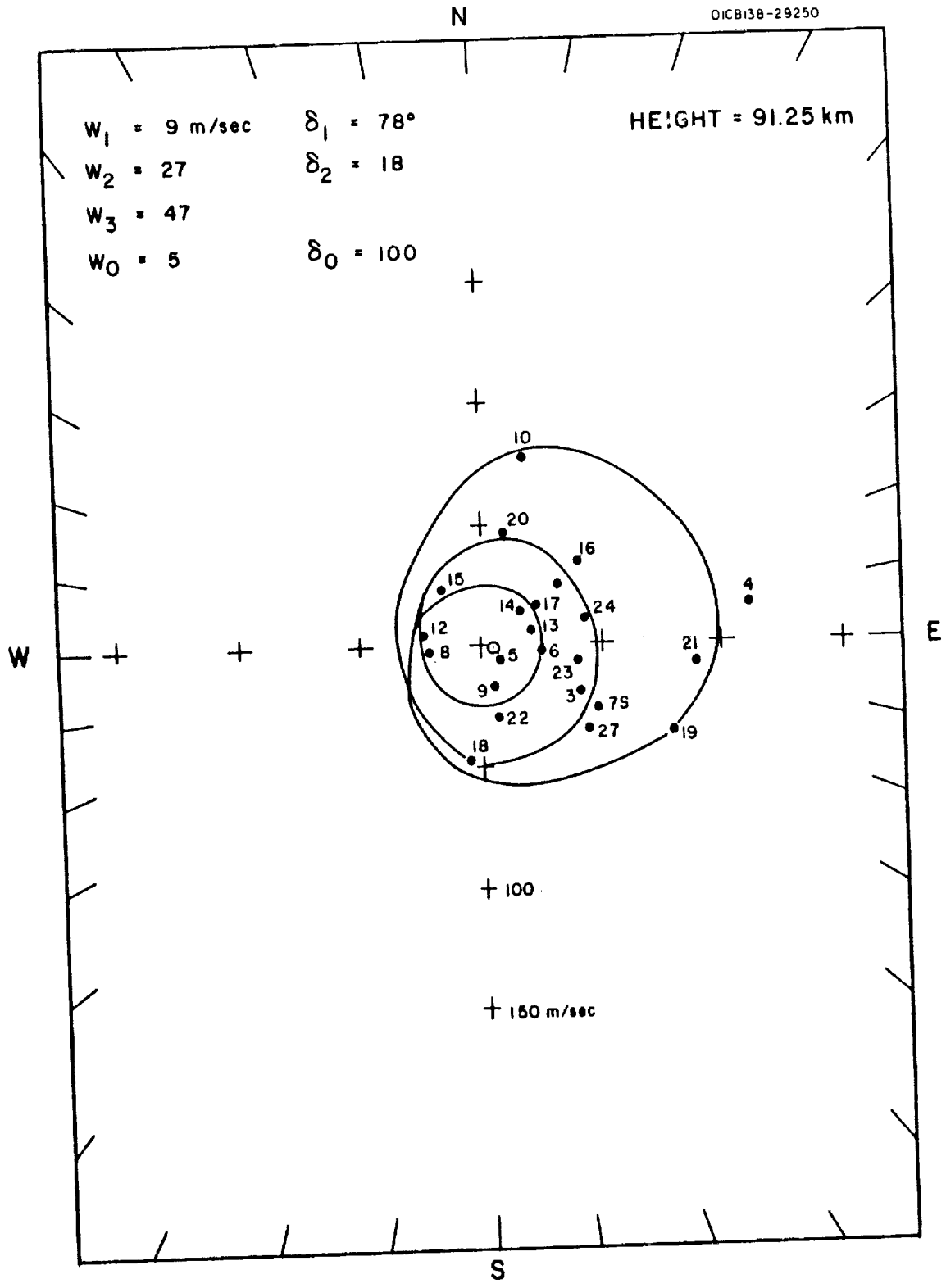

Figure 7. The pattern of wind structure as observed for a height of 91.25 km.

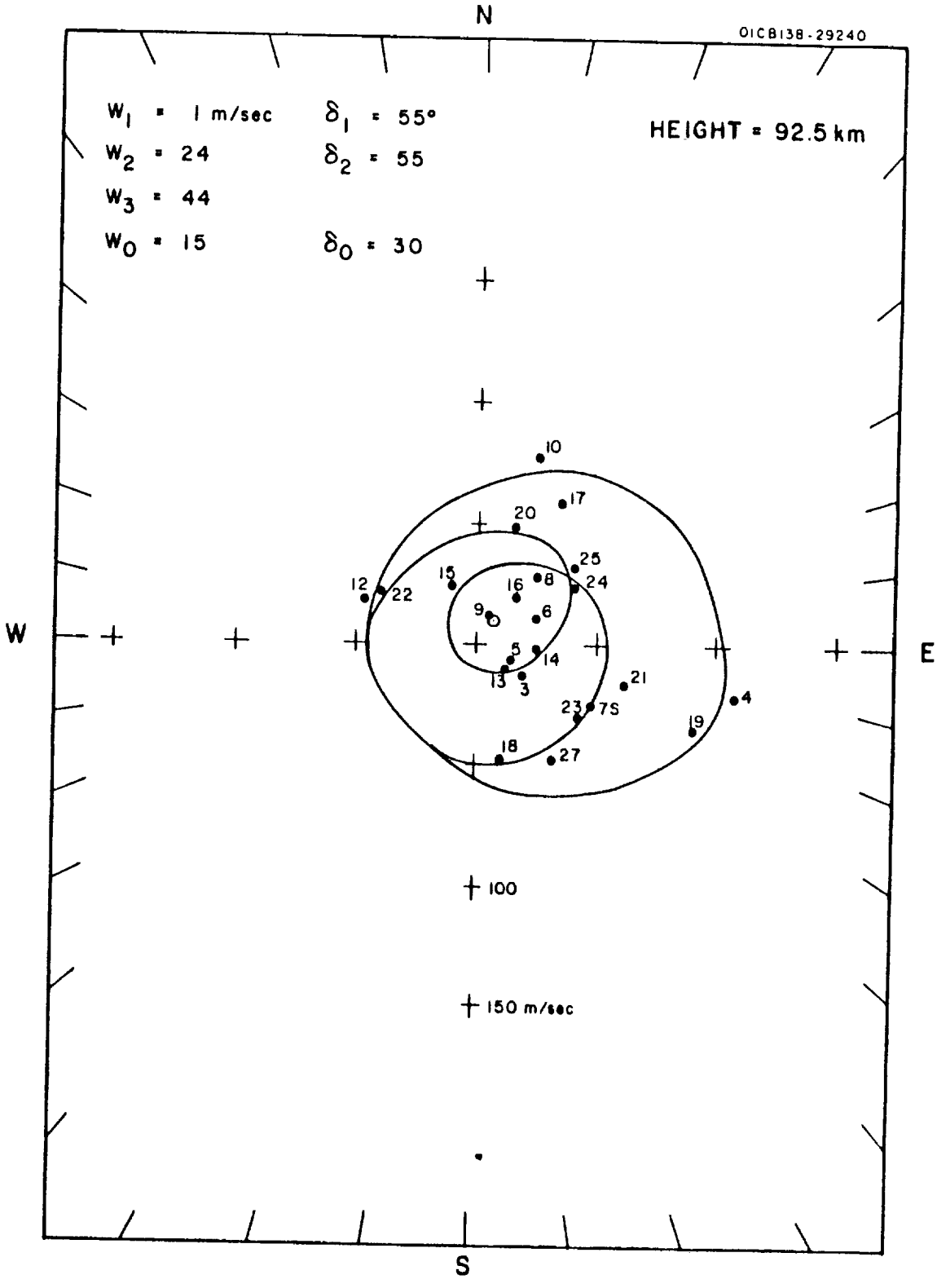

Figure 8. The pattern of wind structure as observed for a height of 92.5 km.

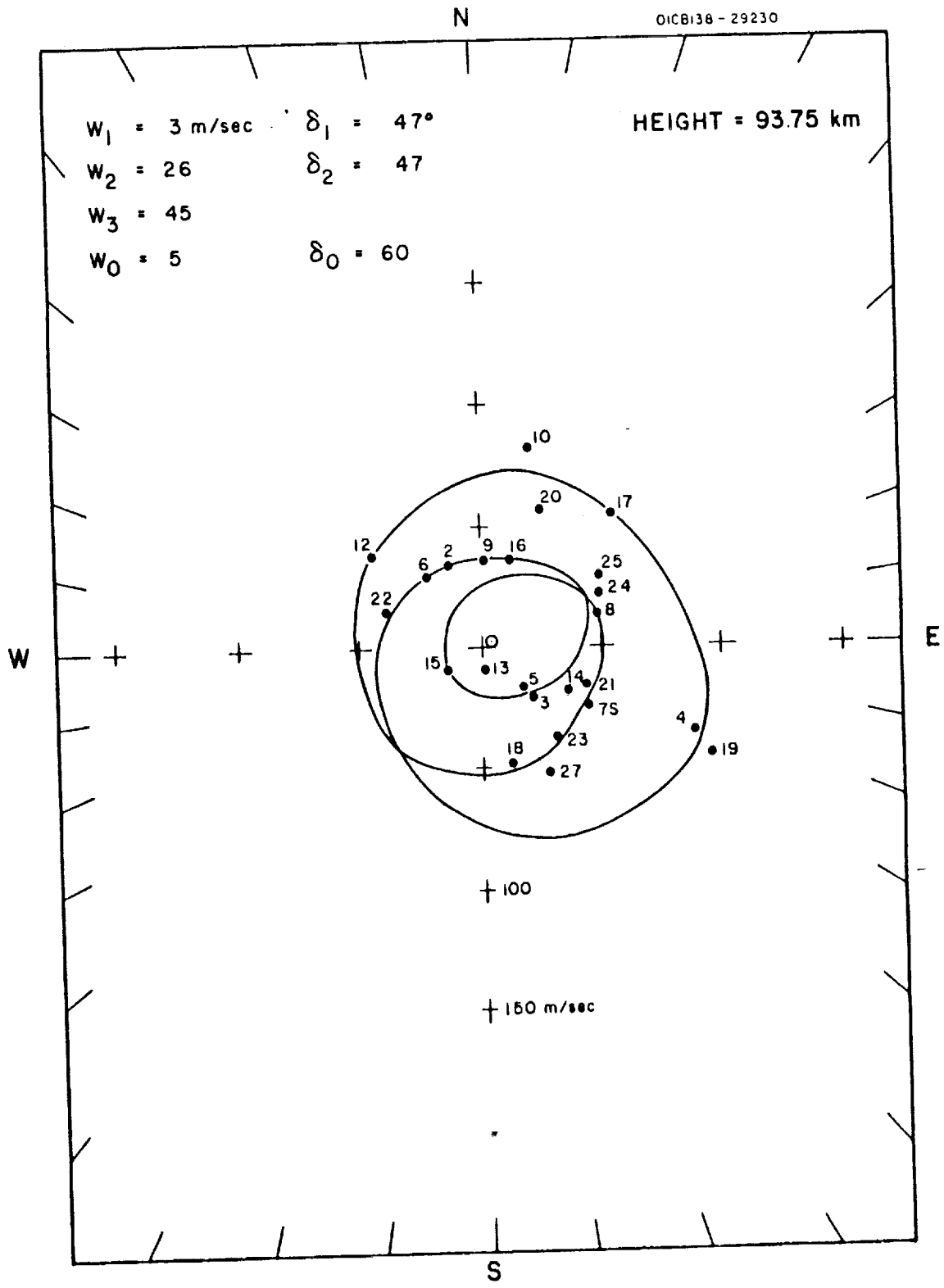

Figure 9. The pattern of wind structure as observed for a height of 93.75 km.

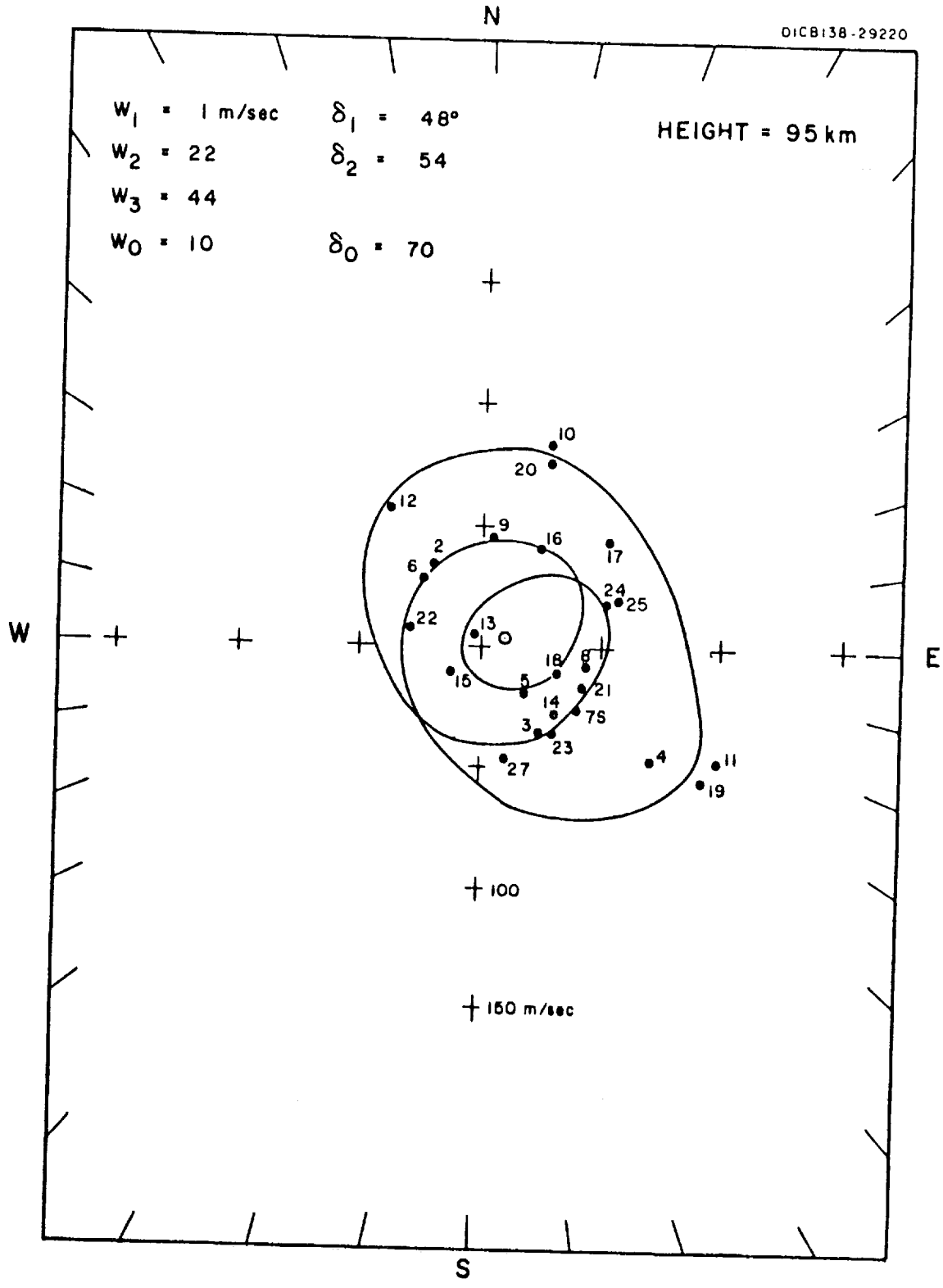

Figure 10. The pattern of wind structure as observed for a height of 95 km.

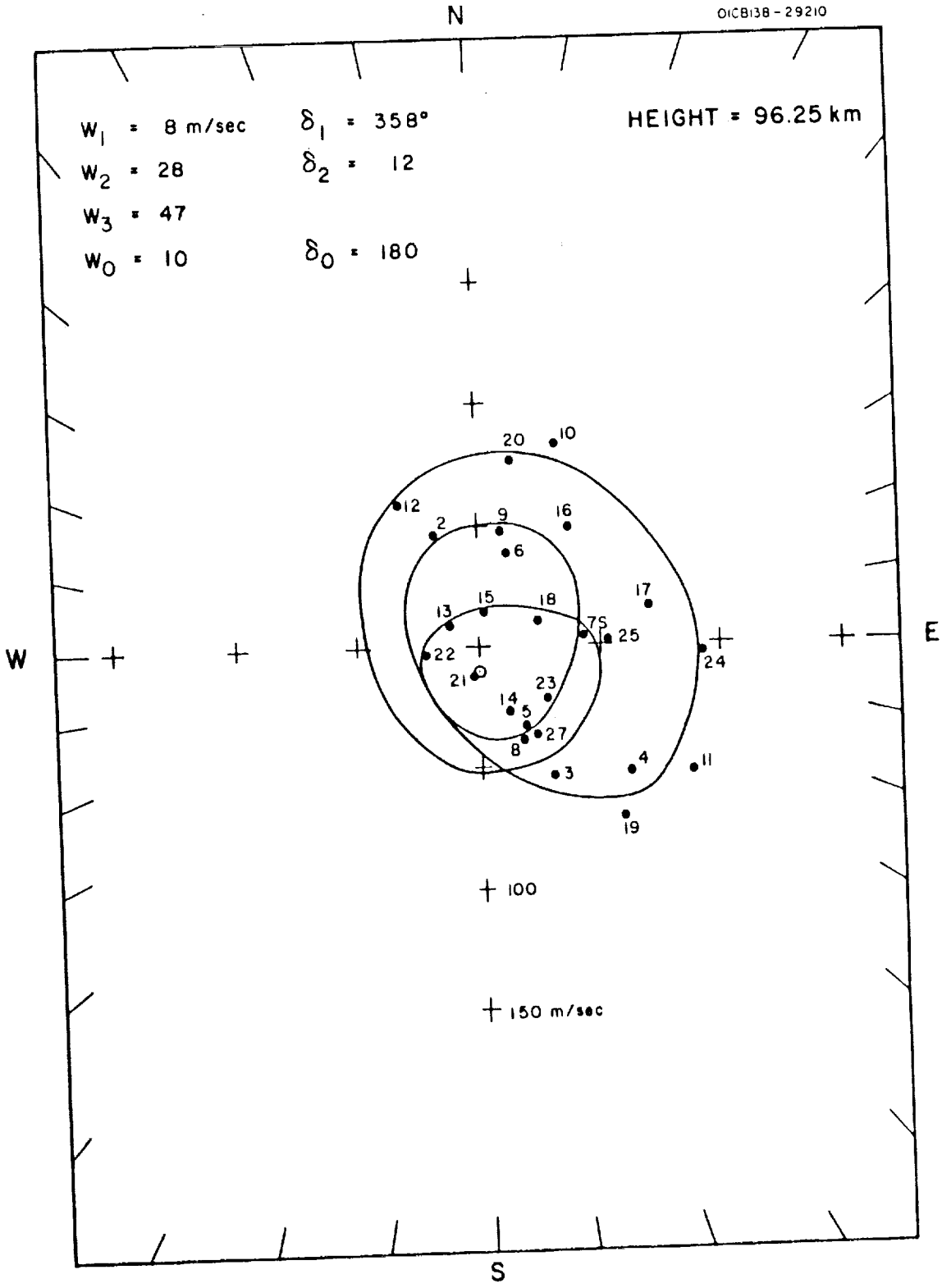

Figure 11. The pattern of wind structure as observed for a height of 96.25 km.

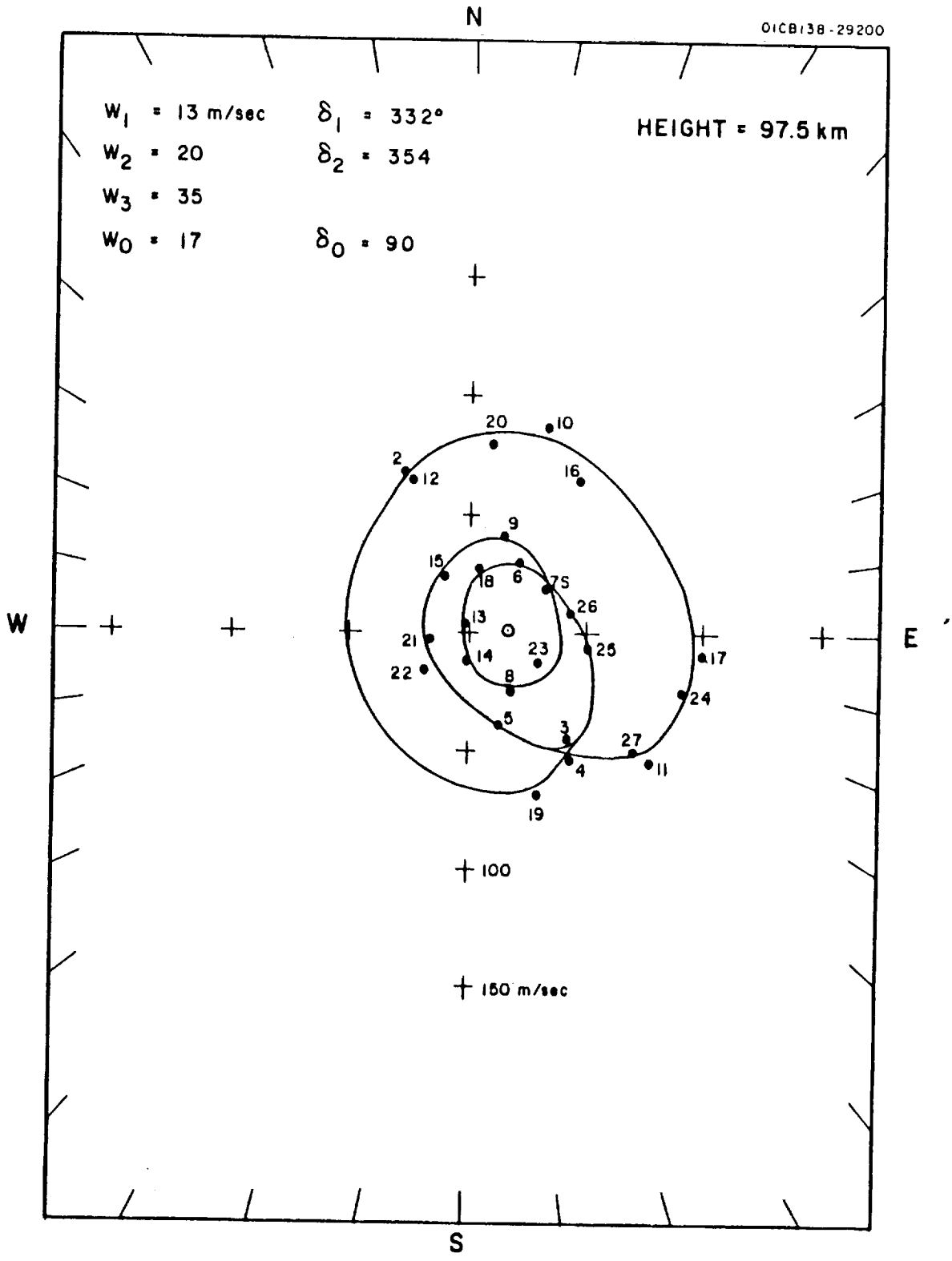

Figure 12. The pattern of wind structure as observed for a height of 97.5 km.

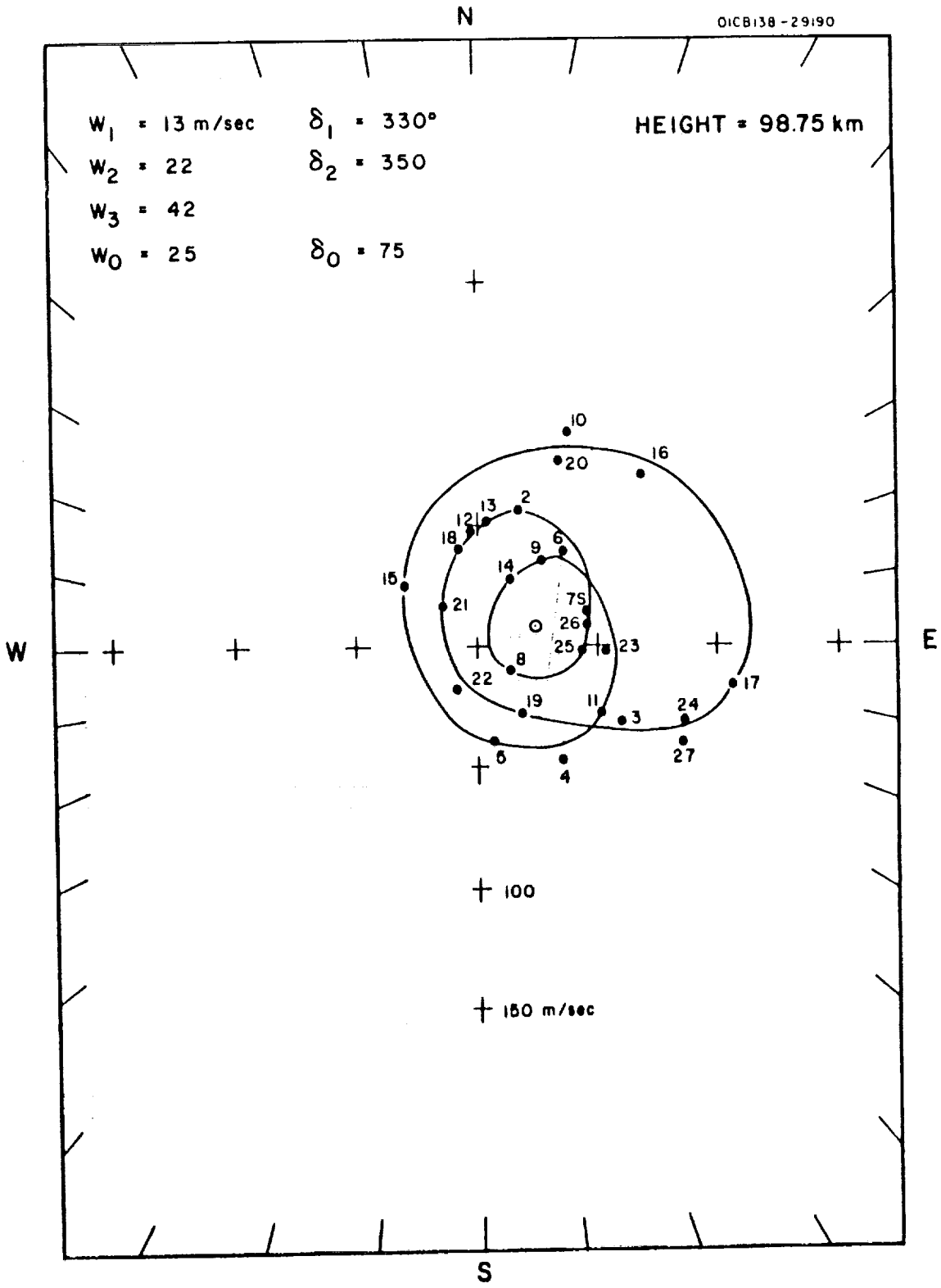

Figure 13. The pattern of wind structure as observed for a height of 98.75 km.

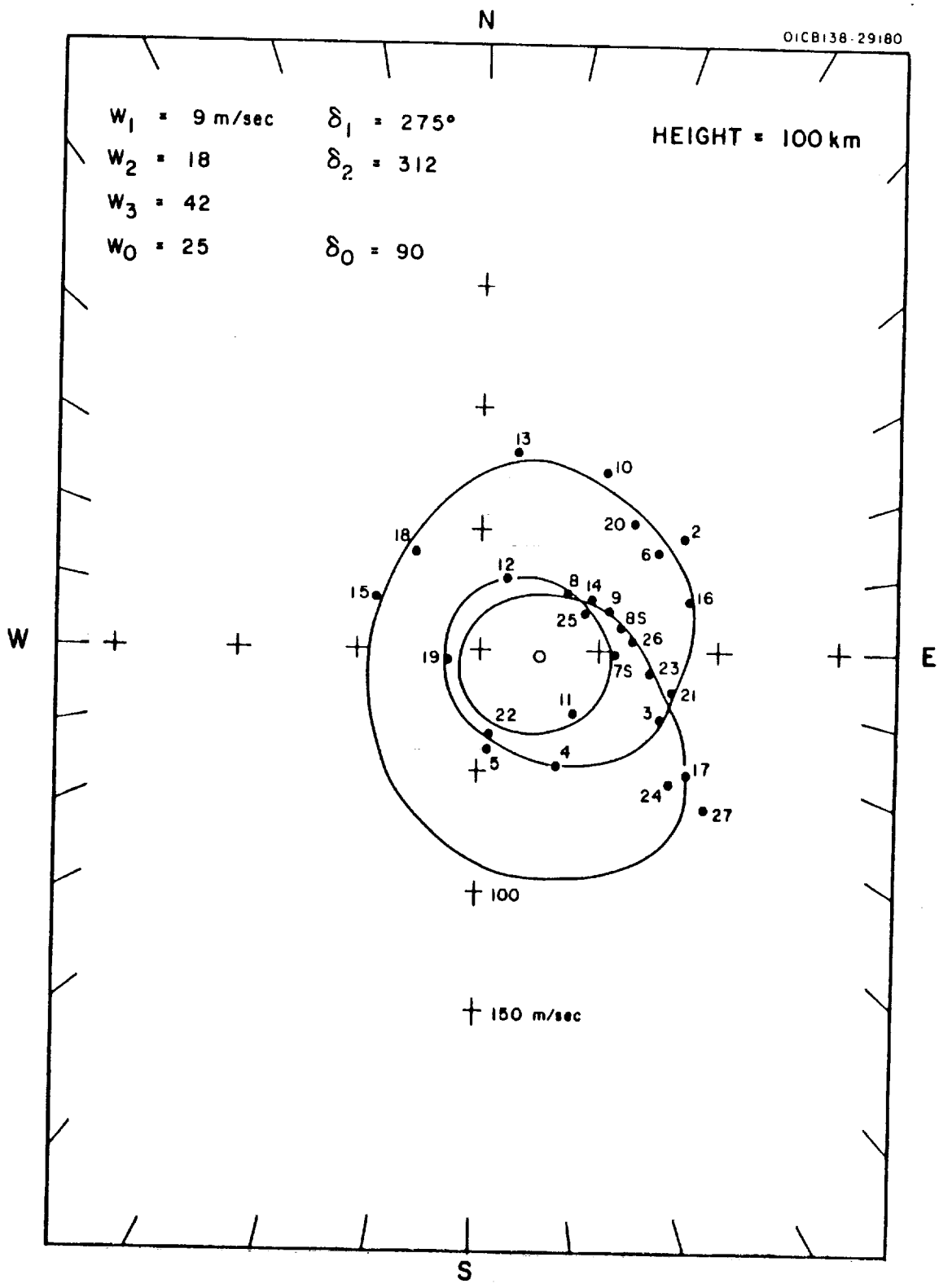

Figure 14. The pattern of wind structure as observed for a height of 100 km.

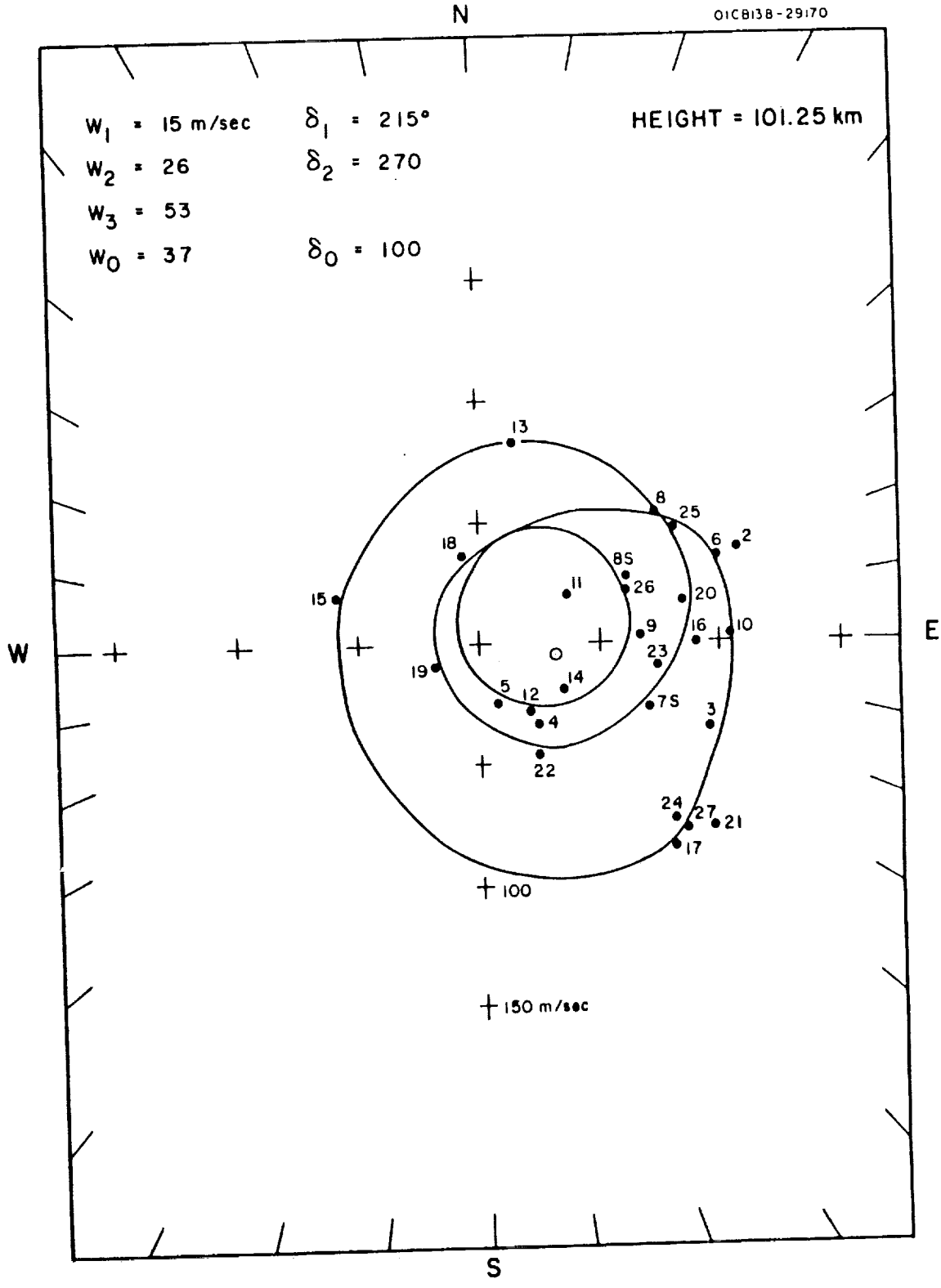

Figure 15. The pattern of wind structure as observed for a height of 101.25 km.

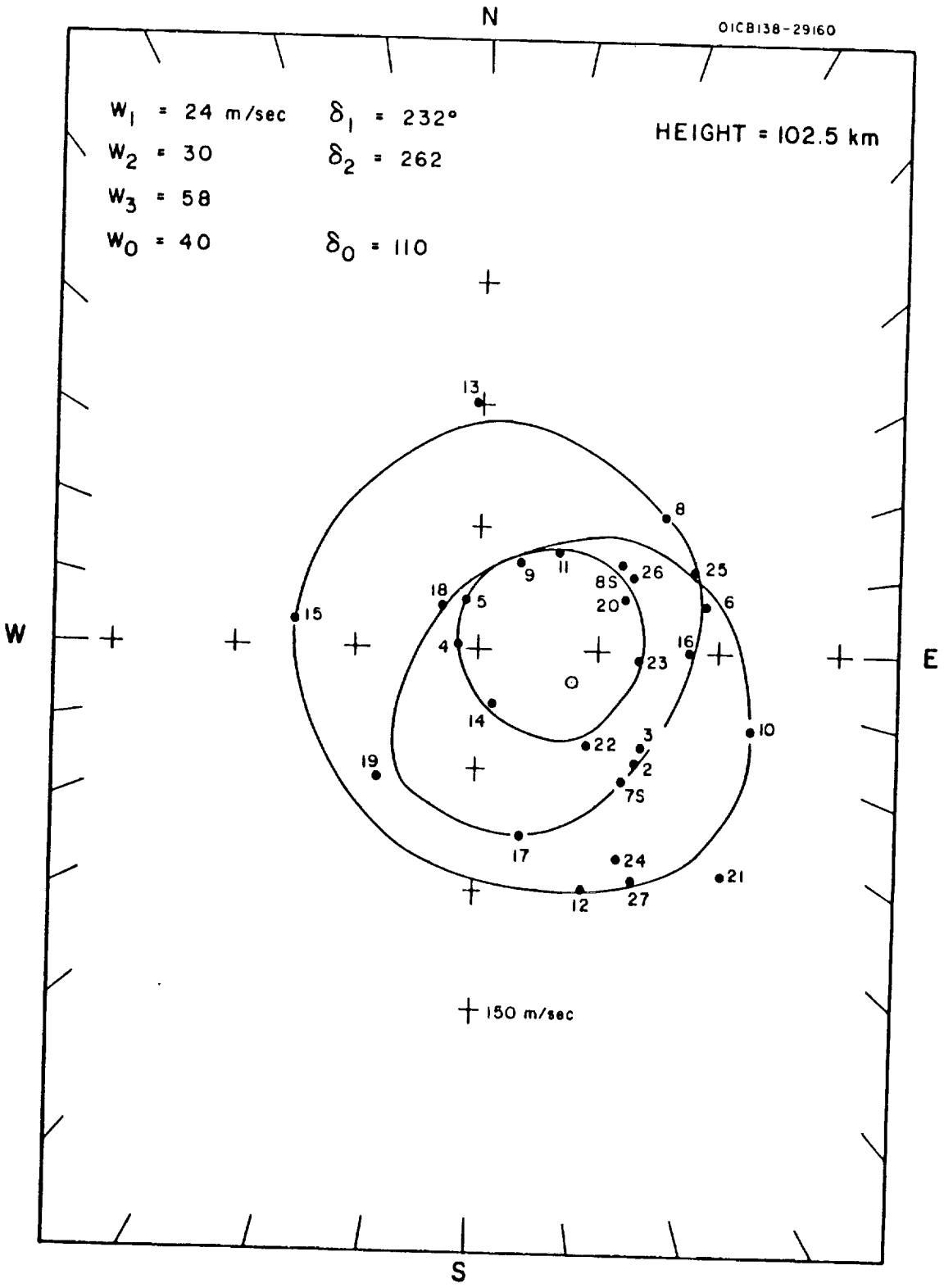

Figure 16. The pattern of wind structure as observed for a height of 102.5 km.

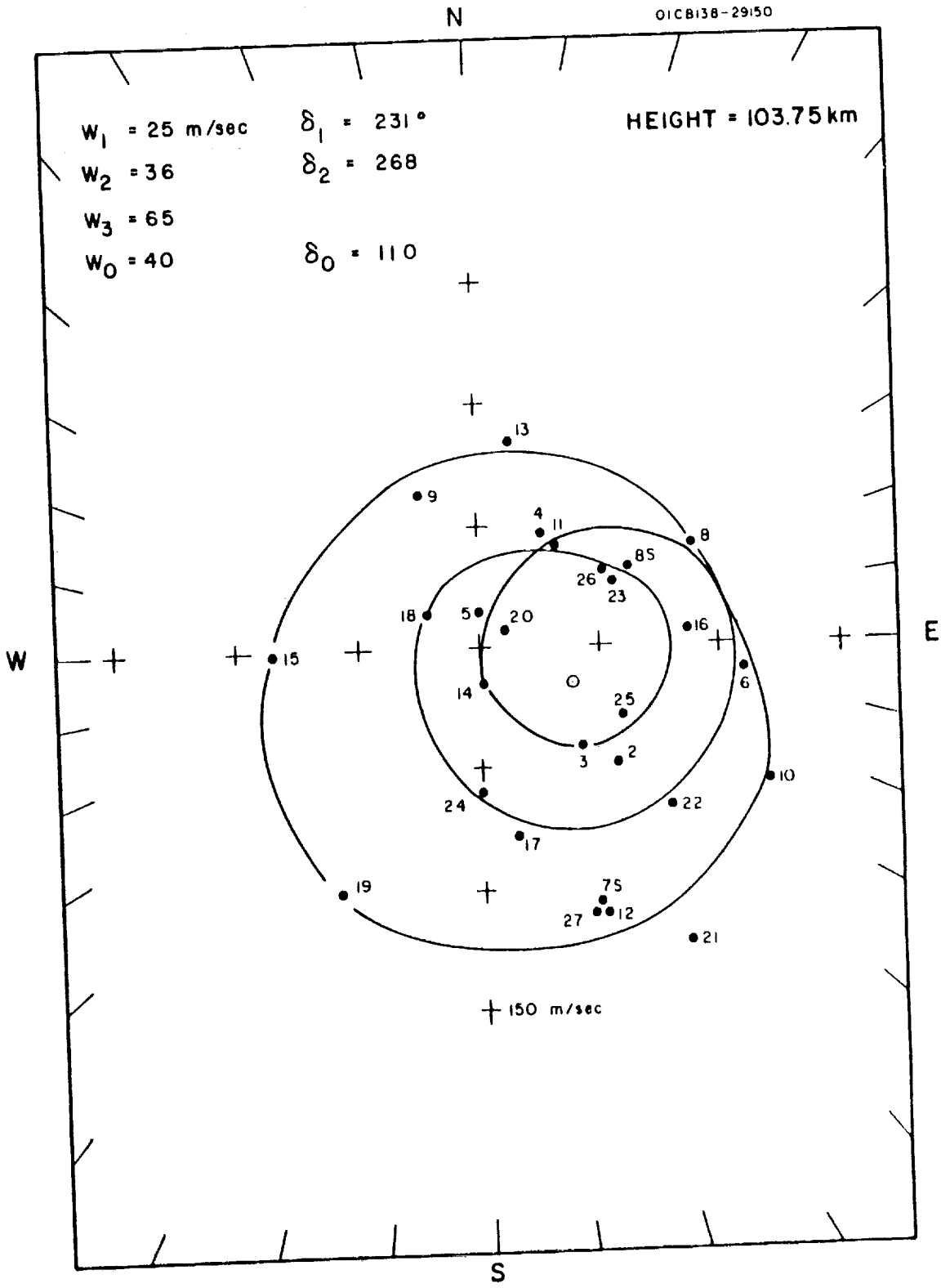

Figure 17. The pattern of wind structure as observed for a height of 103.75 km.

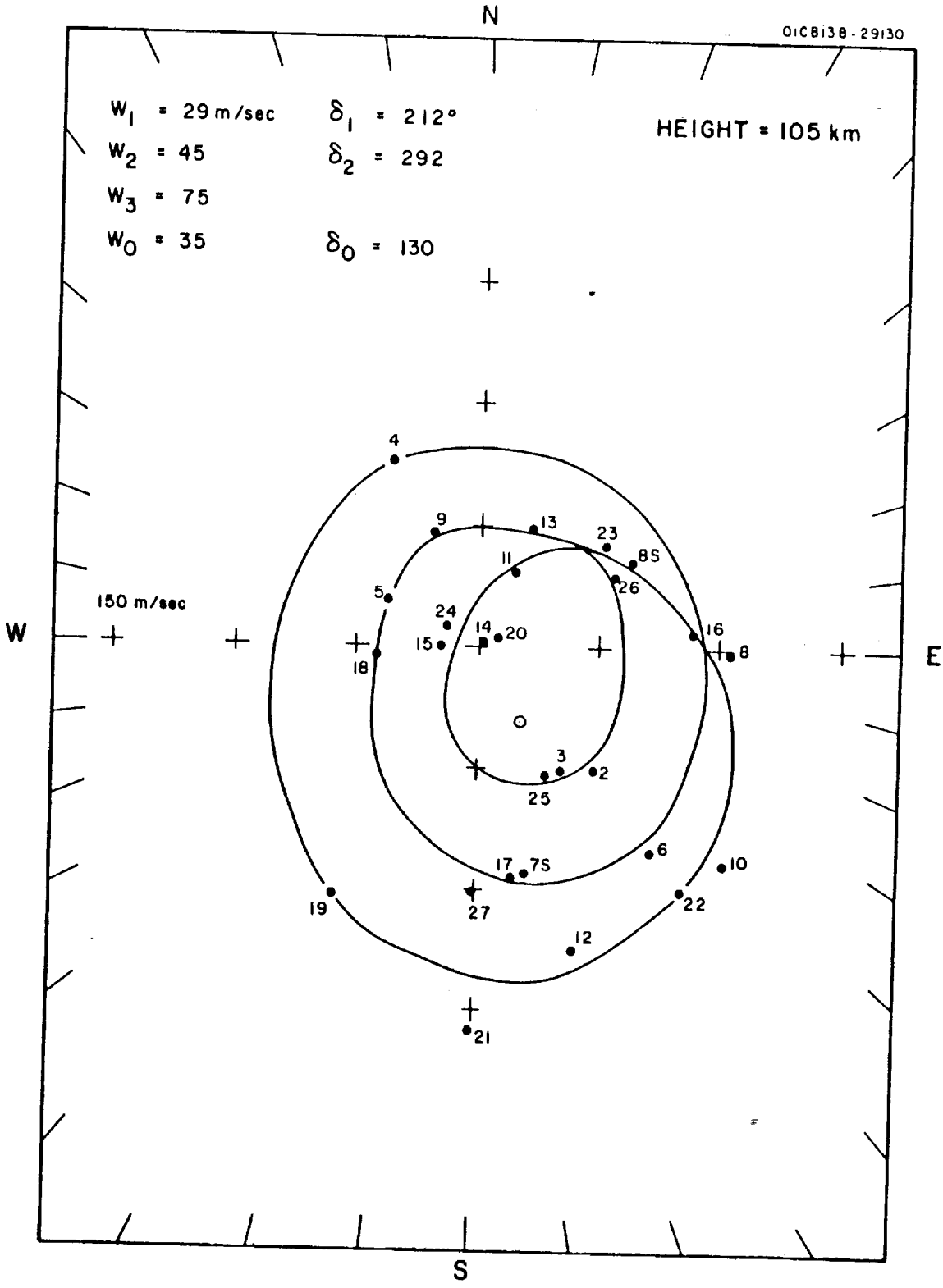

Figure 18. The pattern of wind structure as observed for a height of 105 km.

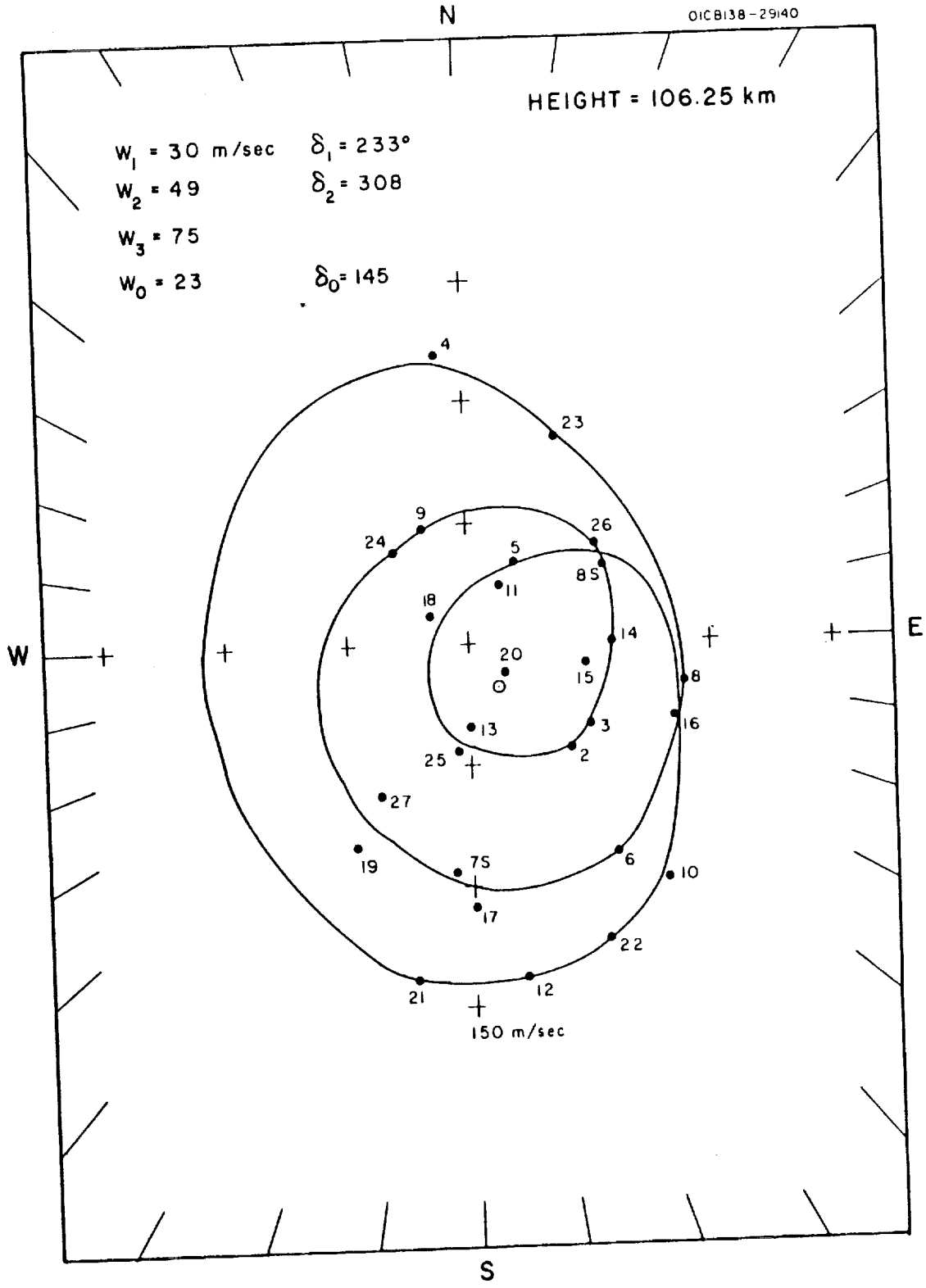

Figure 19. The pattern of wind structure as observed for a height of 106.25 km.

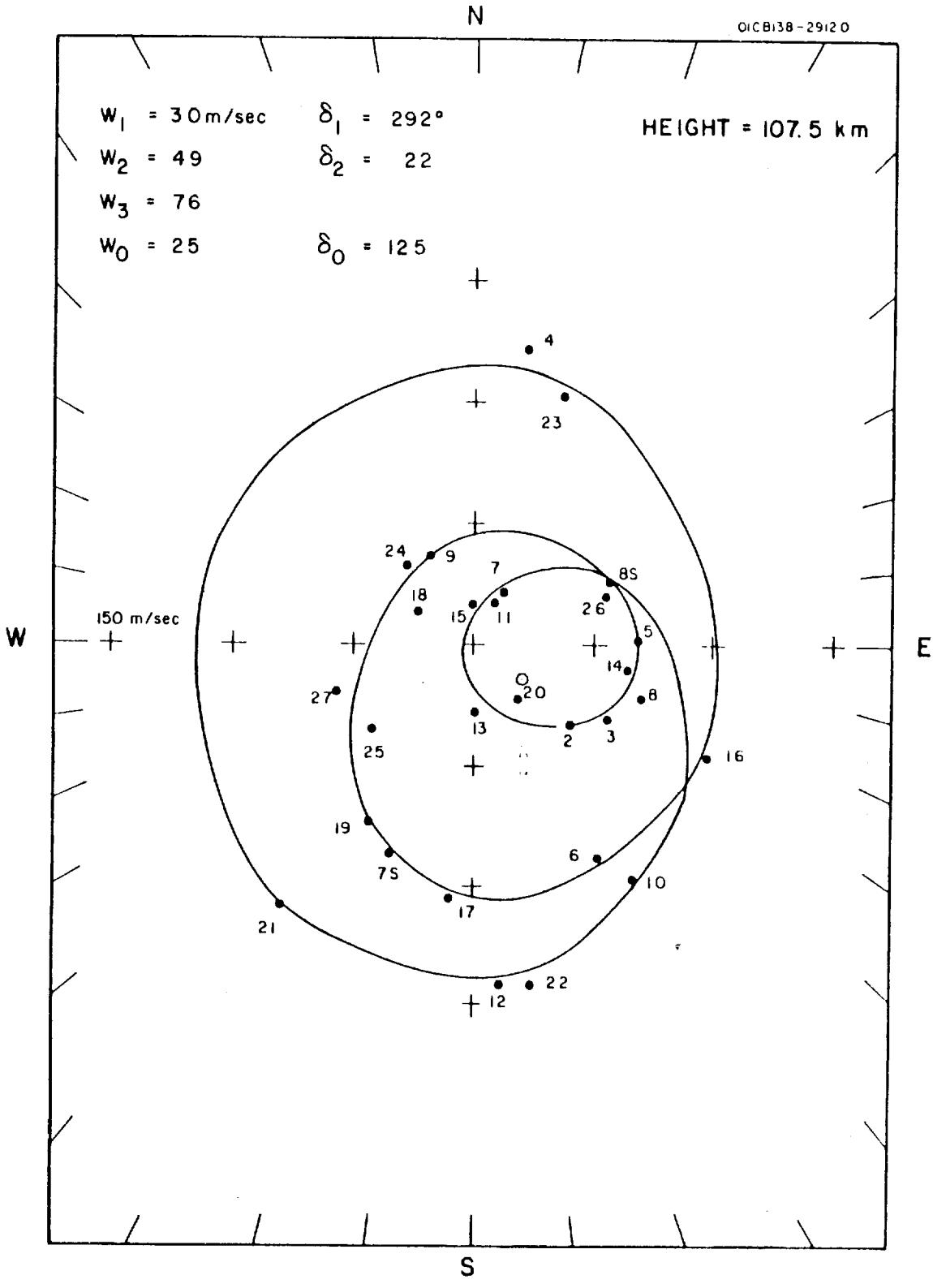

Figure 20. The pattern of wind structure as observed for a height of 107.5 km.

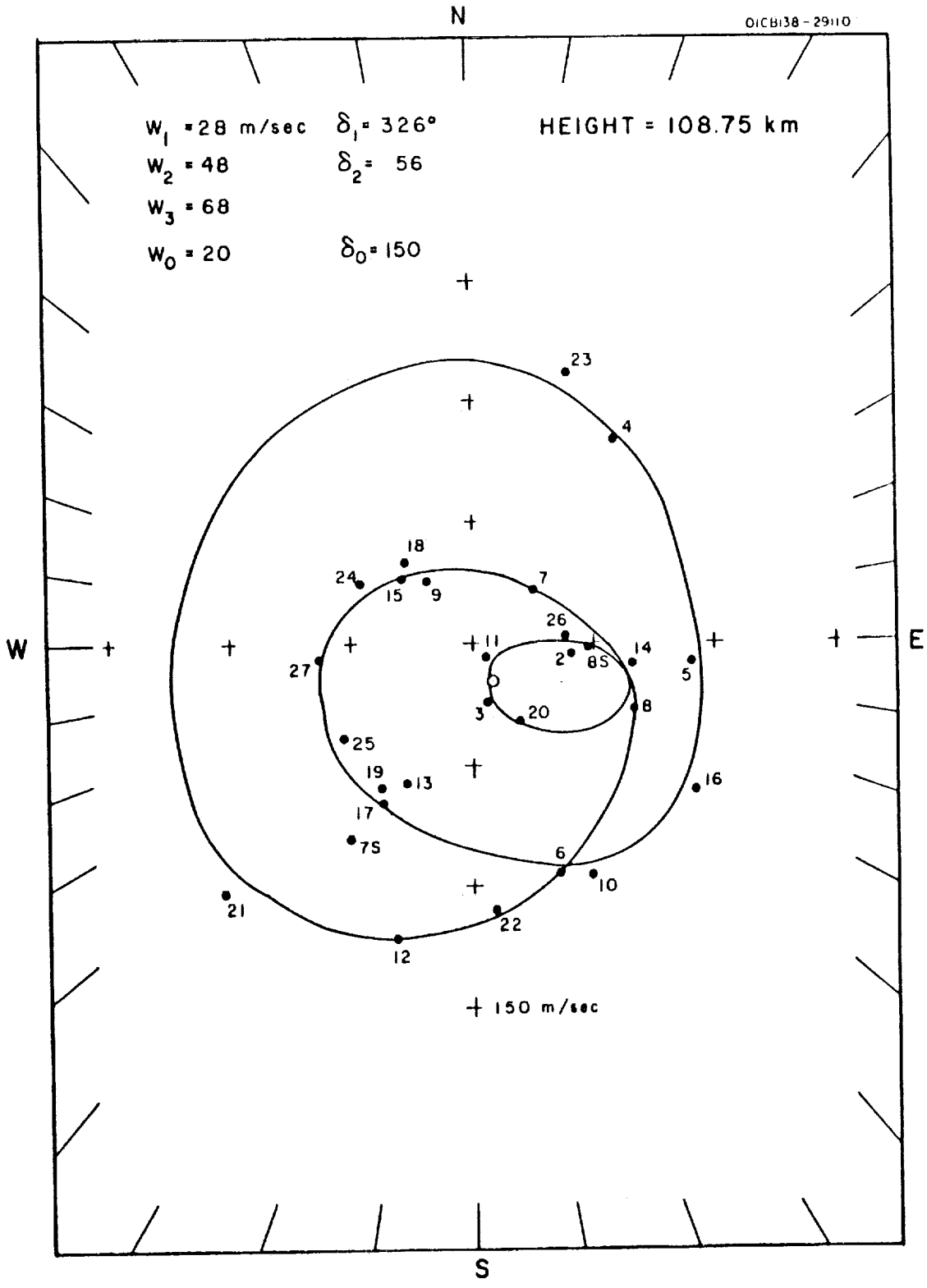

Figure 21. The pattern of wind structure as observed for a height of 108.75 km.

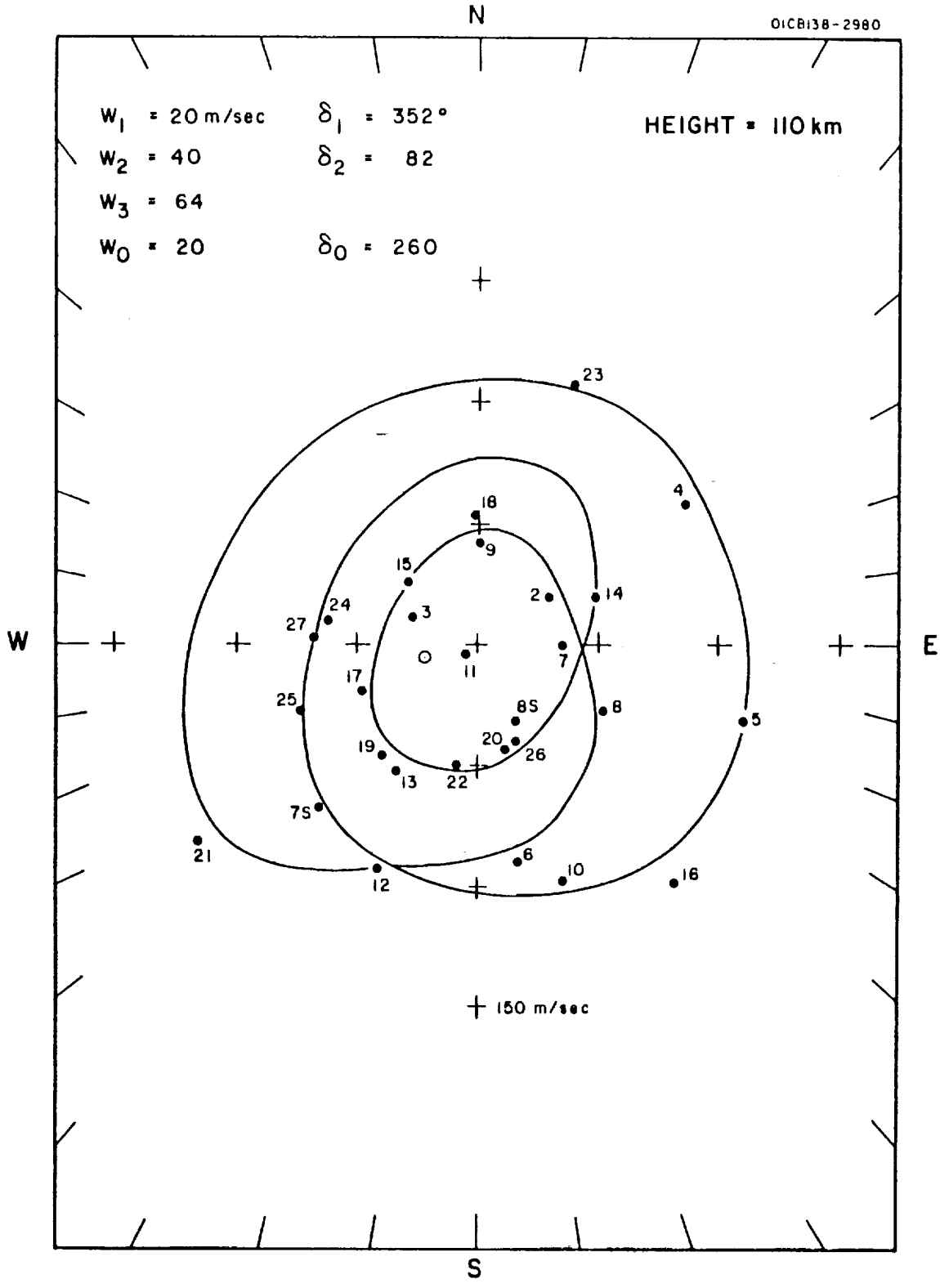

Figure 22. The pattern of wind structure as observed for a height of 110 km.

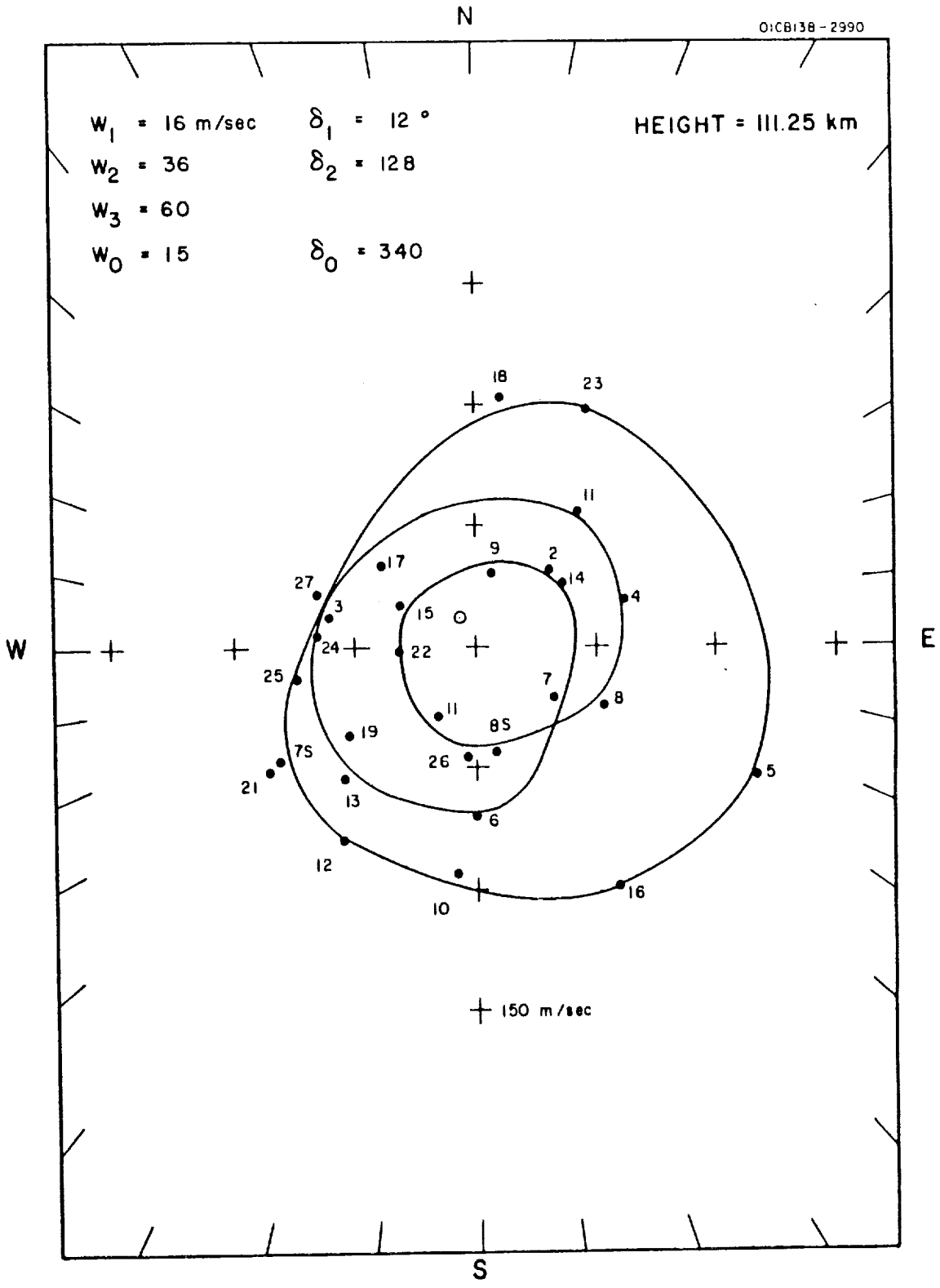

Figure 23. The pattern of wind structure as observed for a height of 111.25 km.

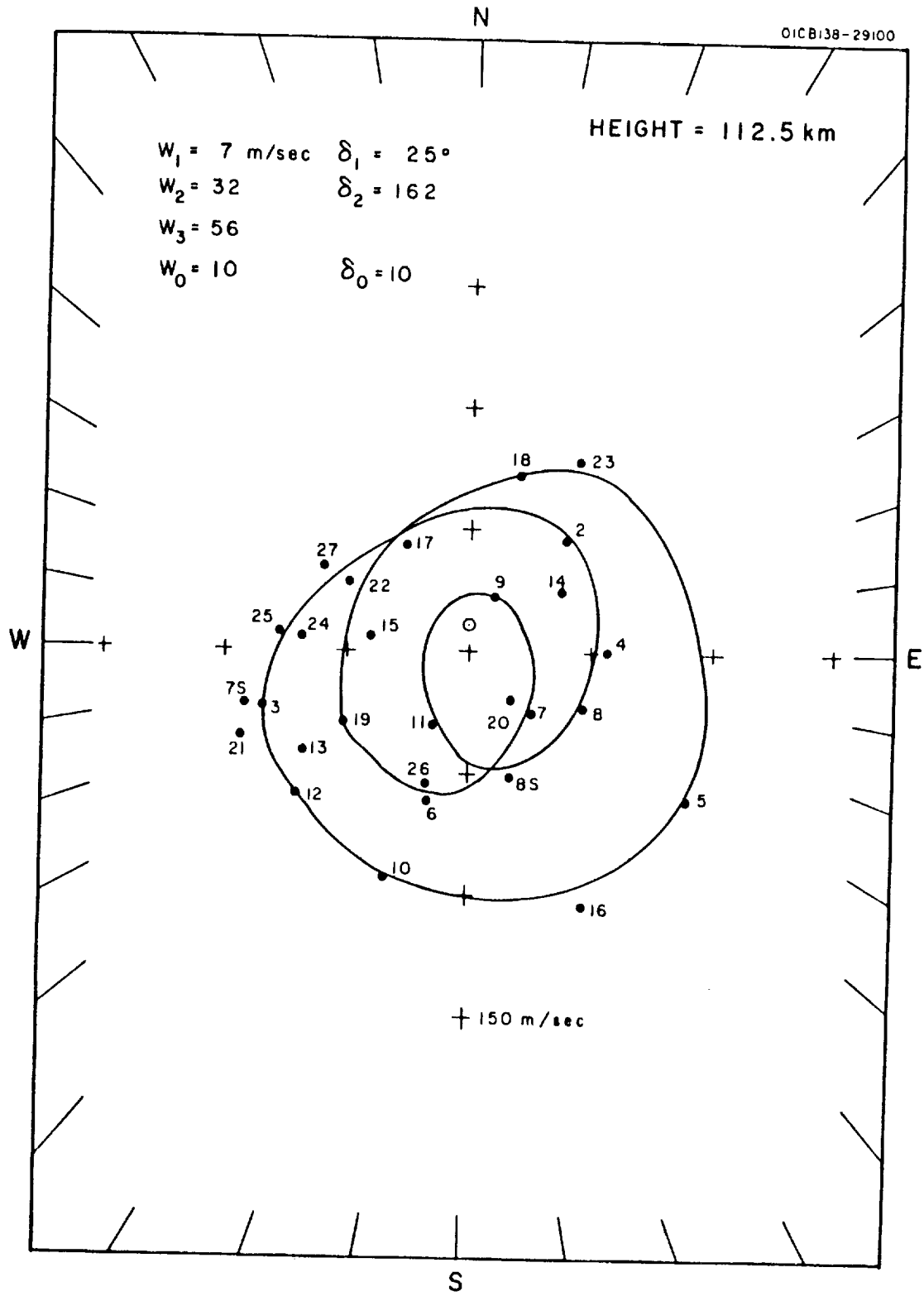

Figure 24. The pattern of wind structure as observed for a height of 112.5 km.

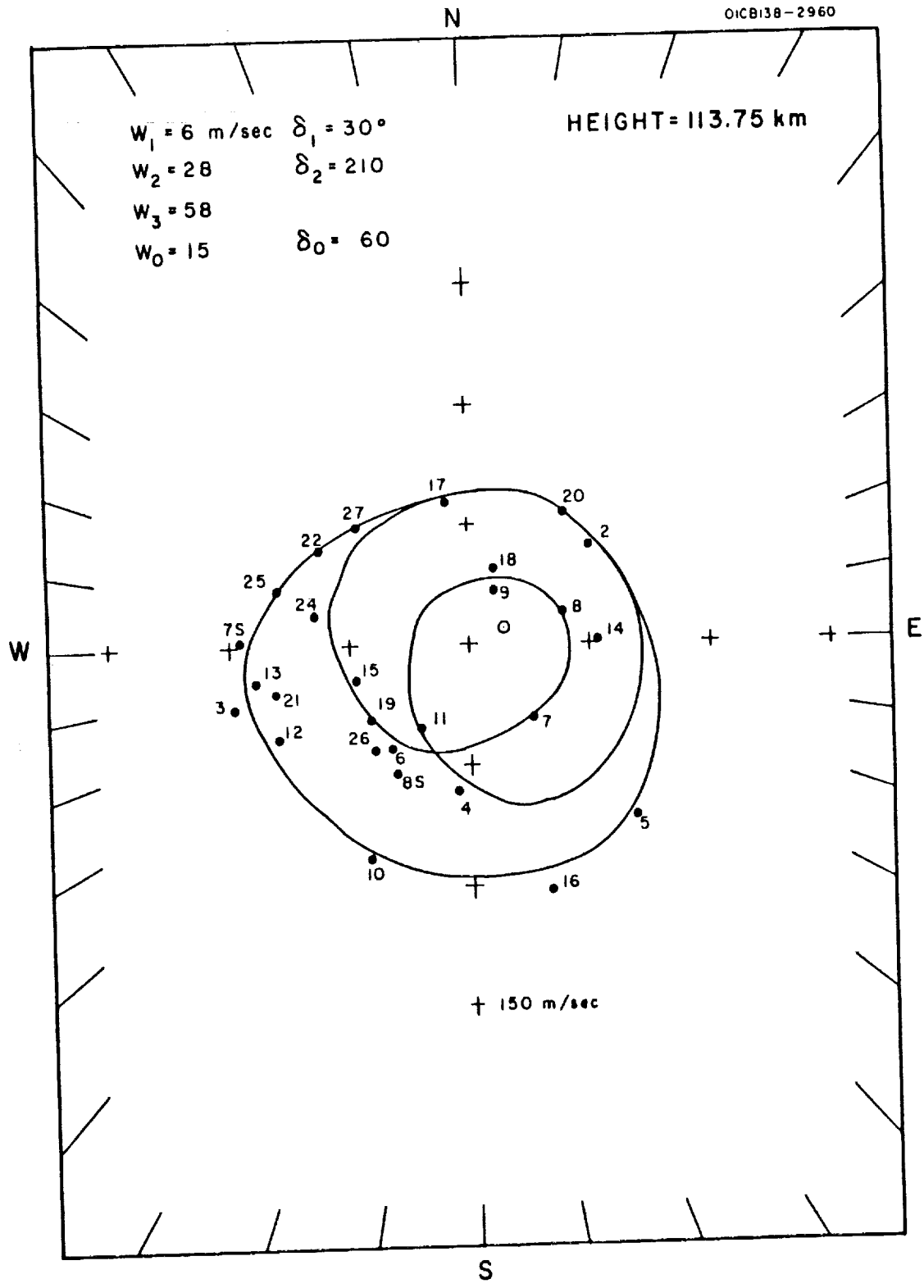

Figure 25. The pattern of wind structure as observed for a height of 113.75 km.

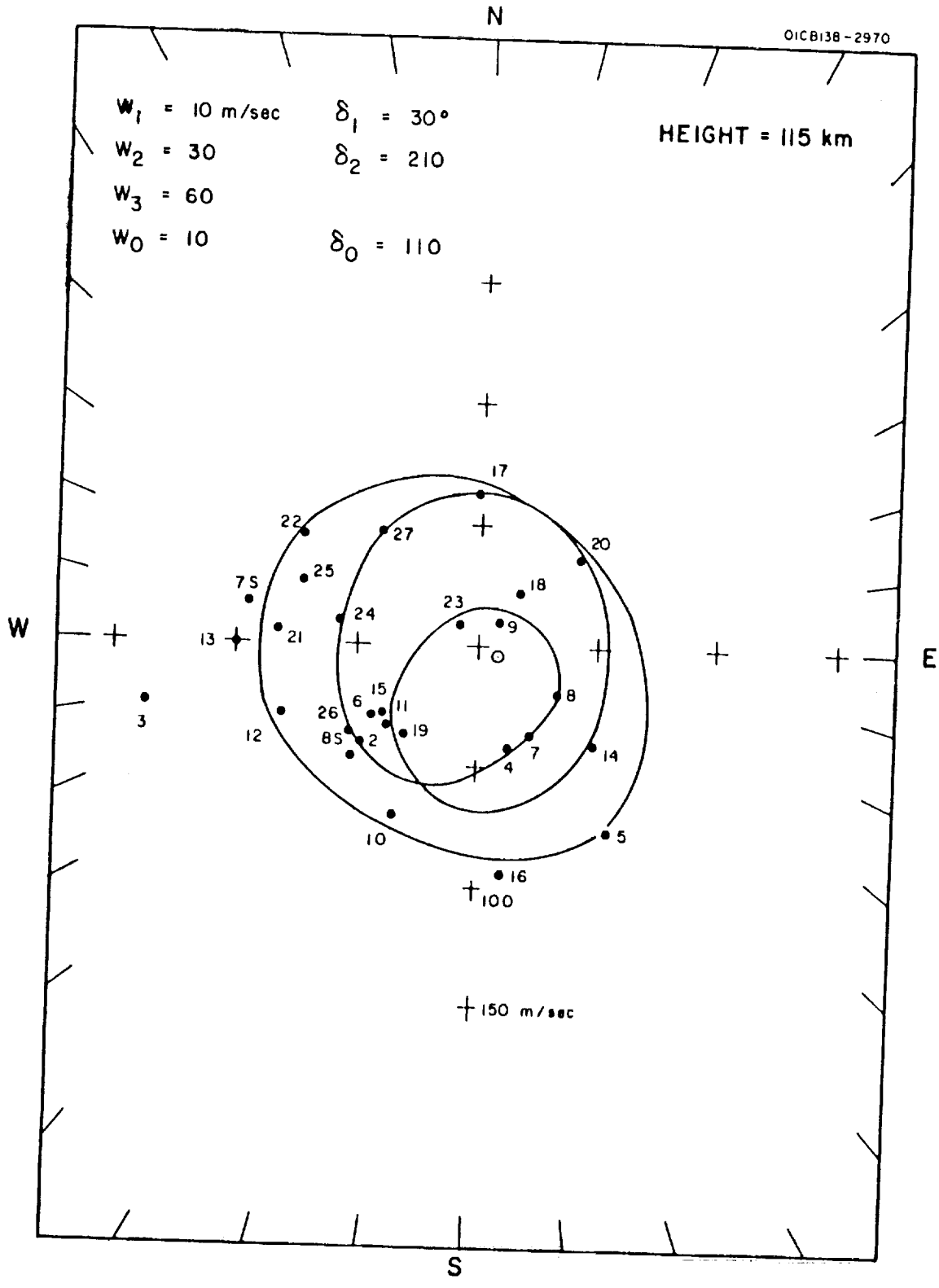

Figure 26. The pattern of wind structure as observed for a height of 115 km.

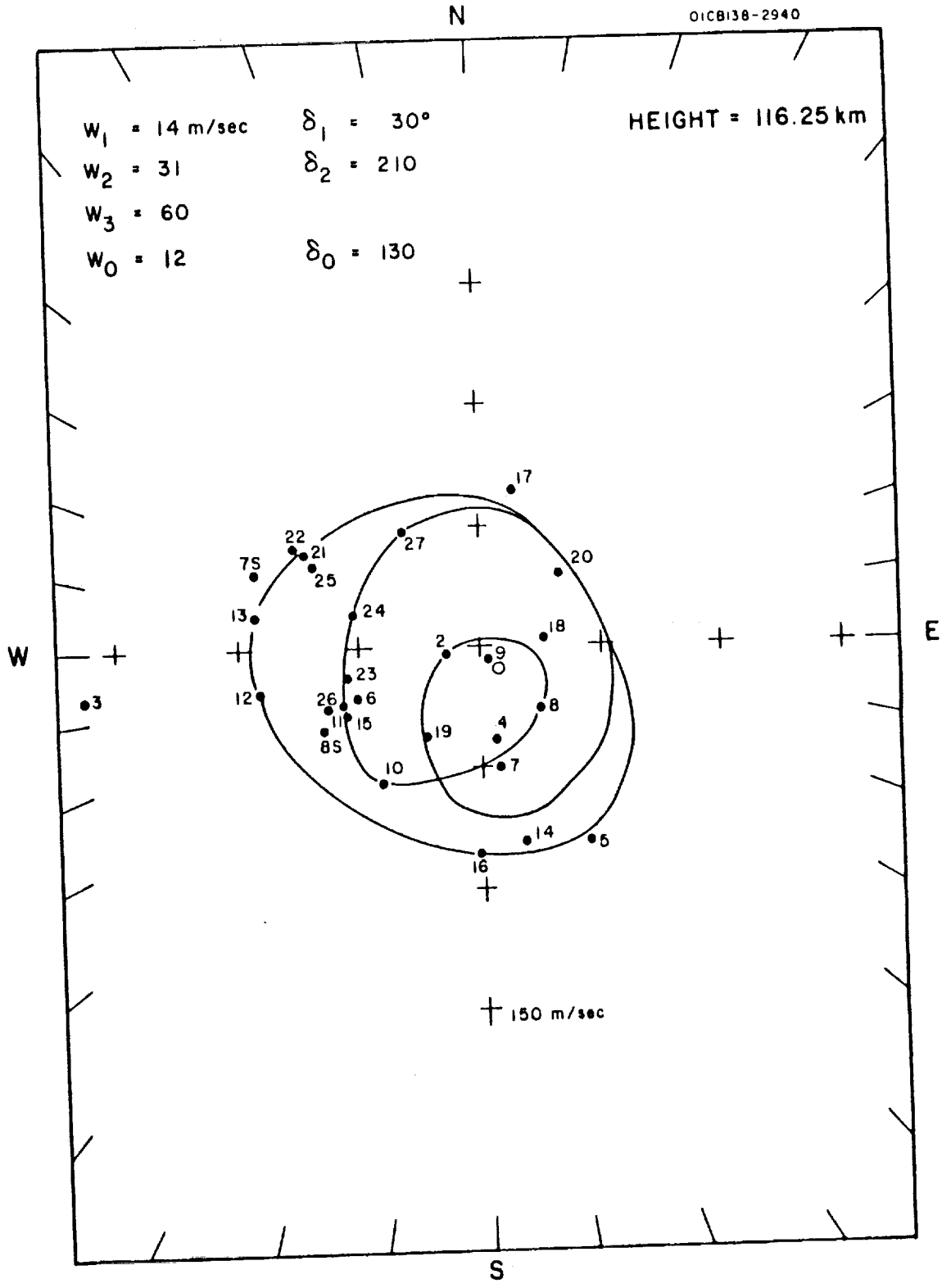

Figure 27. The pattern of wind structure as observed for a height of 116.25 km.

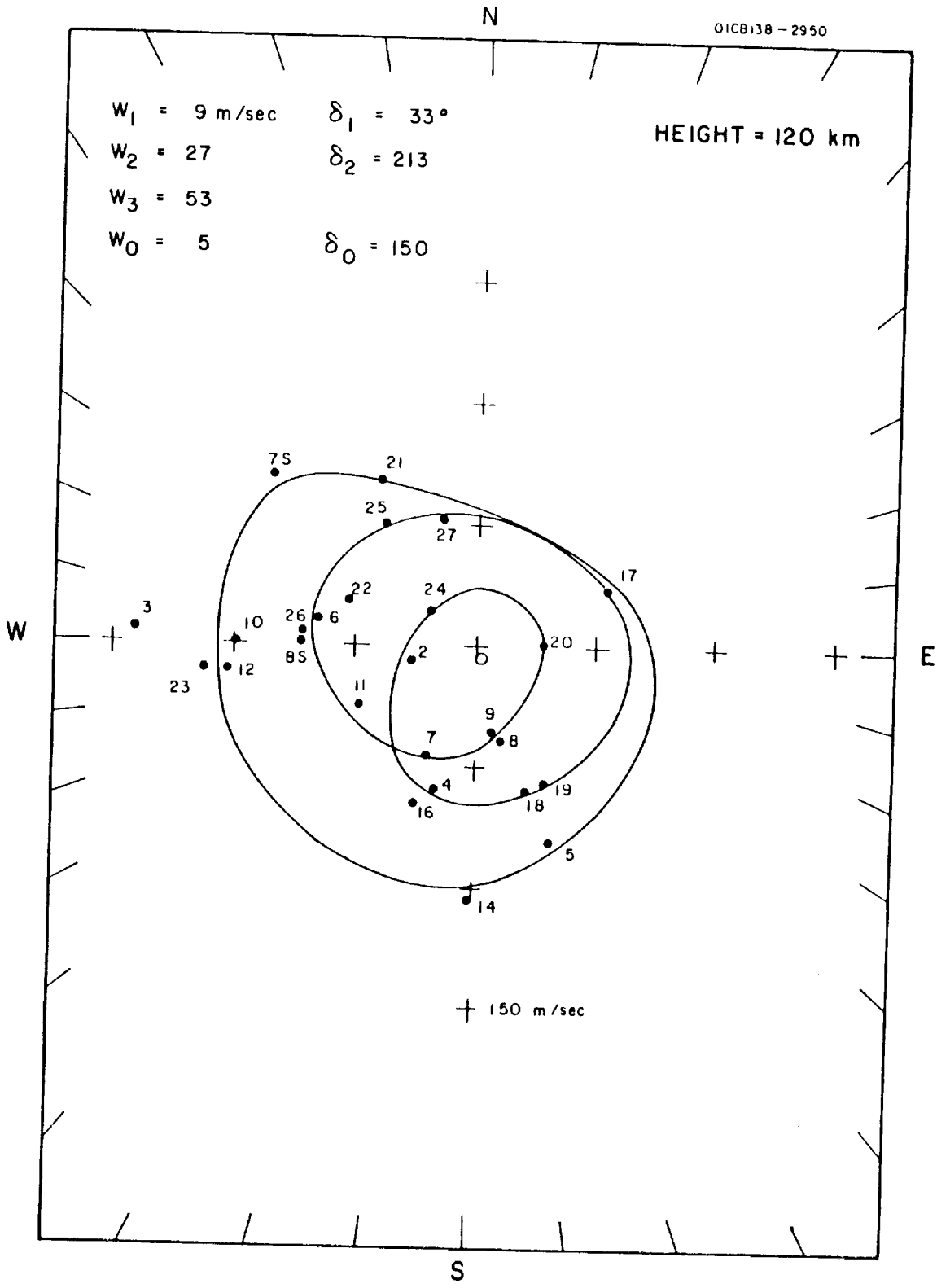

Figure 28. The pattern of wind structure as observed for a height of 120 km.

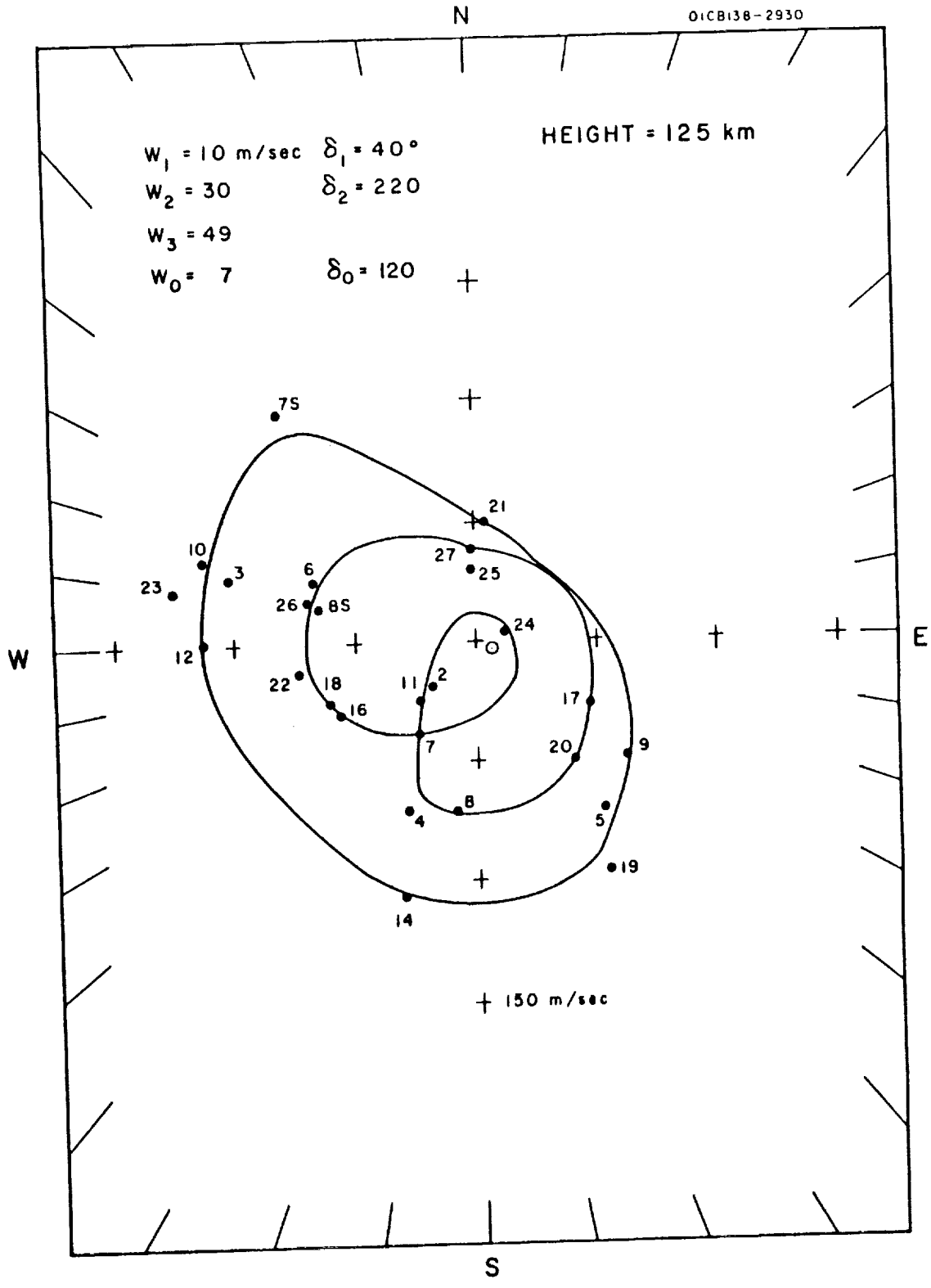

Figure 29. The pattern of wind structure as observed for a height of 125 km.

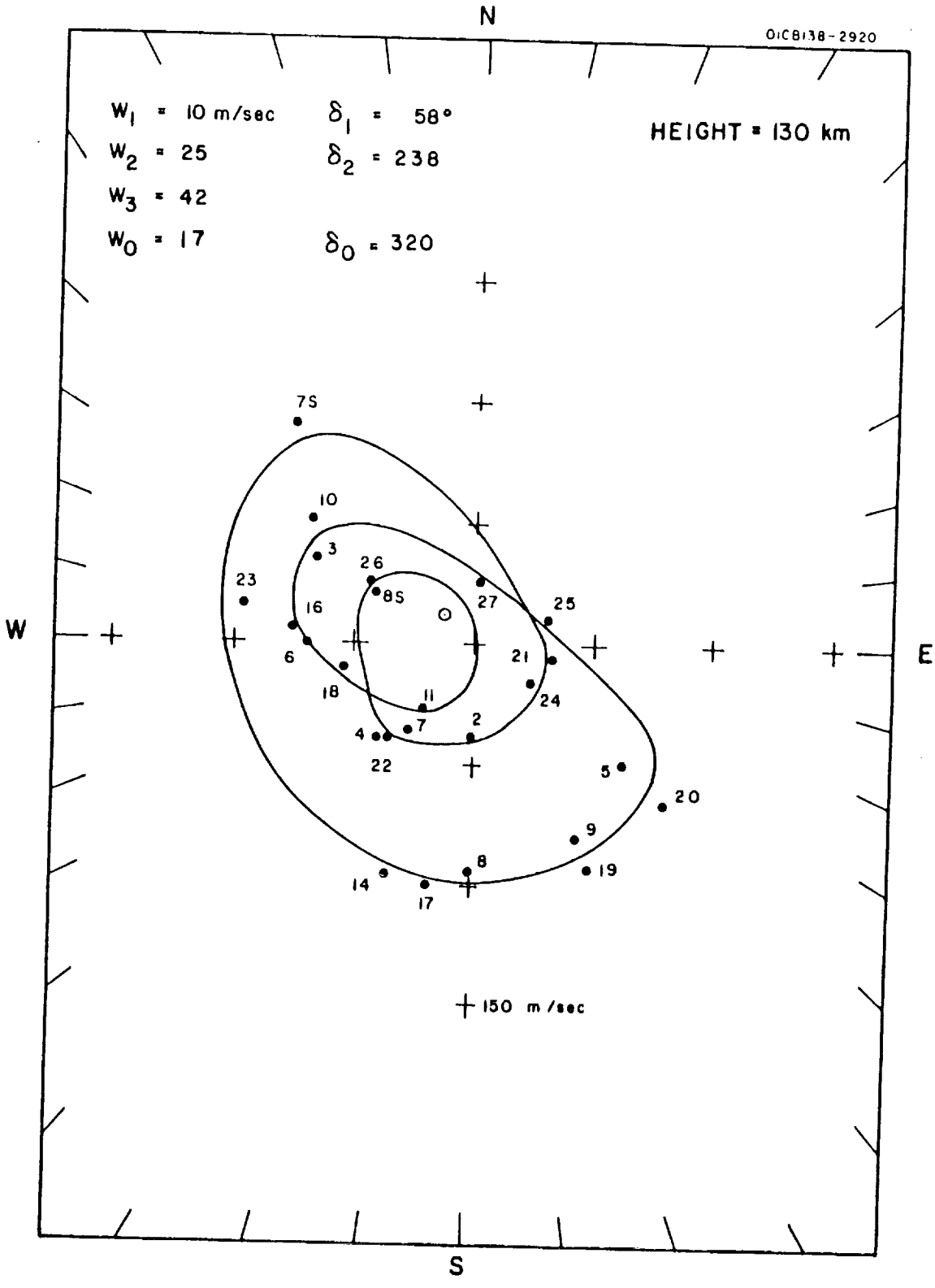

Figure 30. The pattern of wind structure as observed for a height of 130 km.

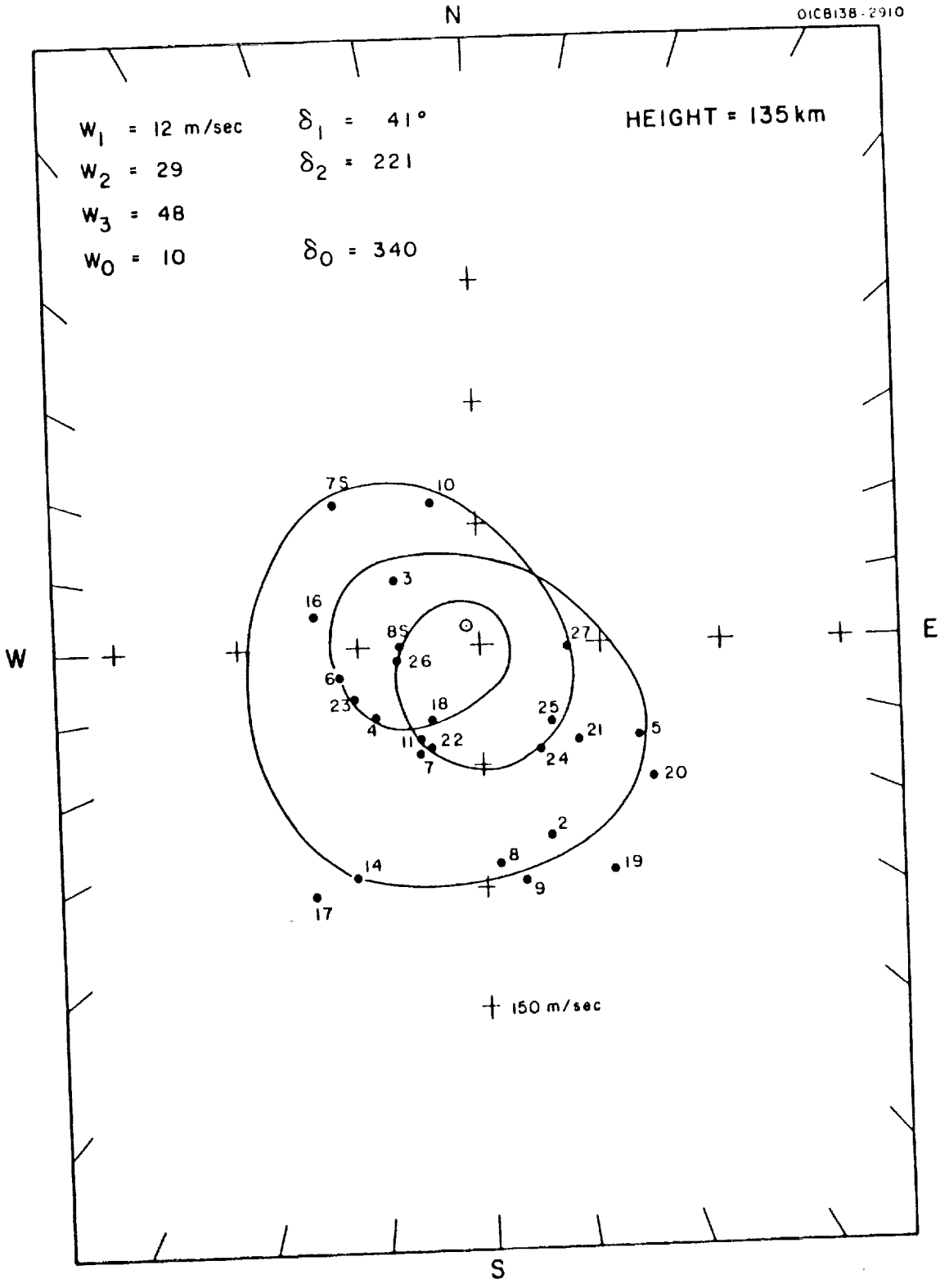

Figure 31. The pattern of wind structure as observed for a height of 135 km.

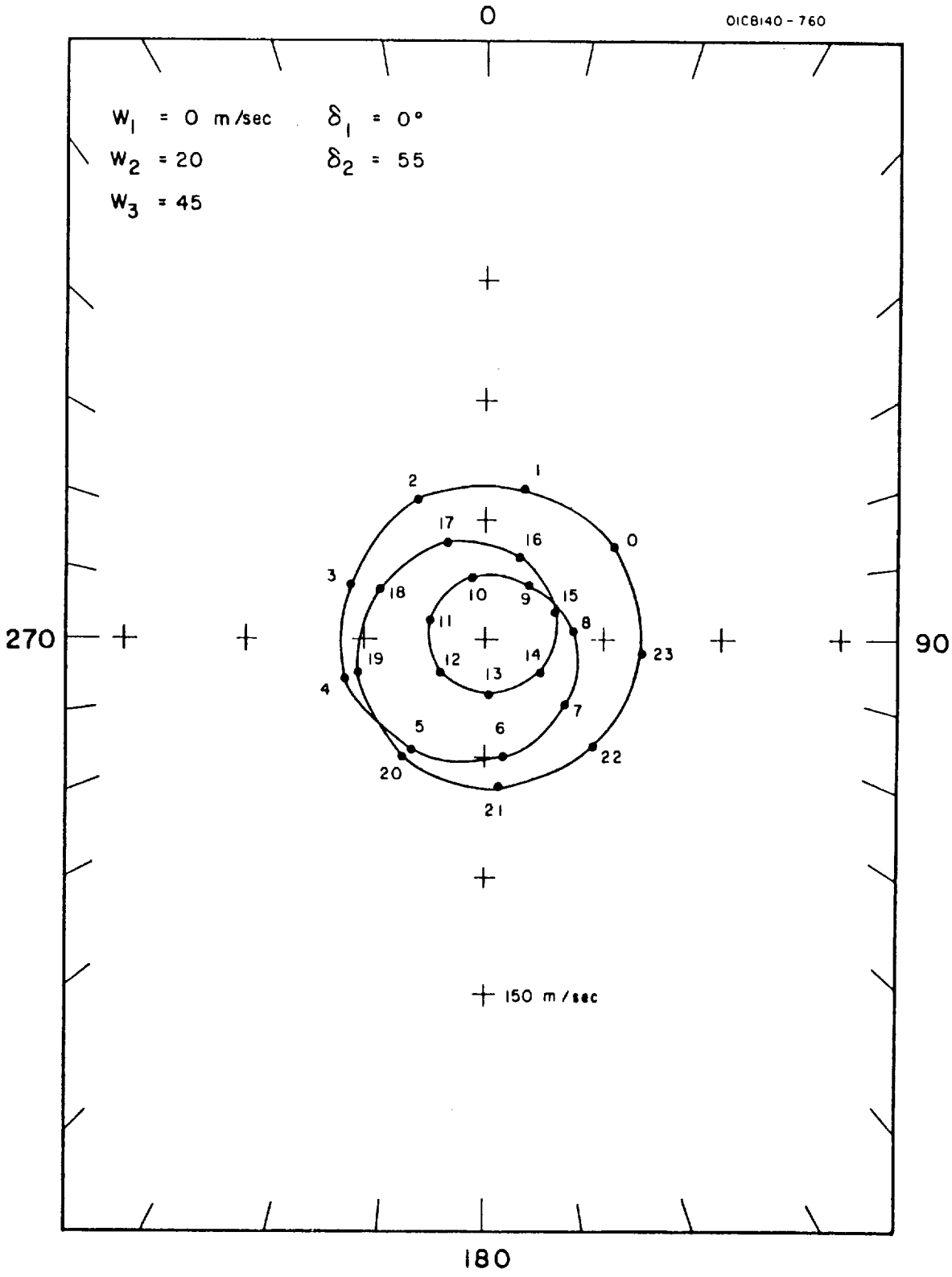

Figure 32. Theoretical figure drawn with $W_1 = 0$, $W_2 = 20$, and $W_3 = 45$ m/sec; $\delta_1 = 0$, $\delta_2 = 55^\circ$. The numbers indicate the local time in hours.

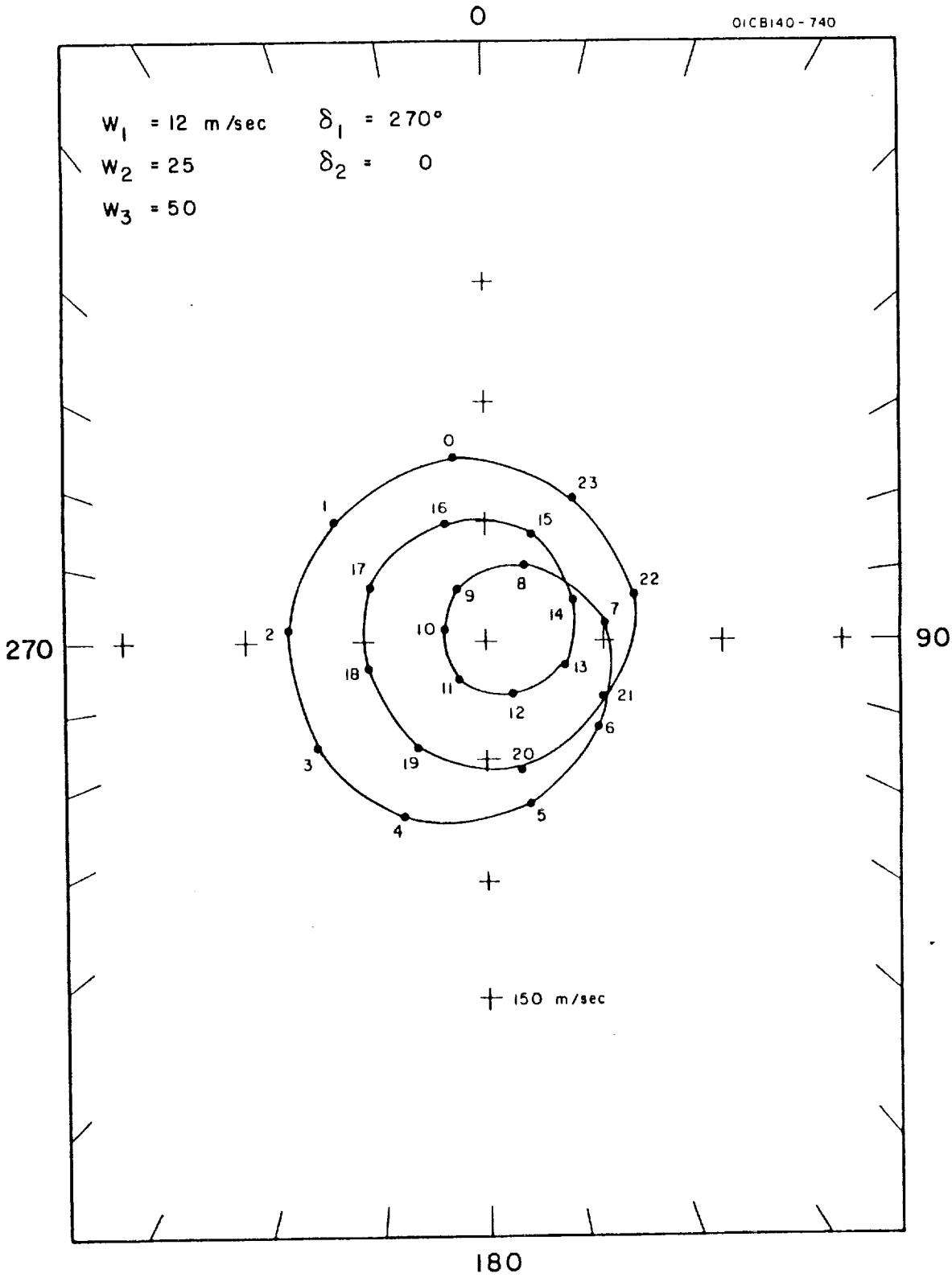

Figure 33. Theoretical figure drawn with $W_1 = 12$, $W_2 = 25$, and $W_3 = 50$ m/sec; $\delta_1 = 270^\circ$, $\delta_2 = 0$. The numbers indicate the local time in hours.

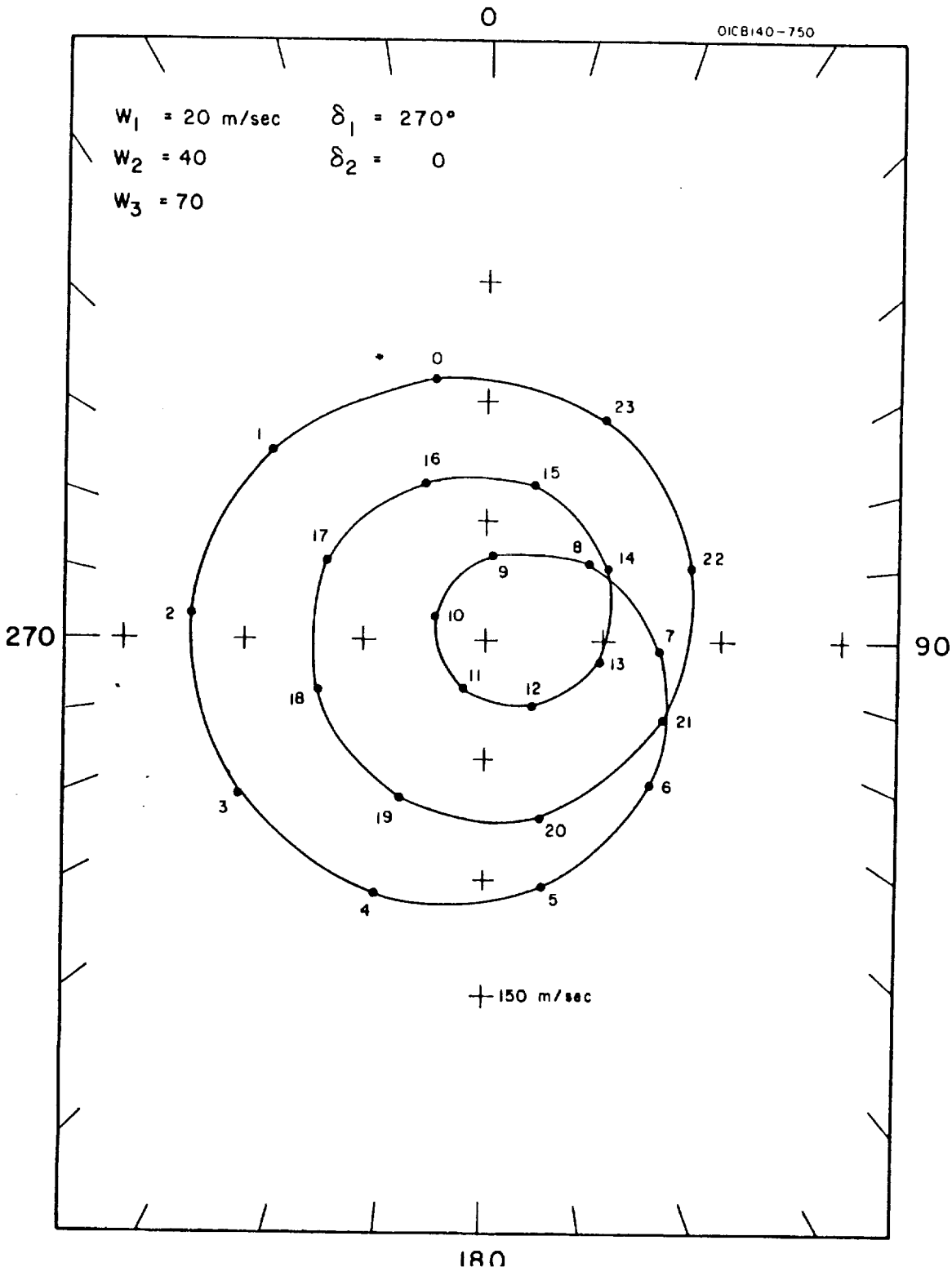

Figure 34. Theoretical figure drawn with W_1 = 20, W_2 = 40, and W_3= 70 m/sec; $\delta_1 = 270^{\circ}$, $\delta_2 = 0$.

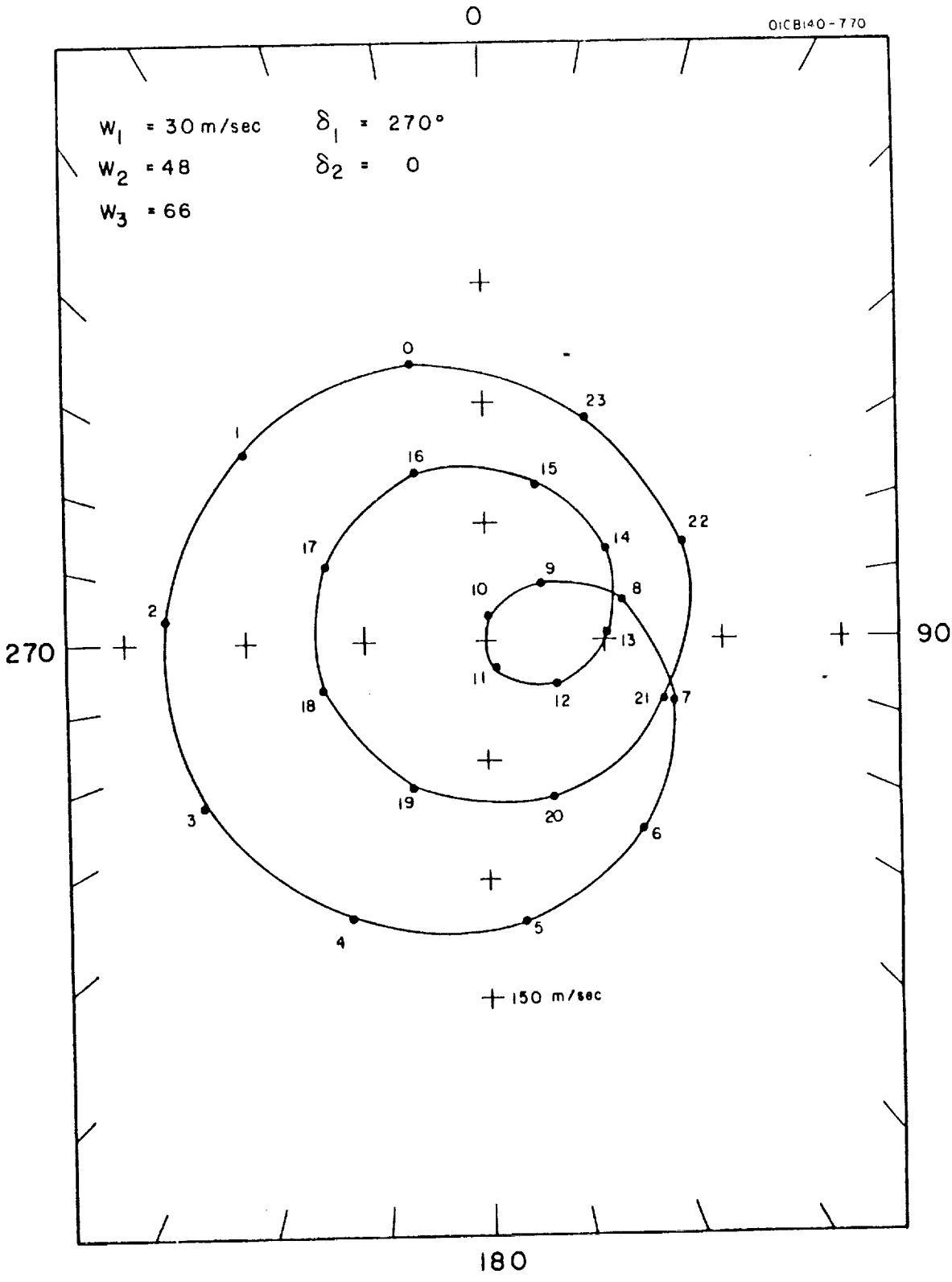

Figure 35. Theoretical figure drawn with W_1 = 30, W_2 = 48, and W_3 = 66 m/sec; $\delta_1 = 270^{\circ}$, $\delta_2 = 0$.

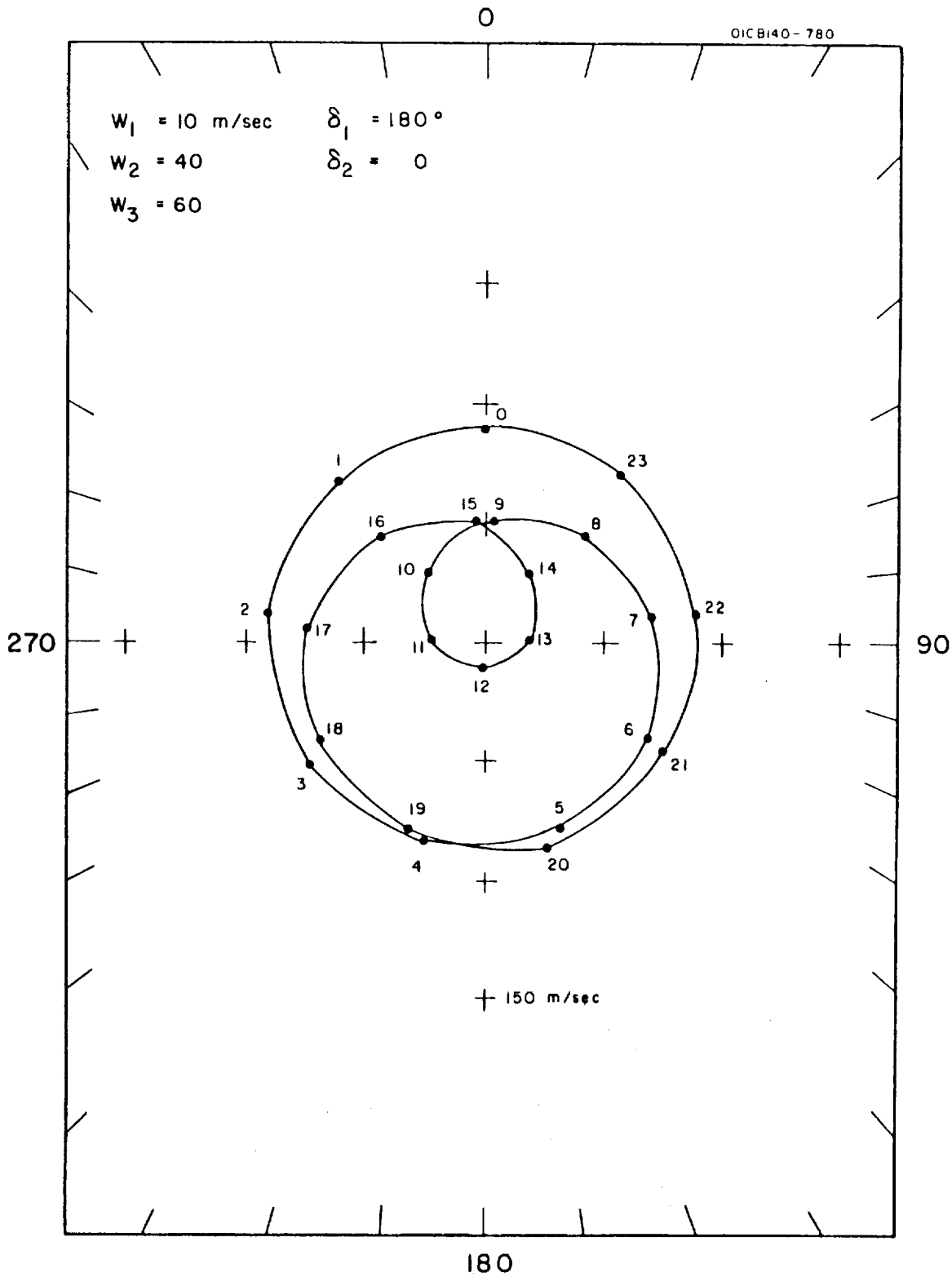

Figure 36. Theoretical figure drawn with W_1 = 10, W_2 = 40, and W_3 = 60 m/sec; $\delta_1 = 180^\circ$, $\delta_2 = 0$.

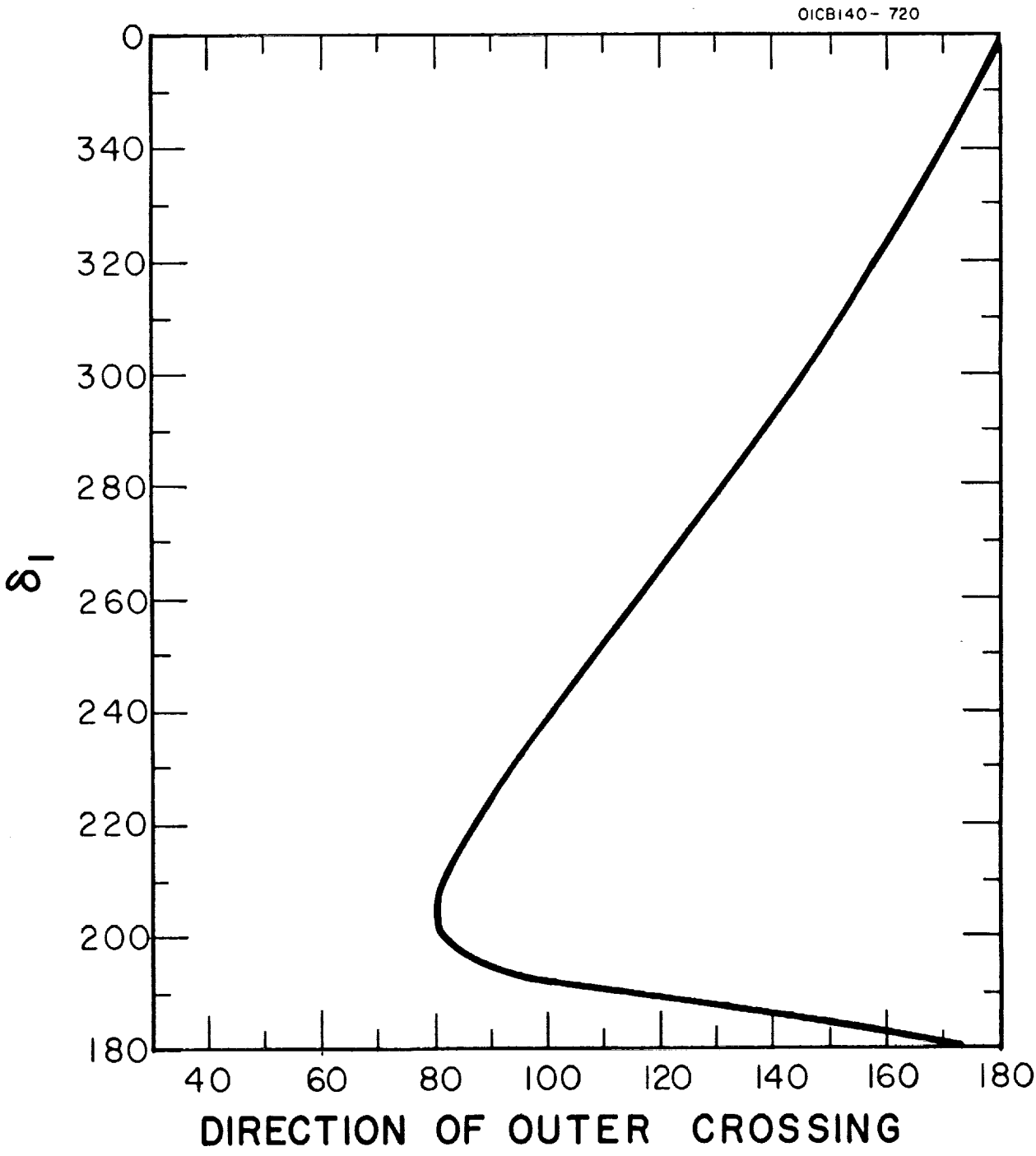

Figure 37. Direction of outer crossing mode as a function of δ_1 from theoretical figures similar to Figure 33.

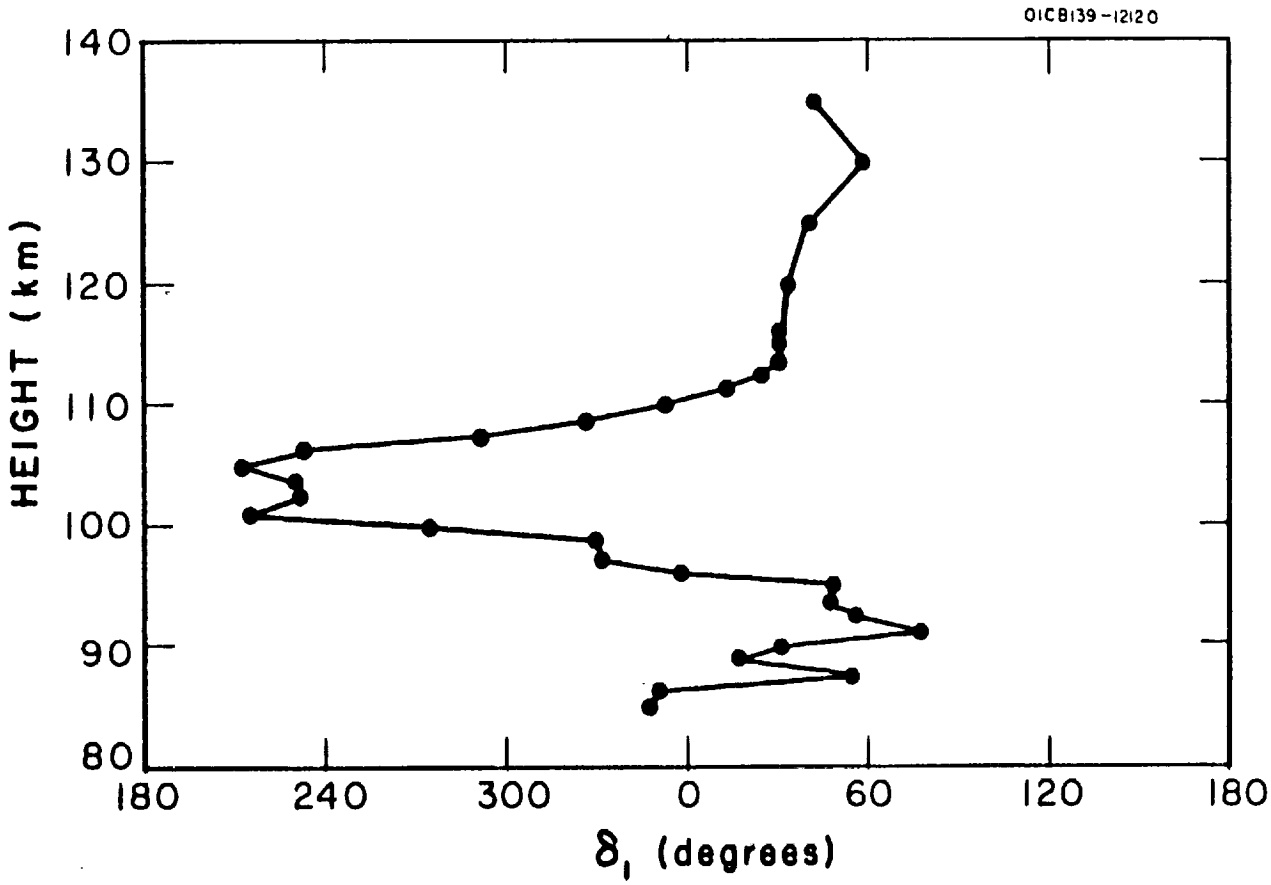

Figure 38. Observed values of δ_1 as a function of height.

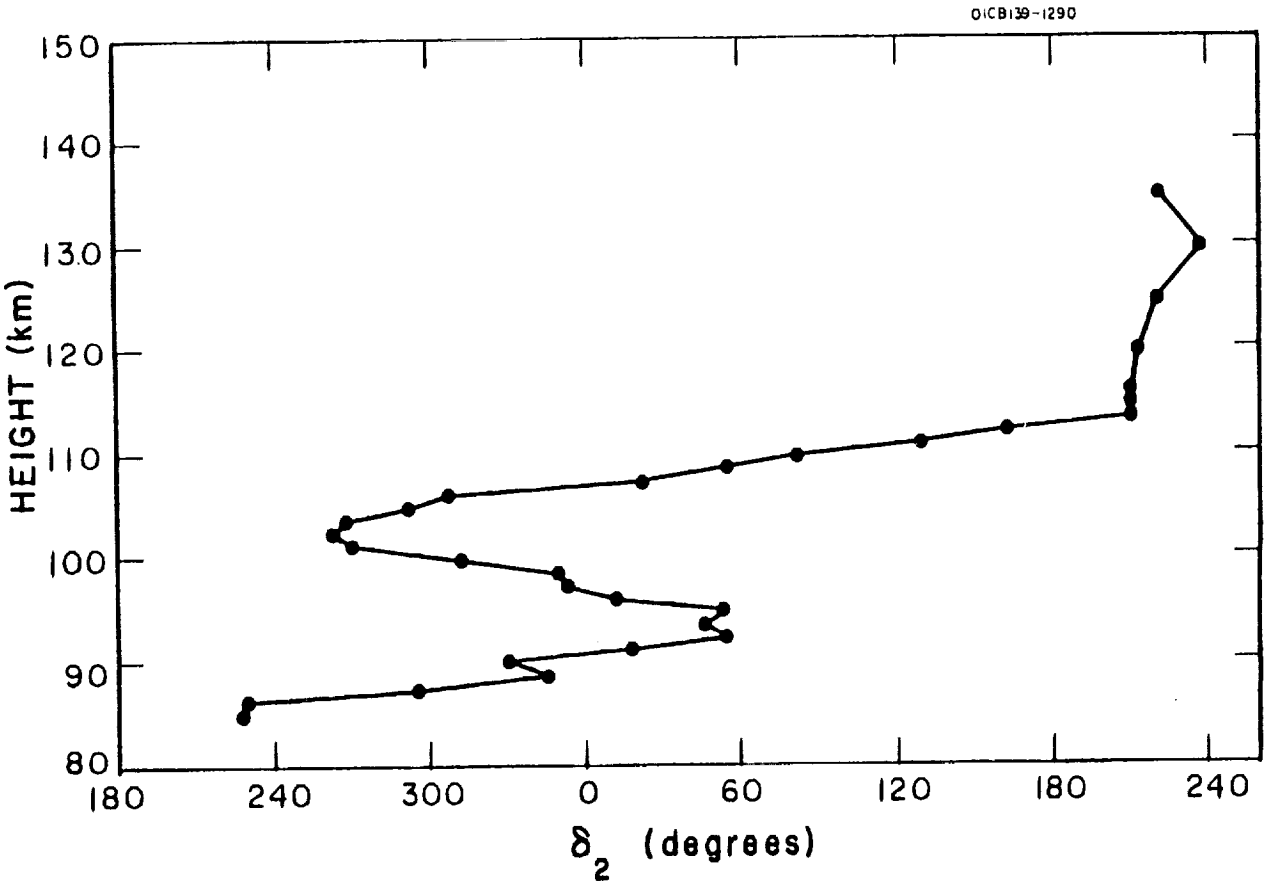

Figure 39. Observed values of δ_2 as a function of height.

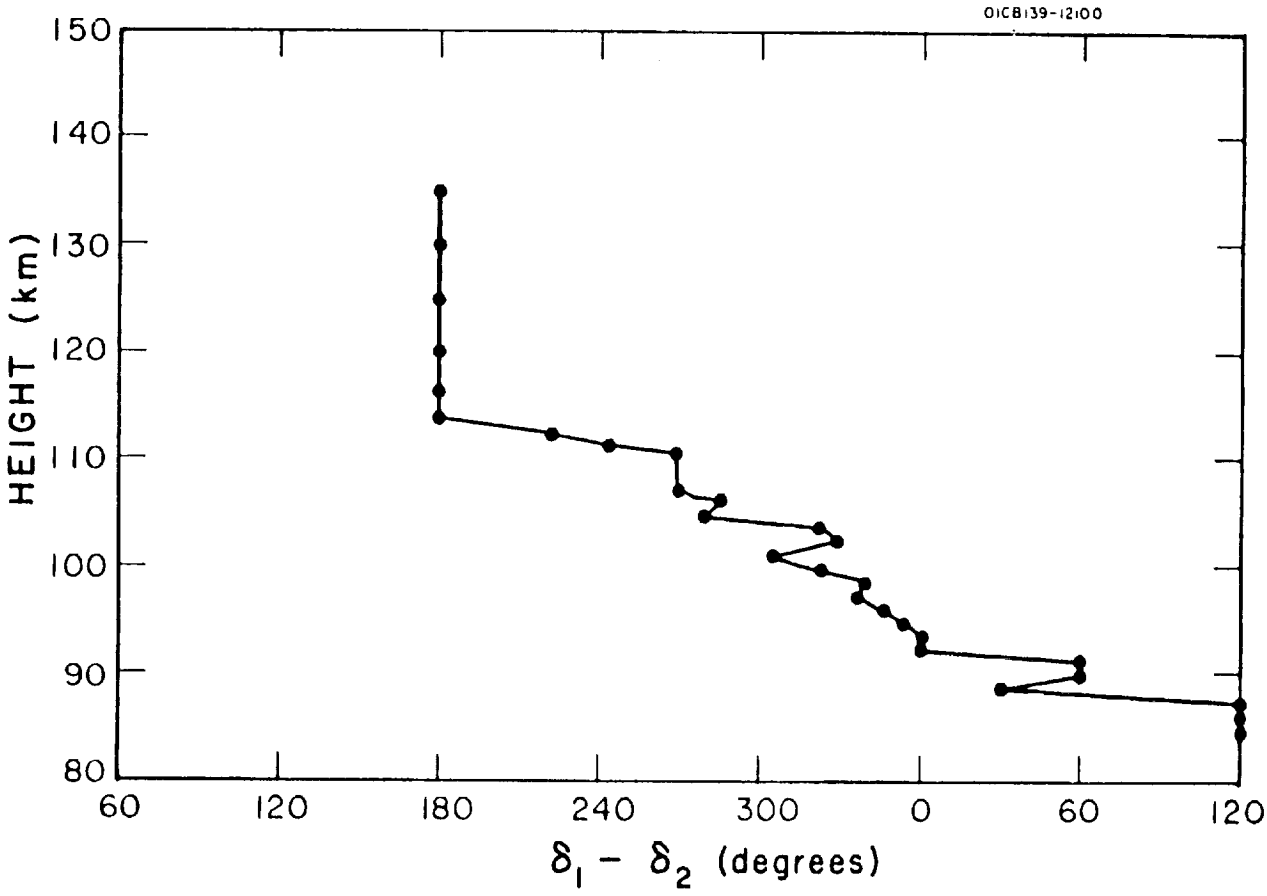

Figure 40. The difference between δ_1 and δ_2 as a function of height.

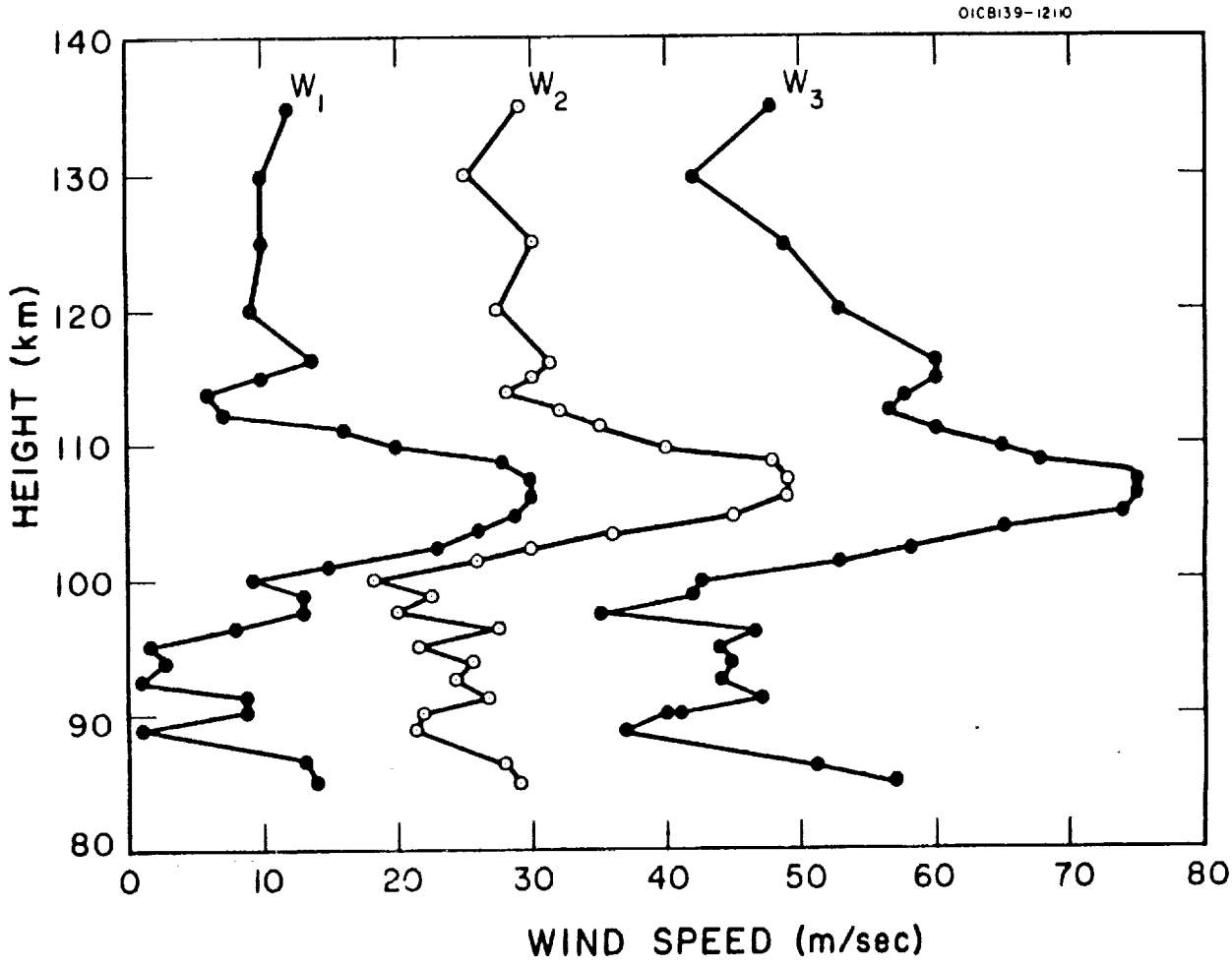

Figure 4 1. Observed values of W_1, W_2, and W_3 as a function of height.

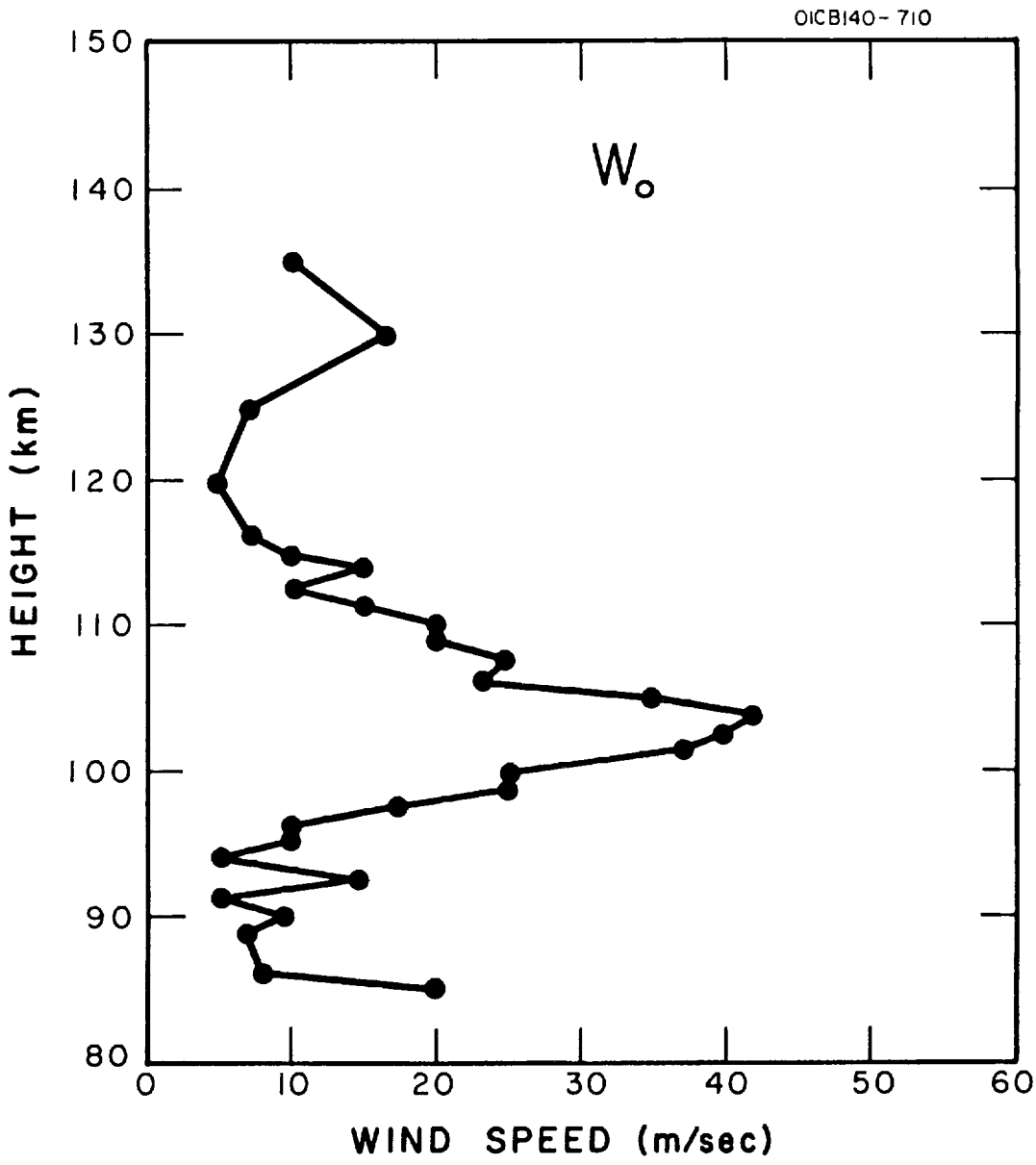

Figure 42. Observed values of W_o as a function of height.

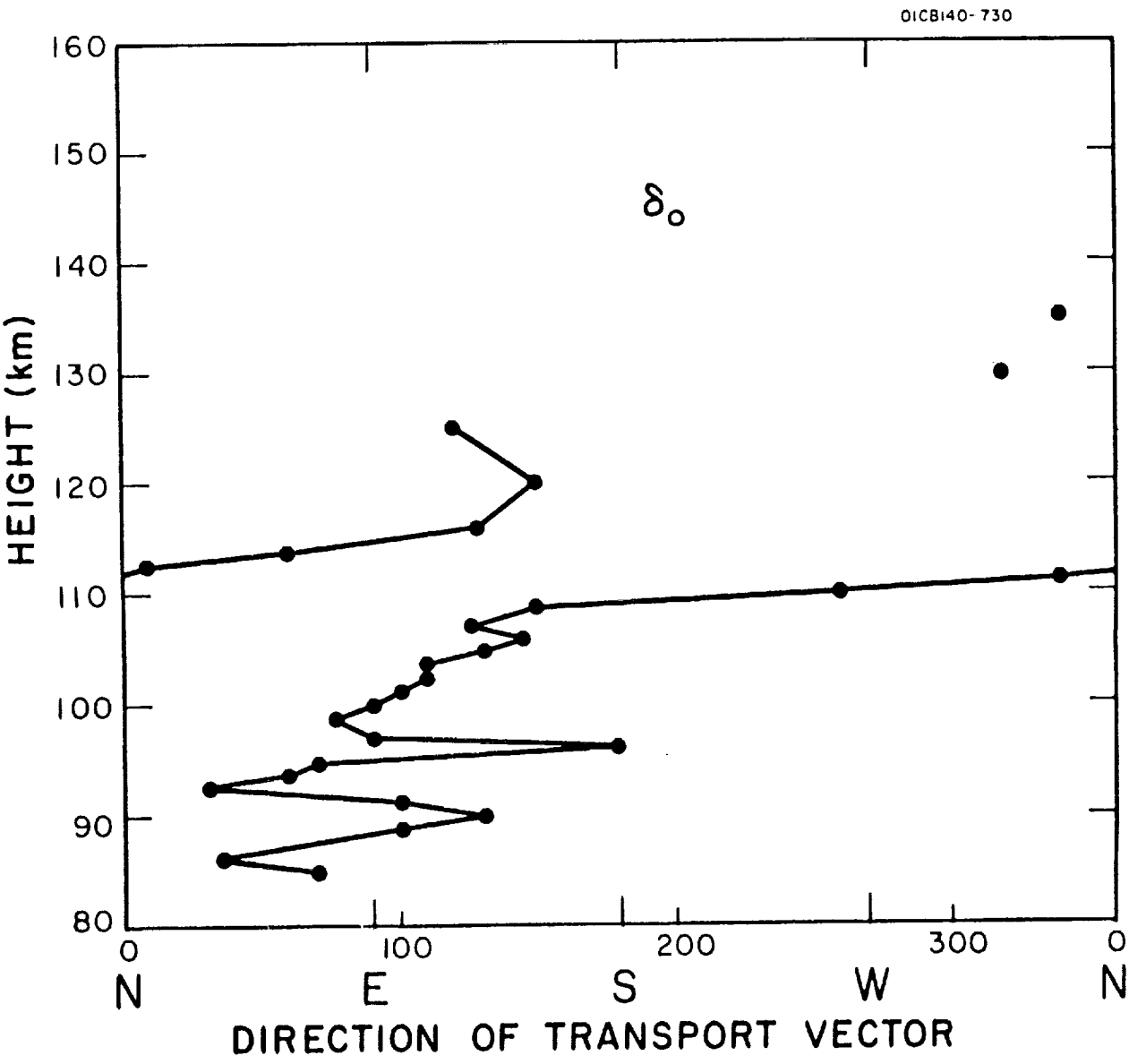

Figure 43. Observed values of δ_o as a function of height.

REFERENCES

1. Geophysics Corporation of America, Final report for the period February 11, 1959 to February 11, 1960, NASA Contract No. NASw-25 Task II, Bedford, Massachusetts (1960).

2. Manring, E., Bedinger, J., Knaflich, H. and Lynch, R., "Upper Atmospheric Wind Profiles Determined from Three Rocket Experiments," NASA Contract No. NAS5-215, Tech. Report 61-1-N, Geophysics Corporation of America, Bedford, Massachusetts (February 1961).

3. Jenkins, R. and Manring, E., "The Design, Construction and Operation of Groundbased Tracking Equipment for Experiments Utilizing Optical Trace Materials to Study Atmospheric Parameters," NASA Contract No. NAS5-215, Tech. Report 61-2-N, Geophysics Corporation of America, Bedford, Massachusetts (March 1961).

4. Levy, R. J. and Manring, E. R., "Photography of Luminous Extended Objects Against a Twilight Sky," NASA Contract No. NAS5-215, Tech. Report 61-4-N, Geophysics Corporation of America, Bedford, Massachusetts (March 1961).

5. Manring, E., Bedinger, J. and Knaflich, H., "Some Measurements of Winds and of the Coefficient of Diffusion in the Upper Atmosphere," Space Research II, Proceedings of the Second International Space Science Symposium Florence, April 10-14, 1961, p. 1107-1124, edited by H. C. van de Hulst, C. de Jager, and A. F. Moore, North-Holland Publishing Co., Amsterdam (1961).

6. Manring, E., Bedinger, J. and Knaflich, H., "Measurement of Winds in the Upper Atmosphere during April 1961," J. Geophys. Res. 67, 3923-3925 (1962).

7. Geophysics Corporation of America, "Study of Winds, Diffusion, and Expansion of Gases in the Upper Atmosphere," Final Report on Contract NAS5-215, NASA Contract No. NAS5-215, Tech. Report 62-13-N, Bedford, Massachusetts (October 1962).

8. Geophysics Corporation of America, "Study of Winds, Diffusion, and Expansion of Gases in the Upper Atmosphere," Final Report on Contract NASw-396, NASA Contract No. NASw-396, Tech. Report 62-16-N, Bedford, Massachusetts (May 1962).

9. Webb, W. L., Christensen, W. I., Varner, E. P. and Spurling, J. P., "Inter-Range Instrumentation Group Participation in the Meteorological Rocket Network," Bull. Am. Meteorol. Soc. 43, 640-649 (1962).

REFERENCES (Continued)

10. Greenhow, J. S. and Neufeld, E. L., "Winds in the Upper Atmosphere," Quart. J. Roy. Meteorol. Soc. 87, 472 (1961).

11. Elford, W. G., "A Study of Winds Between 80 and 100 km in Medium Latitudes," Planetary Space Sci. 1, 94 (1959).

12. Broglio, Luigi, "La seconda fase del programma italiano di ricerca mediante razzi sonda," Scoula D'Ingegneria Aeronautica, Via Eudossiana 18, Rome (1961).

13. Broglio, Luigi, "The Italian Fifth Cycle of Experiments by Sounding Rockets Using Sodium Cloud Technique," Italian Committee for Space Research, National Council of Research (1963).

14. Nordberg, W. and Smith, W., "Preliminary Measurements of Temperatures and Winds Above 50 km over Wallops Island, Virginia," NASA, Tech. Note, D-1694 (1963).

15. Smith, J. W., "Cape Canaveral Wind Summary Surface to 84 km," NASA, MTP-AERO-62-3, Marshall Space Flight Center, Huntsville, Alabama (January 17, 1962).

16. Kiss, E., "Annotated Bibliography of Rocket Meteorology," Meteorological and Geoastrophysical Abstracts 11, 1480-1535 (1960).

17. Murgatroyd, R. J., "Winds and Temperature Between 20-100 km," Quart. J. Roy. Meteorol. Soc. 83, 417-458 (1957).

18. Batten, E. S., "A Model of the Annual Temperature Variations at 30°N between 30 and 60 km," RM-3564-PR, The Rand Corporation, Santa Monica, California (1963).

19. Finger, F. G., Teweles, S. and Mason, R. B., "Synoptic Analysis Based on Meteorological Rocketsonde Data," J. Geophys. Res. 68, 1377-1399 (1963).

20. Greenhow, J. S. and Lovell, A. C. B., "The Upper Atmosphere and Meteors," Physics of the Upper Atmosphere, p. 513-549, edited by J. A. Ratcliffe, Academic Press, New York (1960).

21. Liller, W. and Whipple, F. L., "High-Altitude Winds by Meteor-train Photography," Special Supplement to J. Atmospheric and Terrest. Phys. 1, 112-130 (1954).

22. Hines, C. O., "Internal Atmospheric Gravity Waves at Ionospheric Heights," Canad. J. Phys. 38, 1441 (1960).

REFERENCES (Continued)

23. Siebert, M., "Atmospheric Tides," Advances in Geophysics 7, 105-187, Academic Press, New York (1961).

24. Butler, S. T. and Small, K. A., "The Excitation of Atmospheric Oscillations," Proc. Roy. Soc. A 274, 91-121 (1963).

25. Edwards, H. D., Cooksey, M. M., Justus, C. G., Fuller, R. N., Albritton, D. L. and Rosenberg, N. W., "Upper-Atmosphere Wind Measurements Determined from 12 Rocket Experiments," J. Geophys. Res. 68, 3021-3032 (1963).

26. Rosenberg, N. W., Edwards, H. D. and Wright, J. W., "Ionospheric Winds: Motions into Night and Sporadic E Correlations," to be published in Space Research IV, North-Holland Publishing Co., Amsterdam.

27. Edwards, H. D., Justus, C. G. and Kurts, D. C., "Upper Atmosphere Winds for Evening Twilight," submitted to J. Geophys. Res. for publication.

APPENDIX A

Wind measurements from 22 sodium vapor trails over Wallops Island are included. A plot of both wind speed and direction of trail transport is given as a function of altitude for each trail. The time, date and altitude range is shown on each plot. The figure numbers correspond to flight numbers in Table 2 of this report.

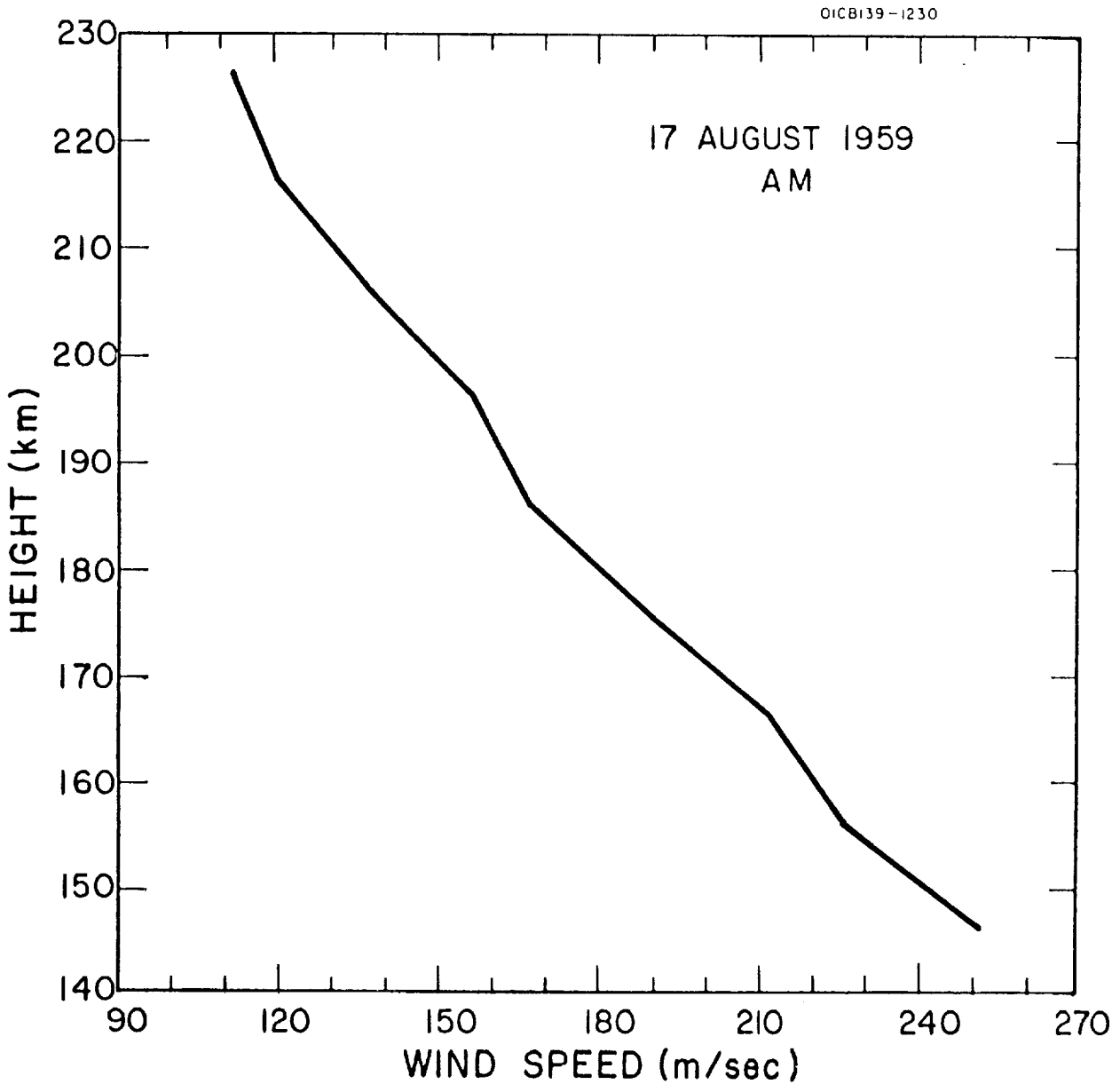

Figure A.1a. Wind speed as a function of height for morning twilight of 17 August 1959.

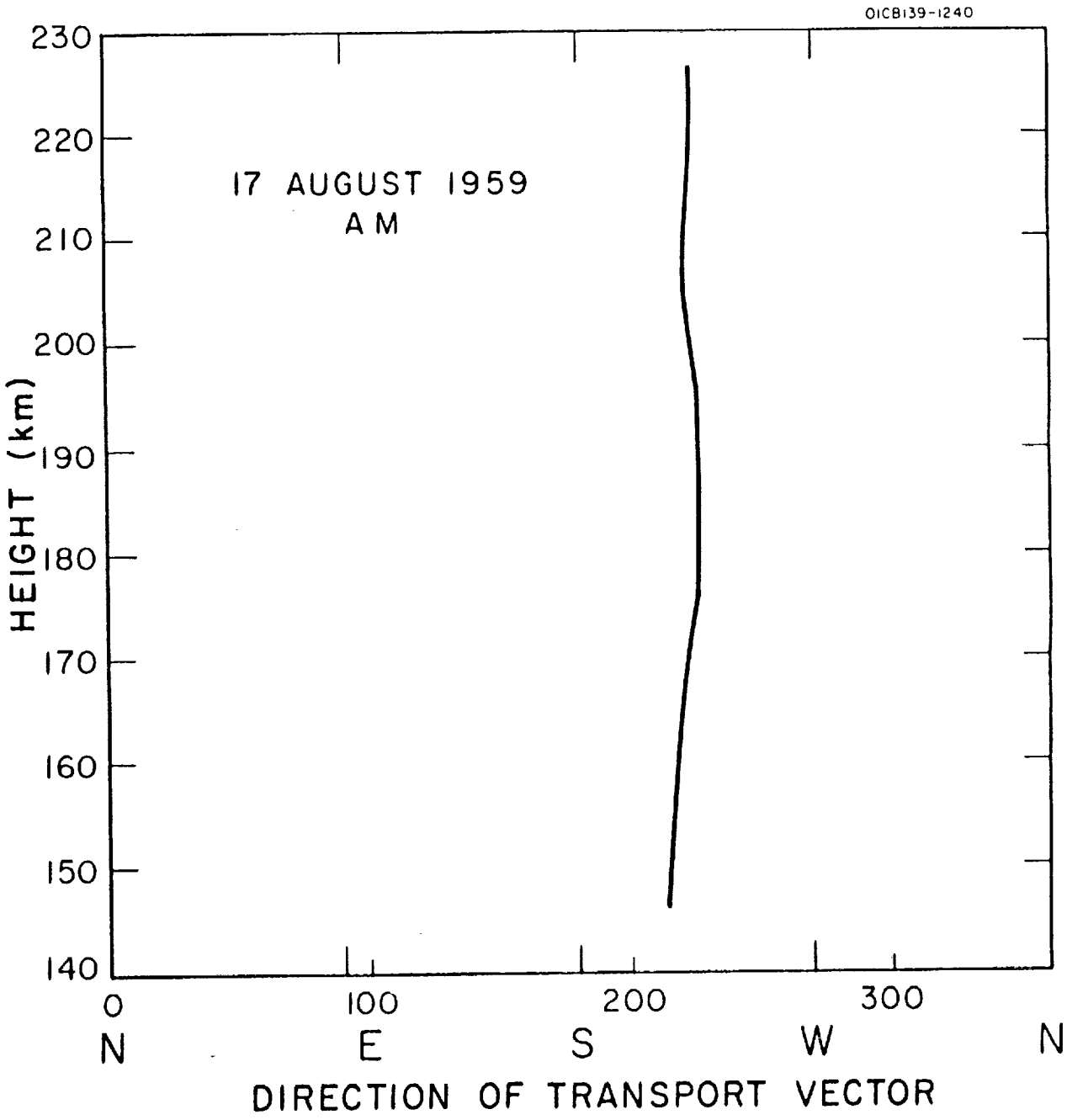

Figure A.1b. Direction of transport vector as a function of height for morning twilight of 17 August 1959.

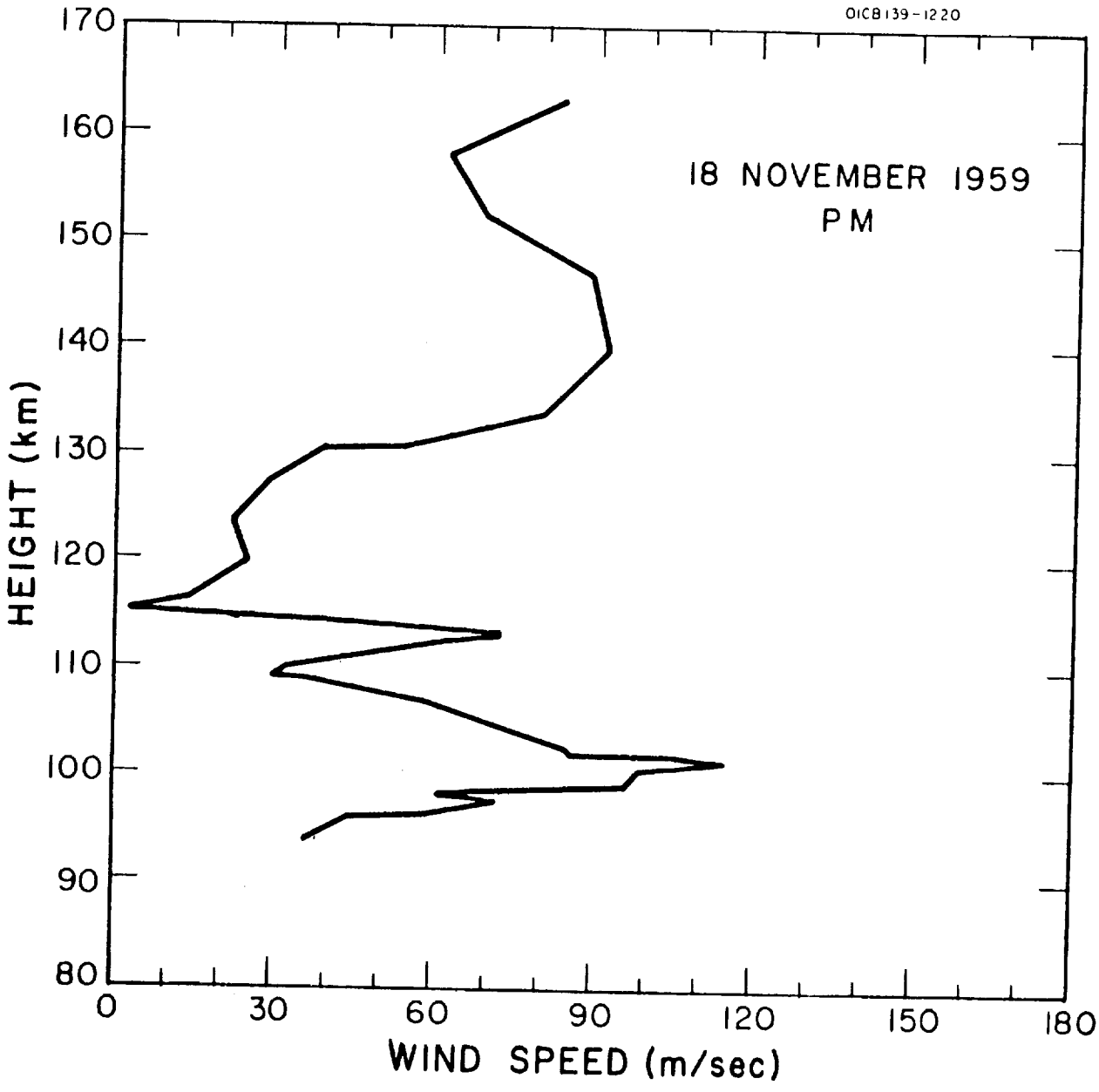

Figure A.2a. Wind speed as a function of height for evening twilight of 18 November 1959.

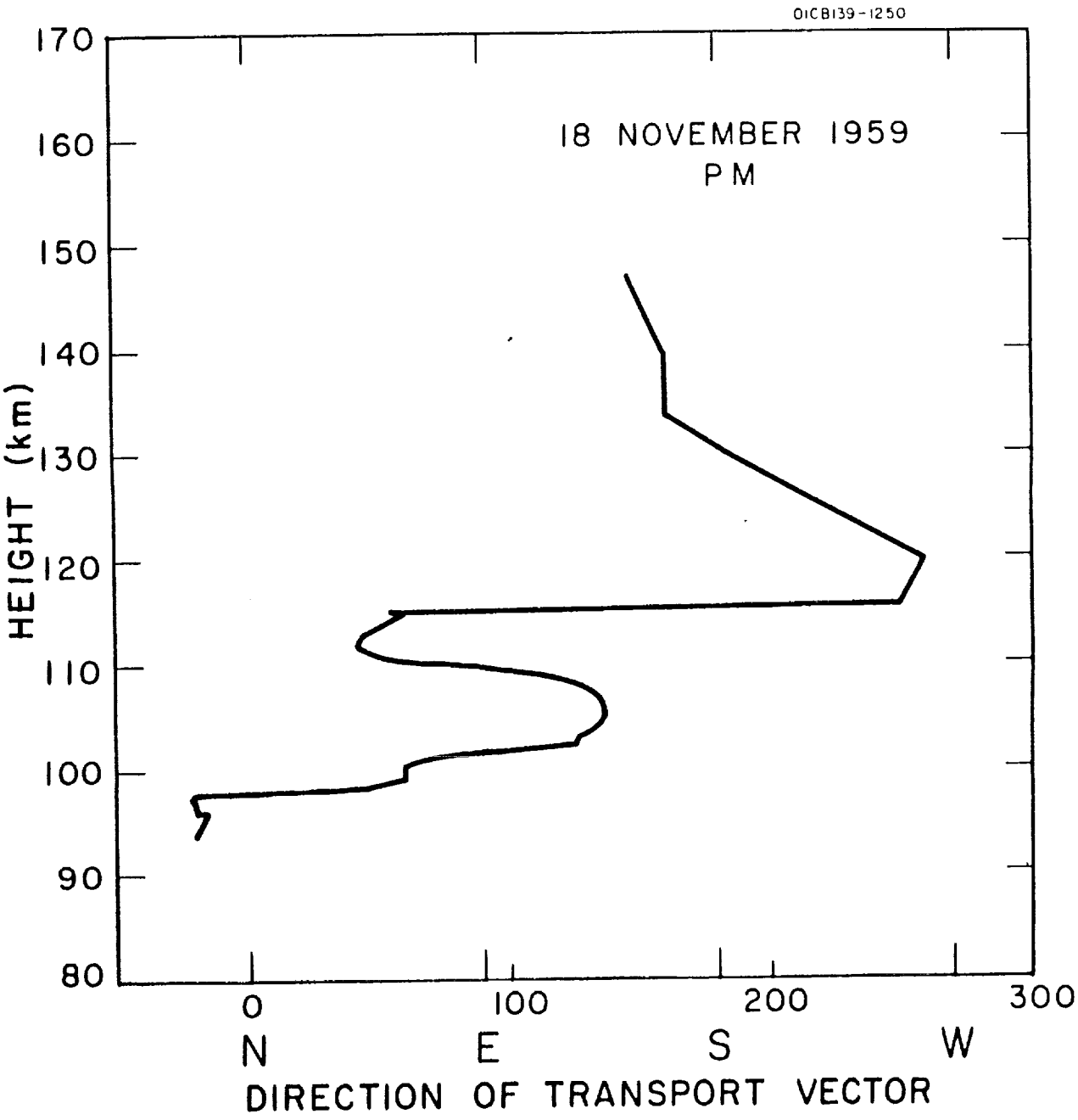

Figure A.2b. Direction of transport vector as a function of height for evening twilight of 18 November 1959.

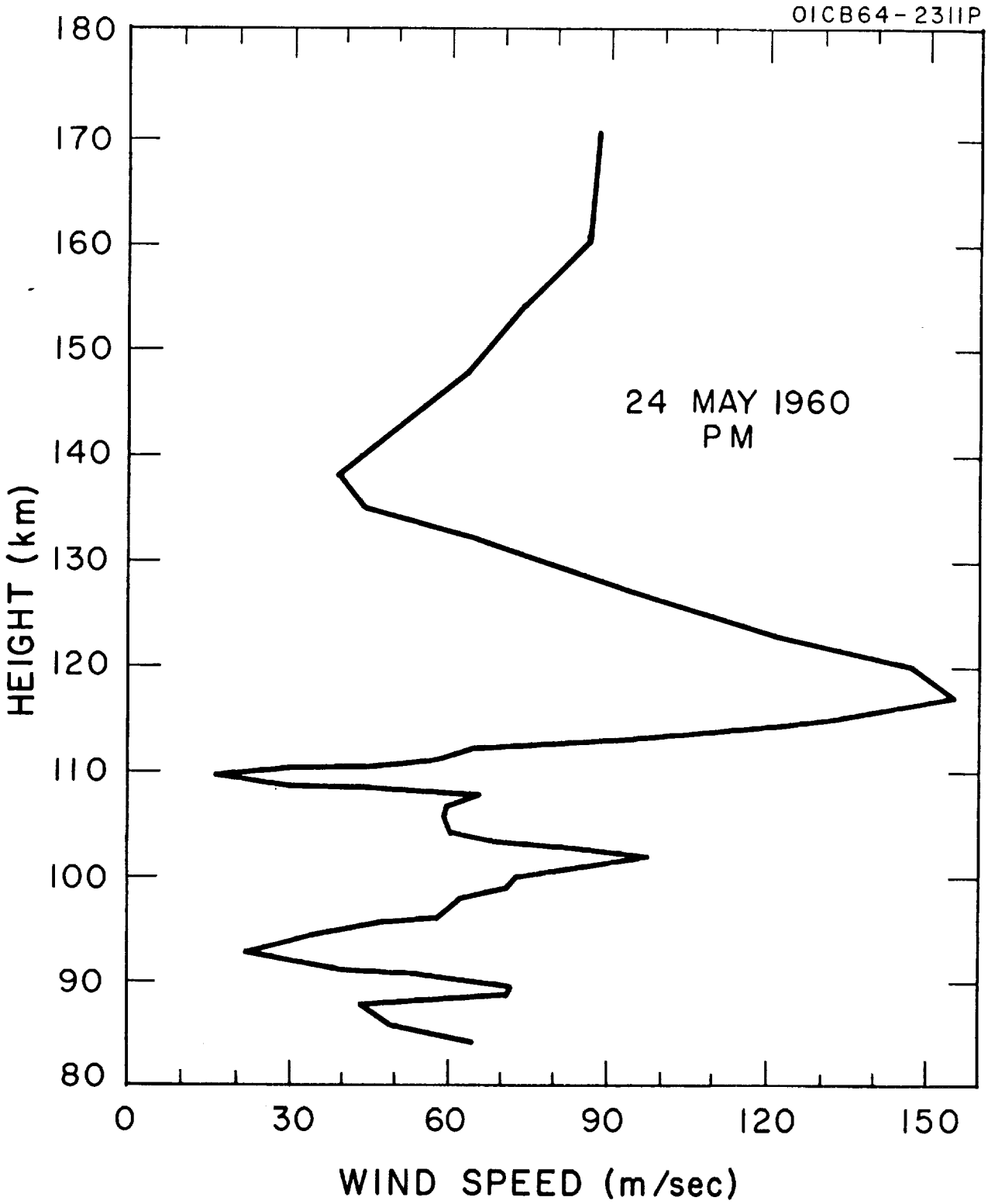

Figure A.3a. Wind speed as a function of height for evening twilight of 24 May 1960.

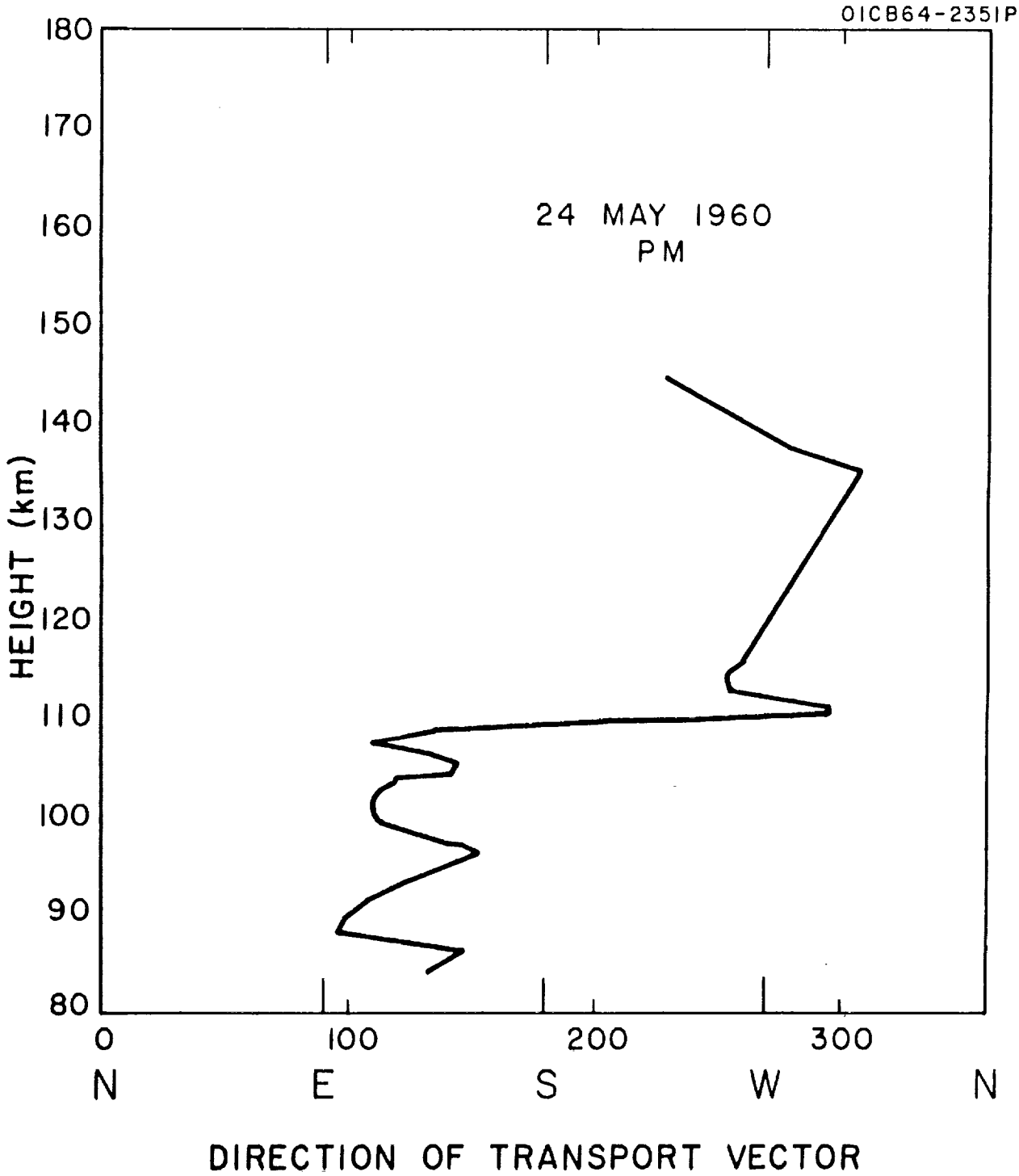

Figure A.3b. Direction of transport vector as a function of height for evening twilight of 24 May 1960.

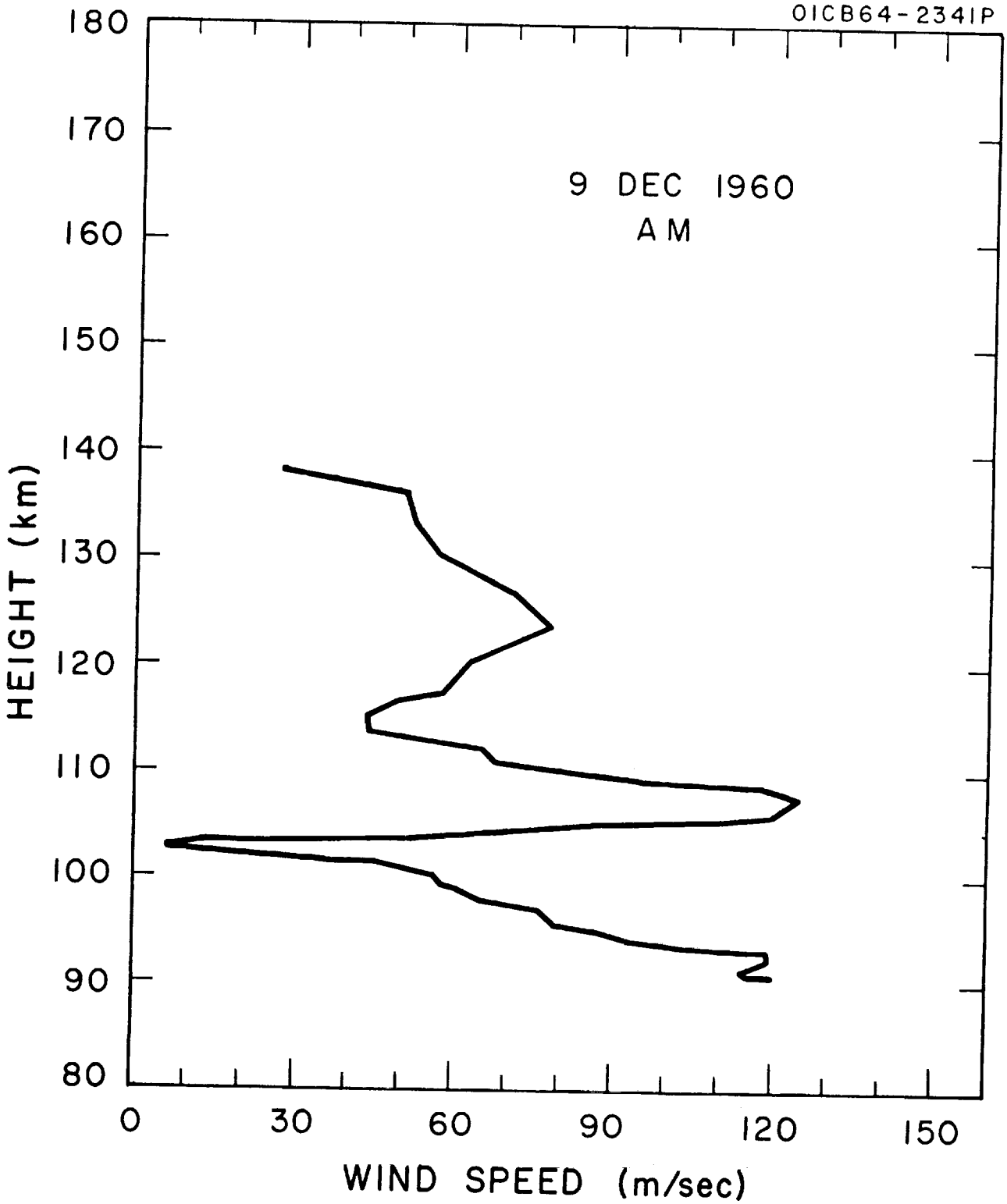

Figure A.4a. Wind speed as a function of height for morning twilight of 9 December 1960.

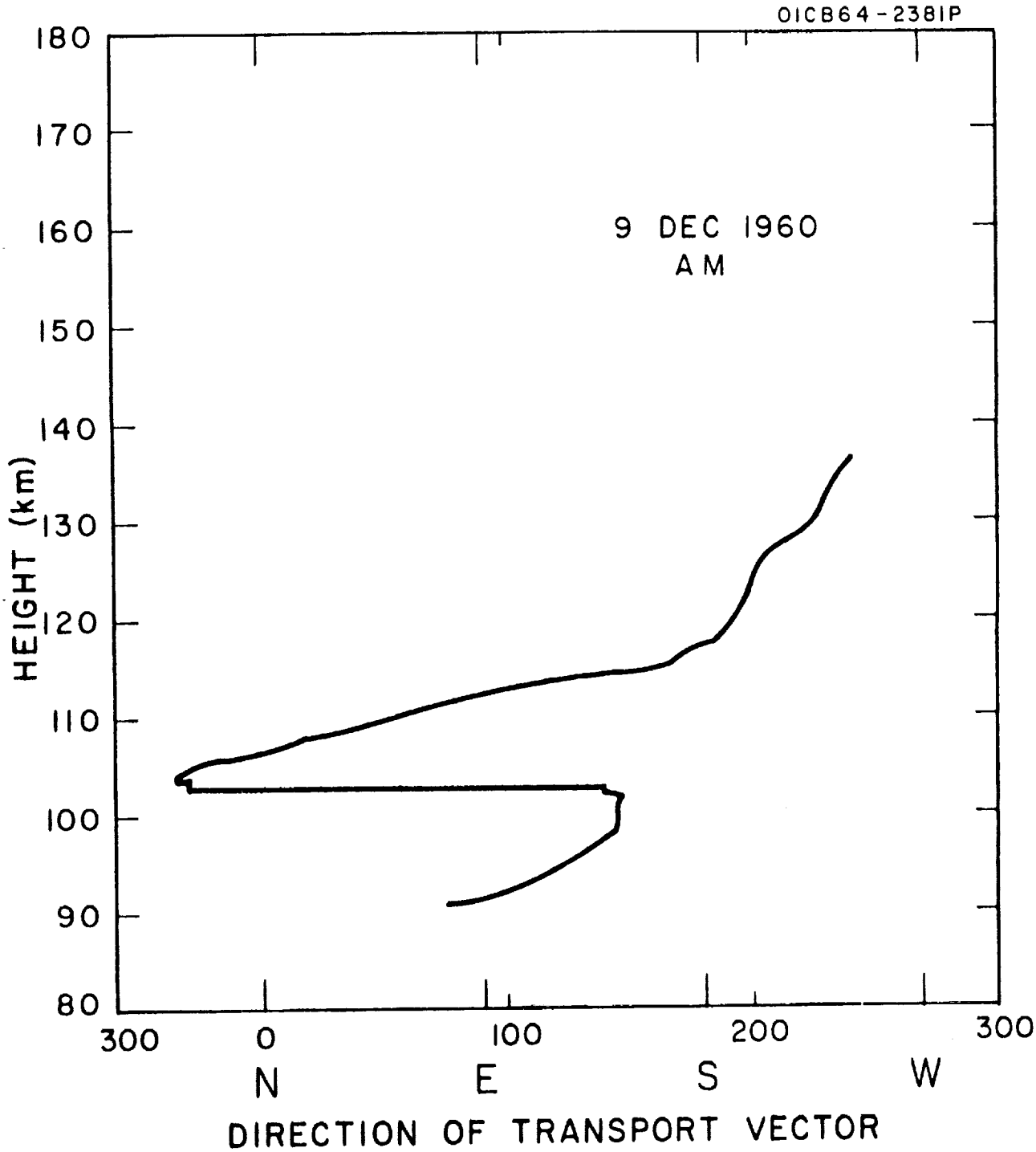

Figure A.4b. Direction of transport vector as a function of height for morning twilight of 9 December 1960.

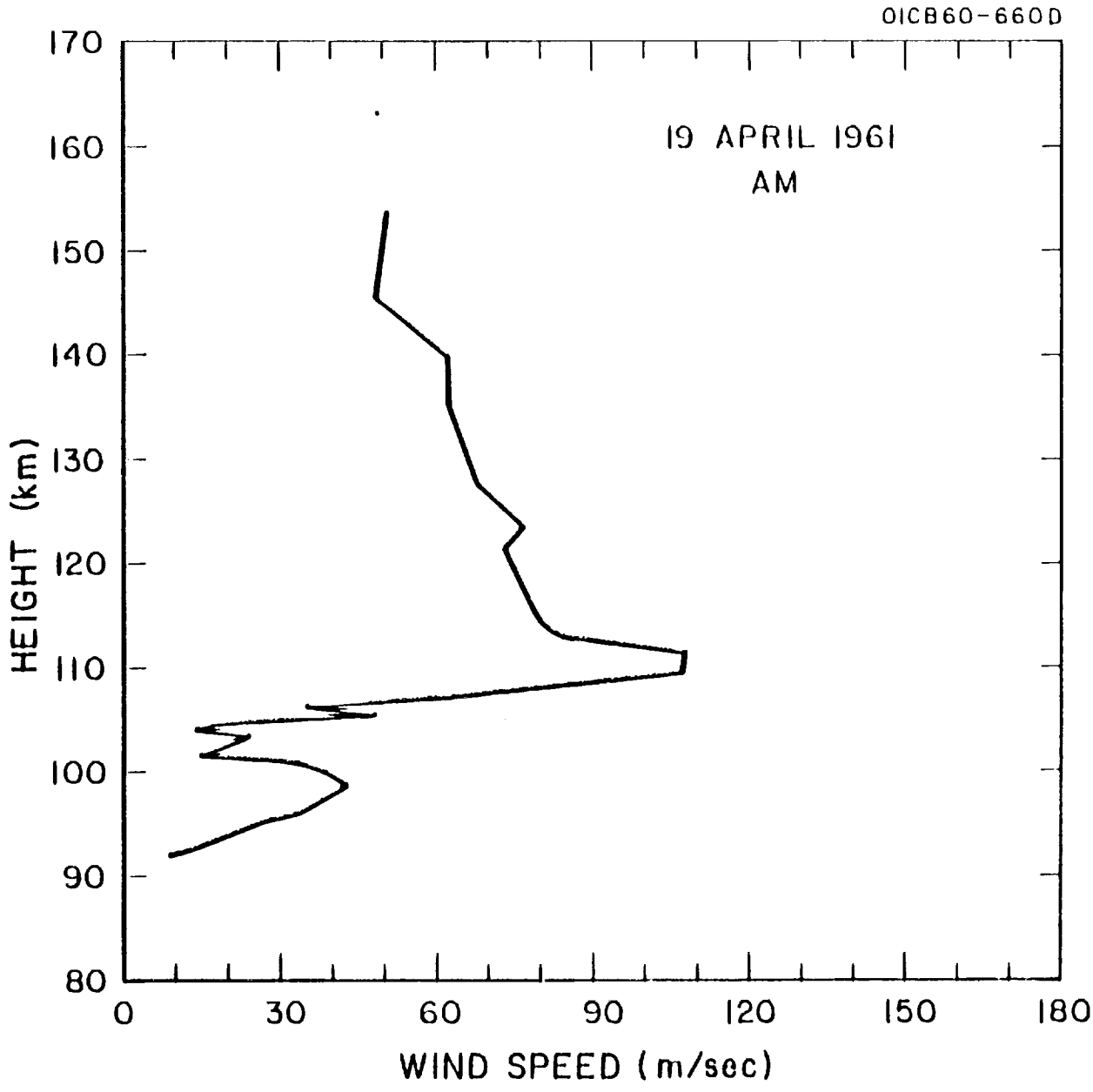

Figure A.5a. Wind speed as a function of height for morning twilight of 19 April 1961.

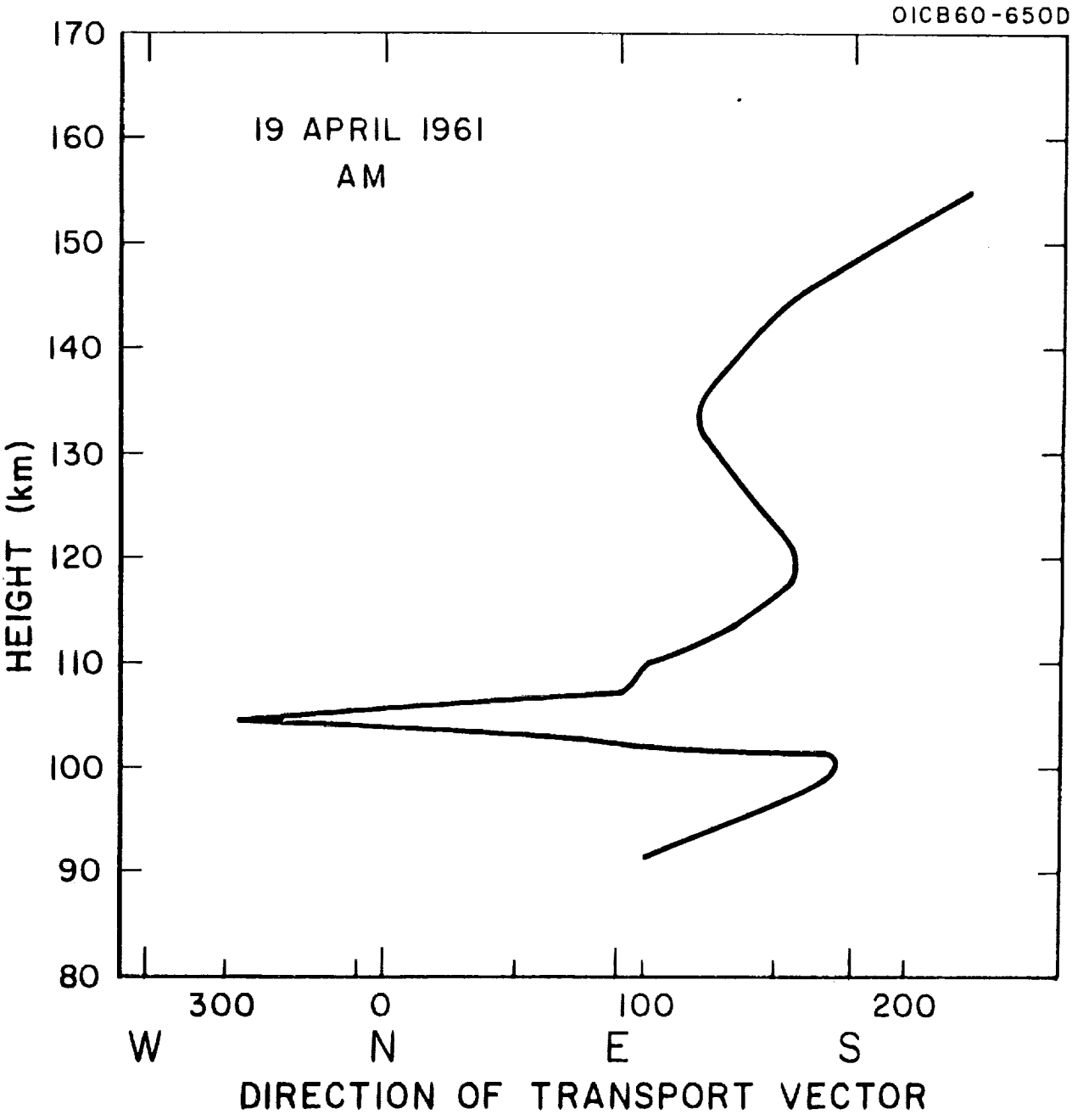

Figure A.5b. Direction of transport vector as a function of height for morning twilight of 19 April 1961.

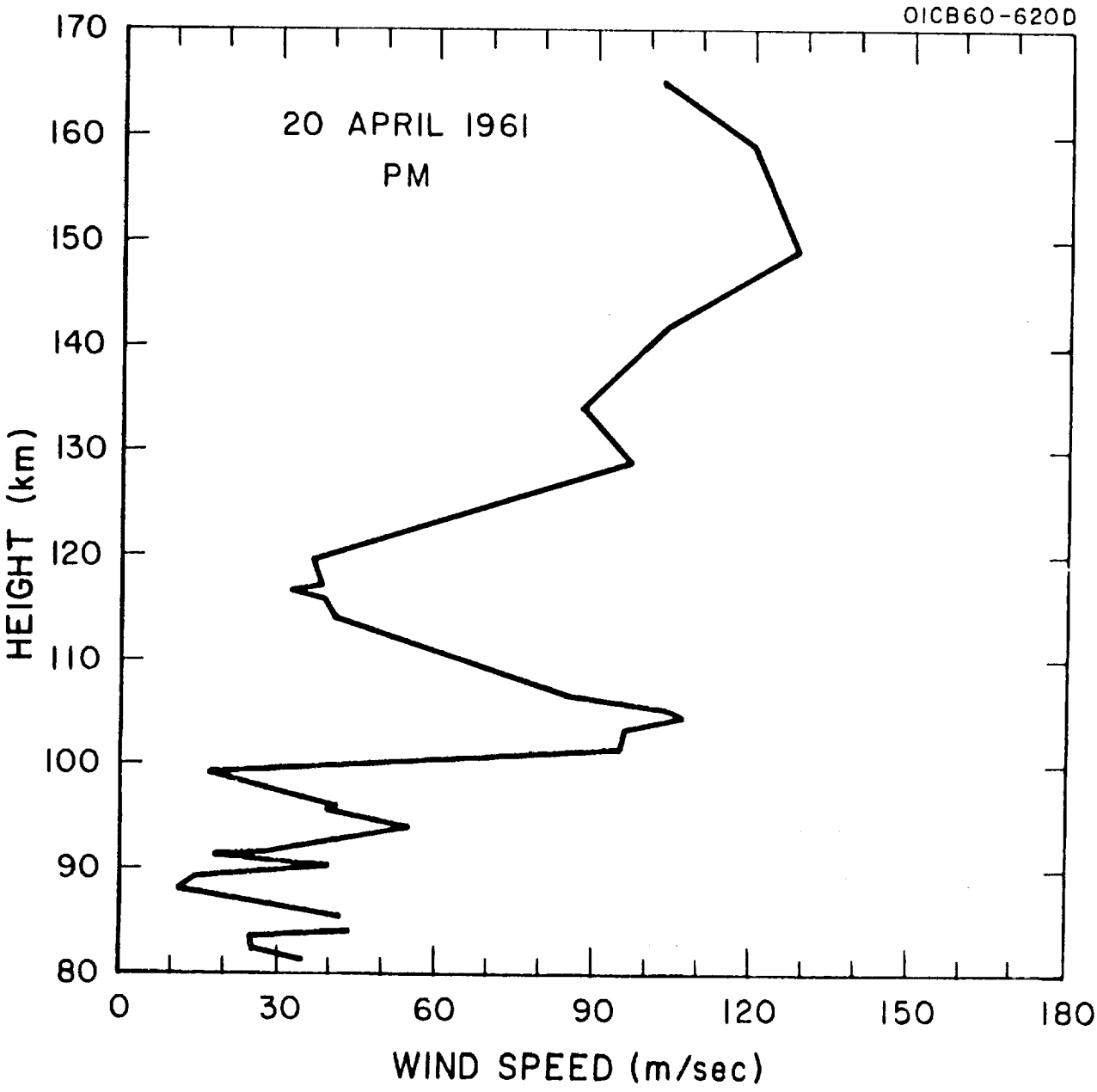

Figure A.8a. Wind speed as a function of height for evening twilight of 20 April 1961.

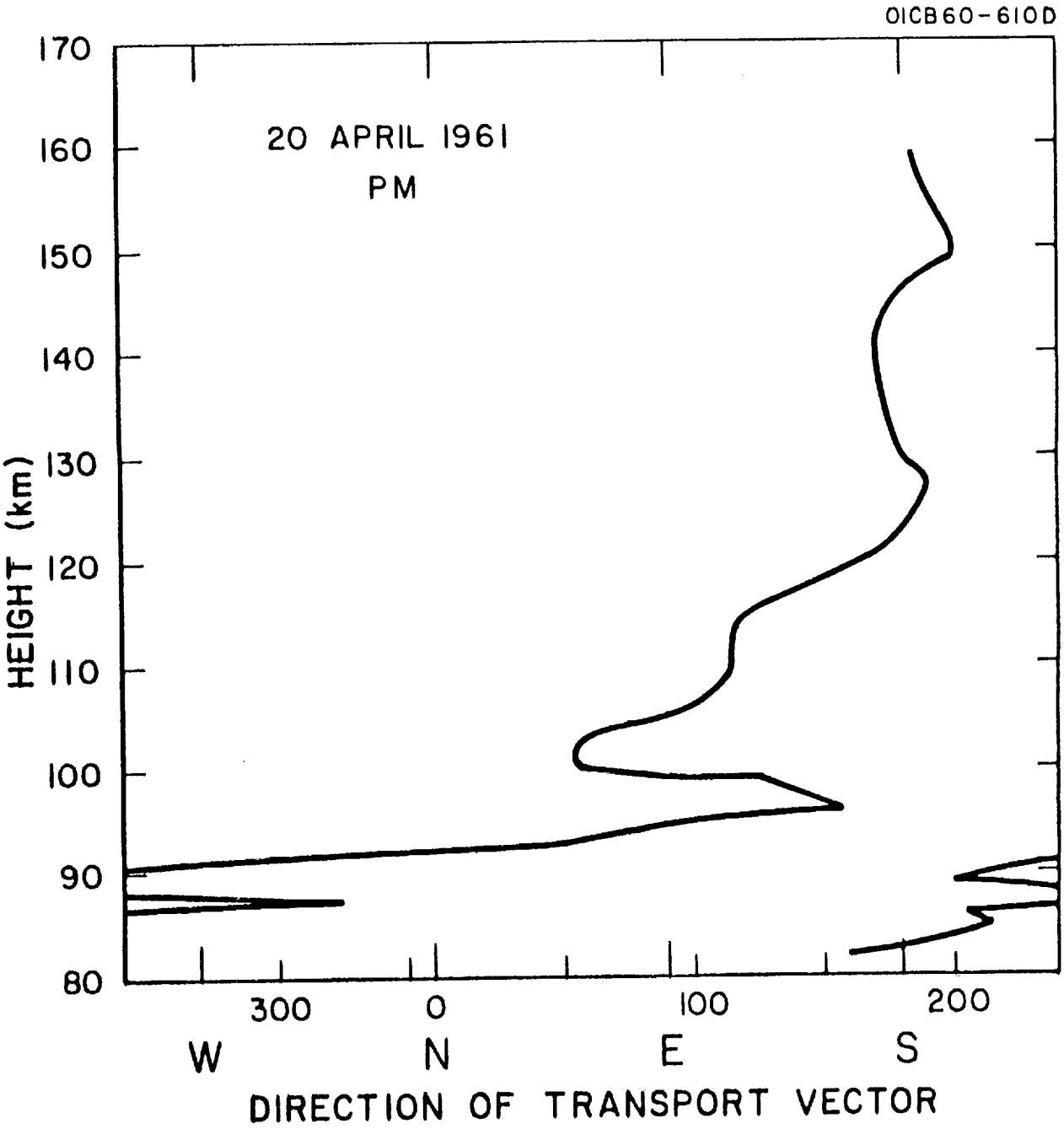

Figure A.8b. Direction of transport vector as a function of height for evening twilight of 20 April 1961.

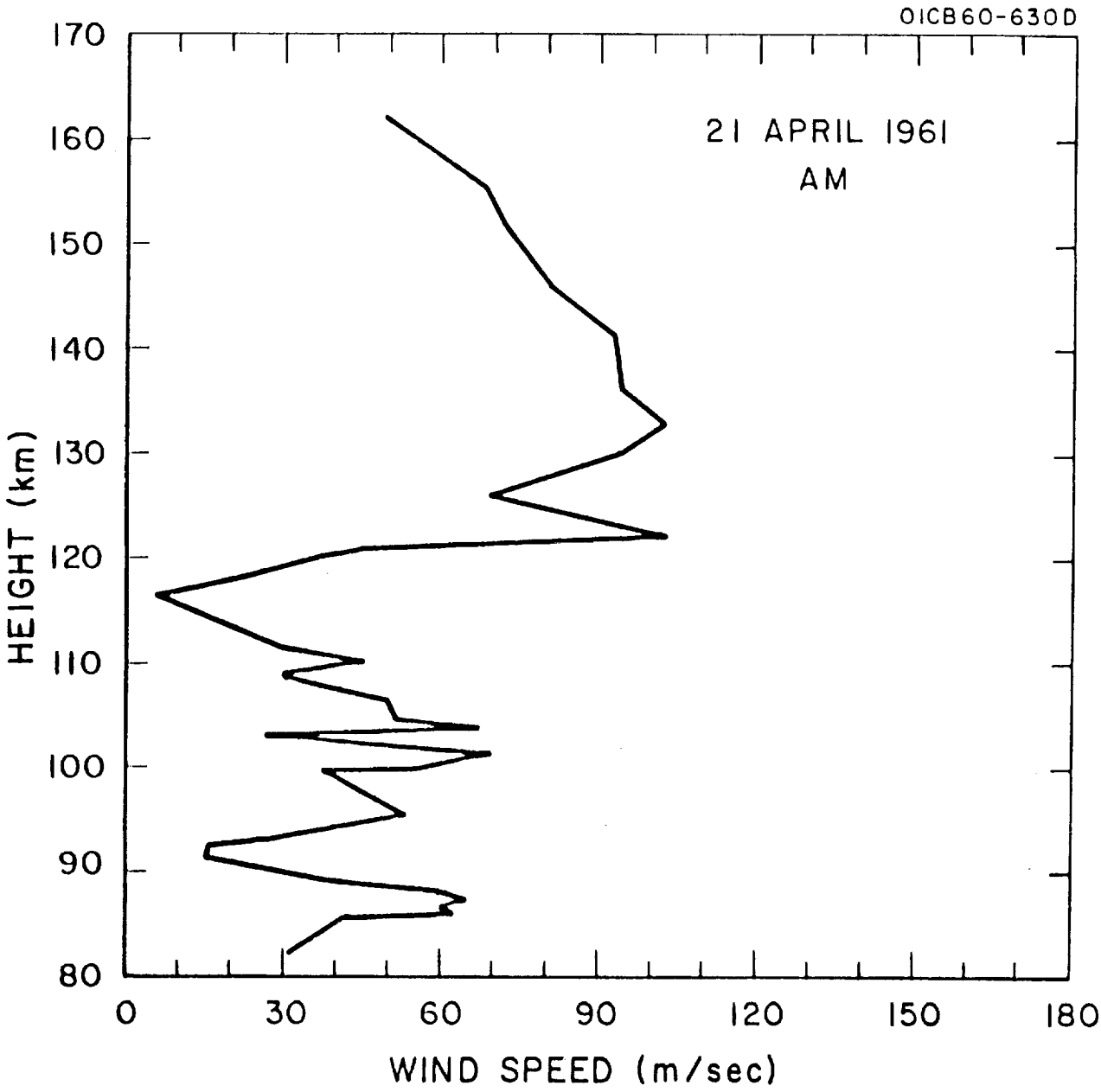

Figure A.9a. Wind speed as a function of height for morning twilight of 21 April 1961.

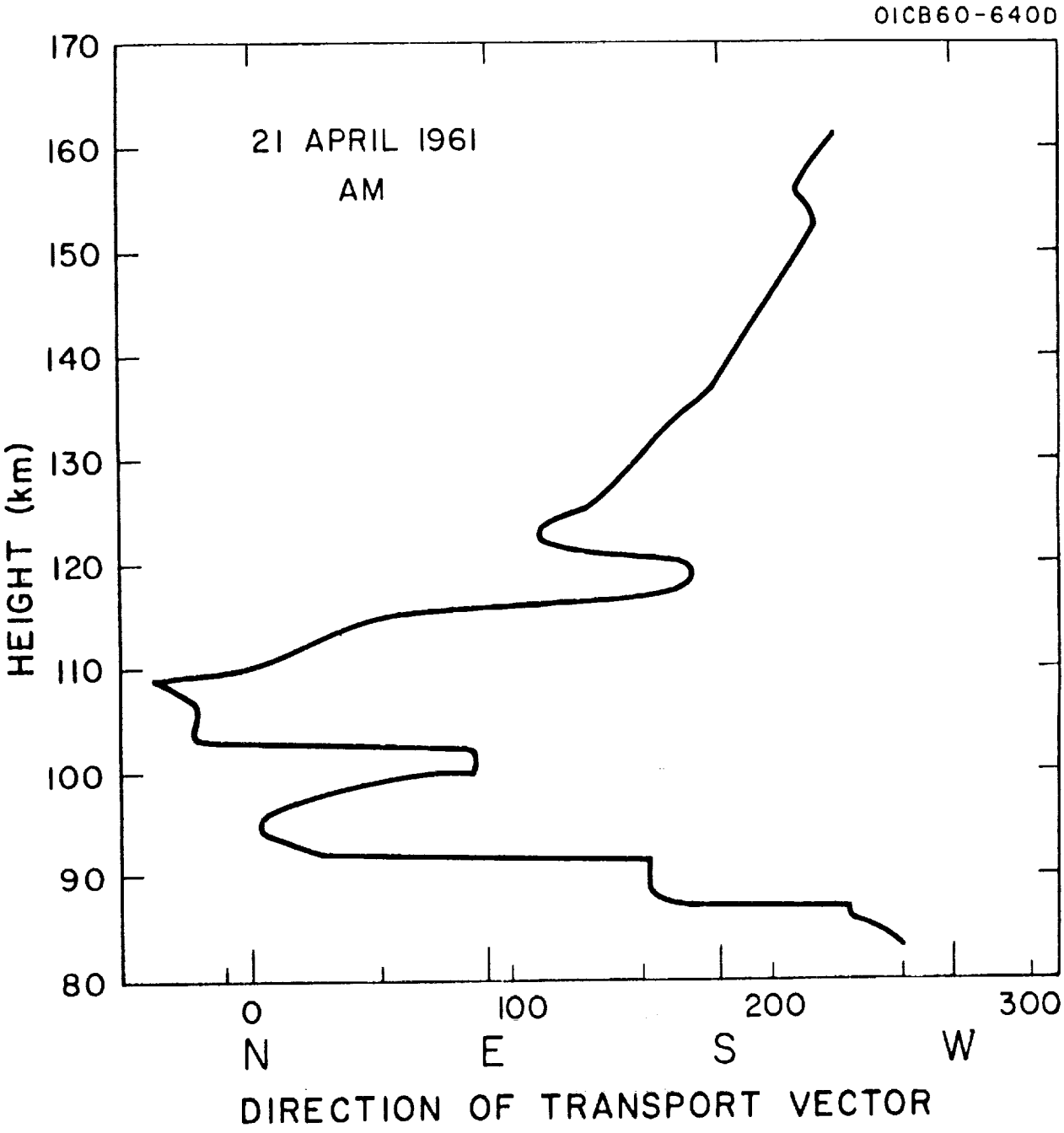

Figure A.9b. Direction of transport vector as a function of height for morning twilight of 21 April 1961.

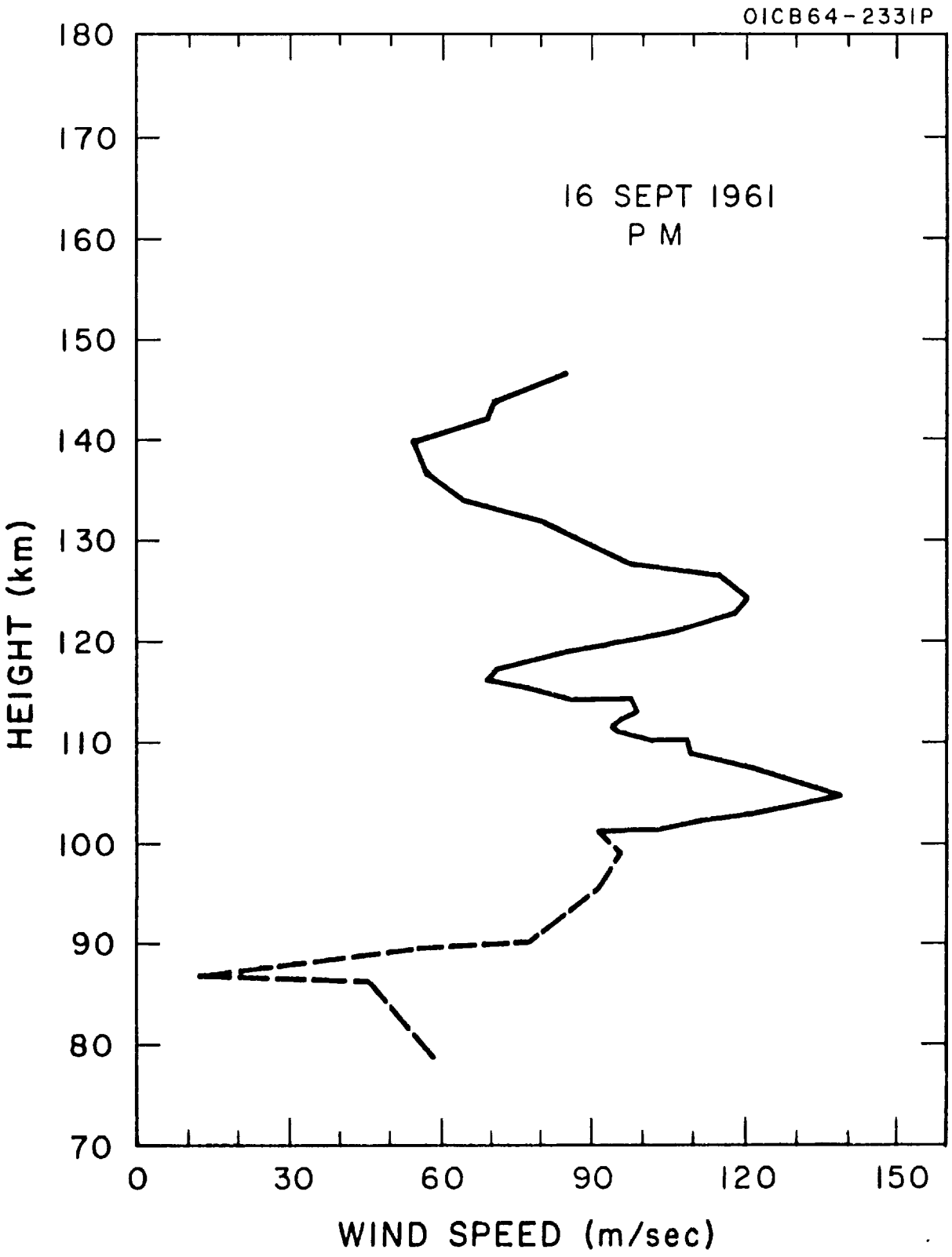

Figure A.10a. Wind speed as a function of height for evening twilight of 16 September 1961.

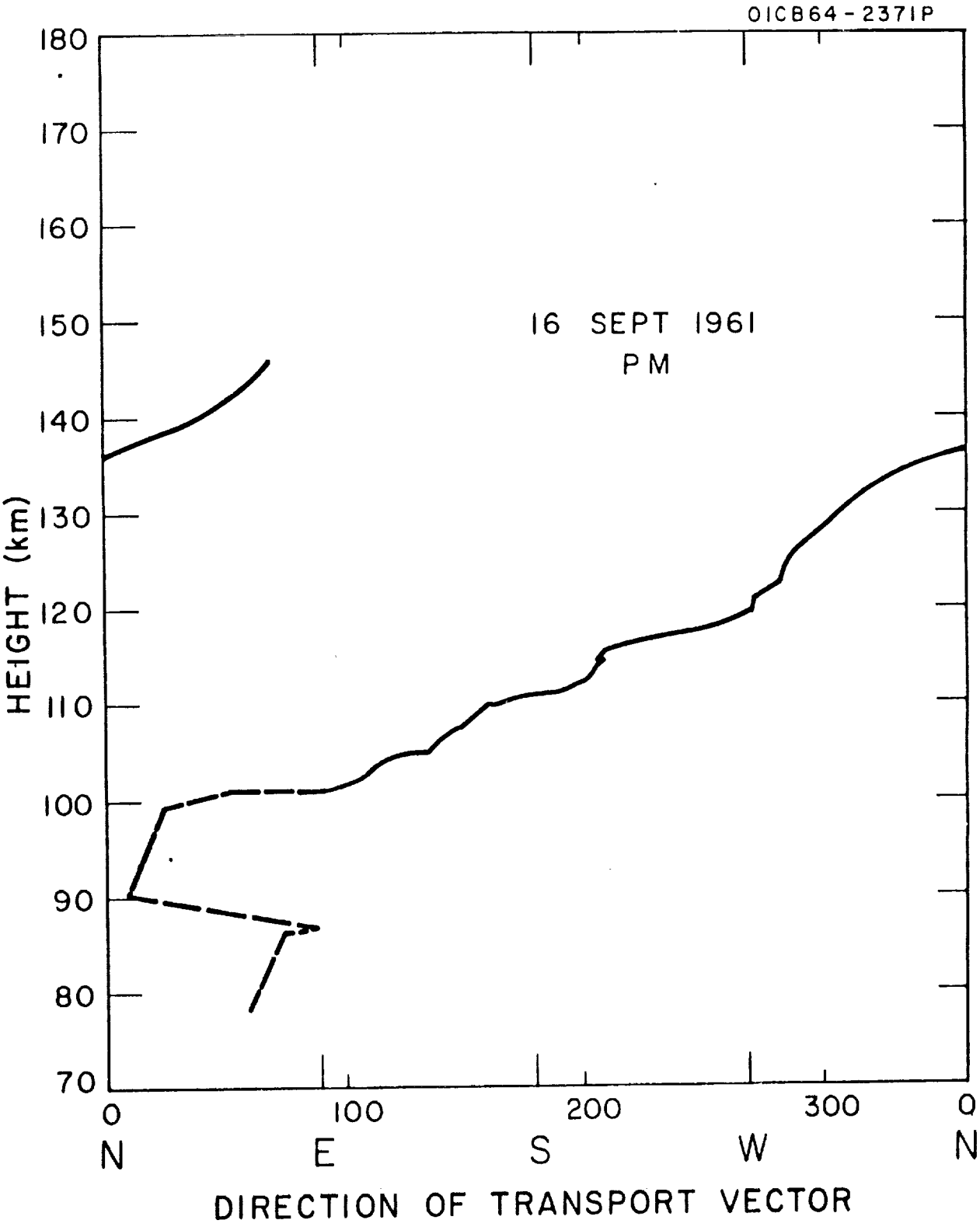

Figure A.10b. Direction of transport vector as a function of height for evening twilight of 16 September 1961.

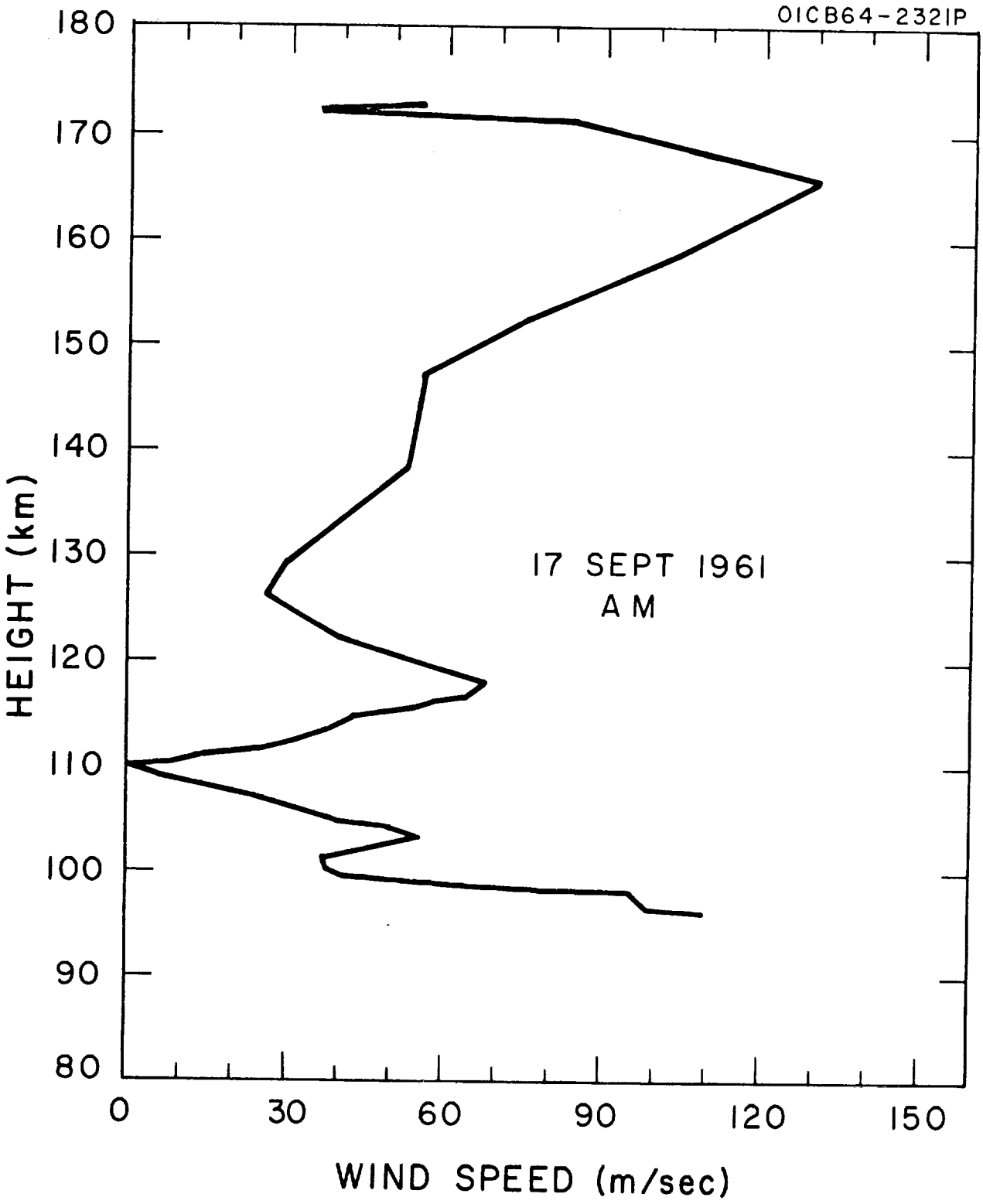

Figure A.11a. Wind speed as a function of height for morning twilight of 17 September 1961.

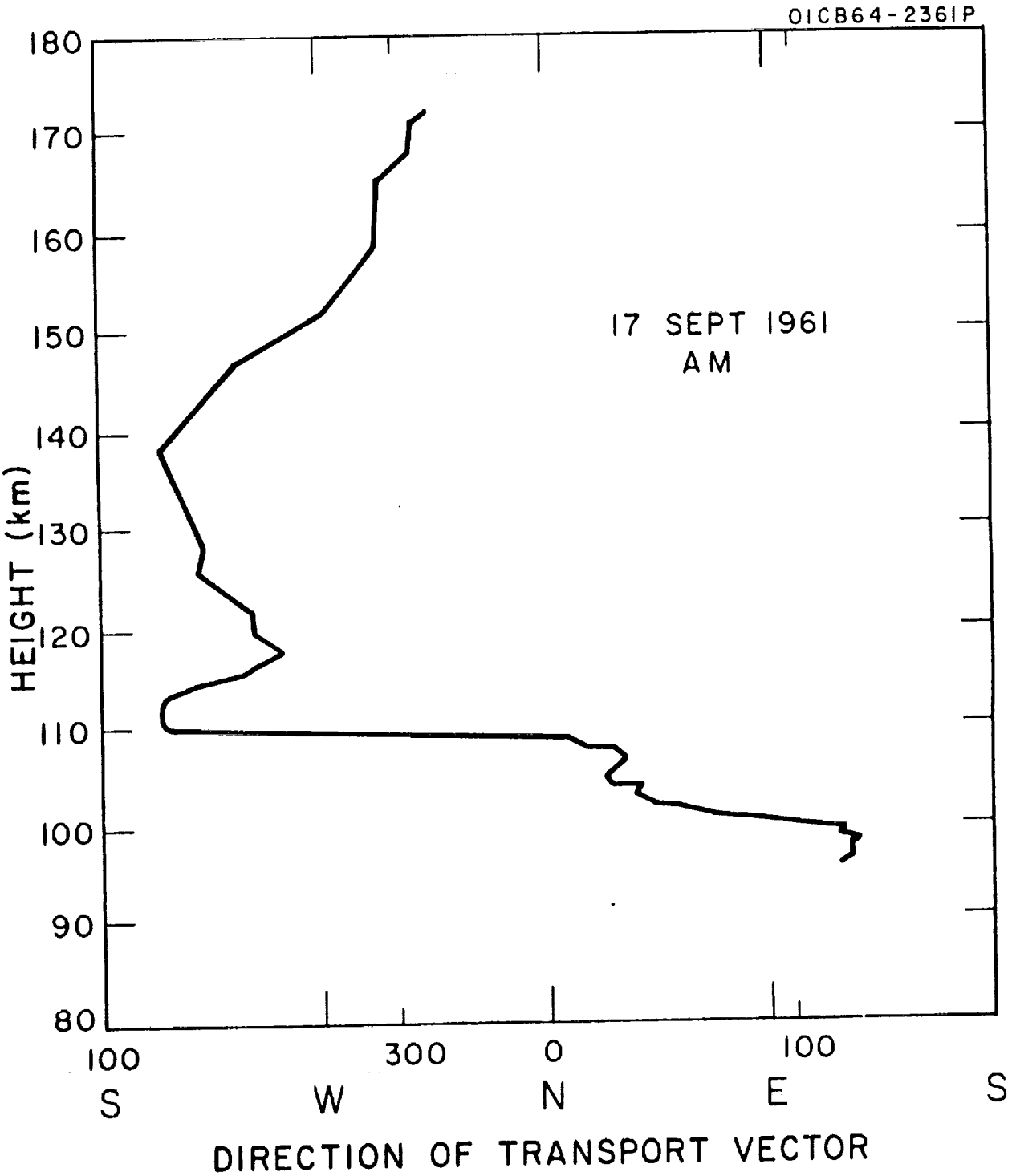

Figure A.11b. Direction of transport vector as a function of height for morning twilight of 17 September 1961.

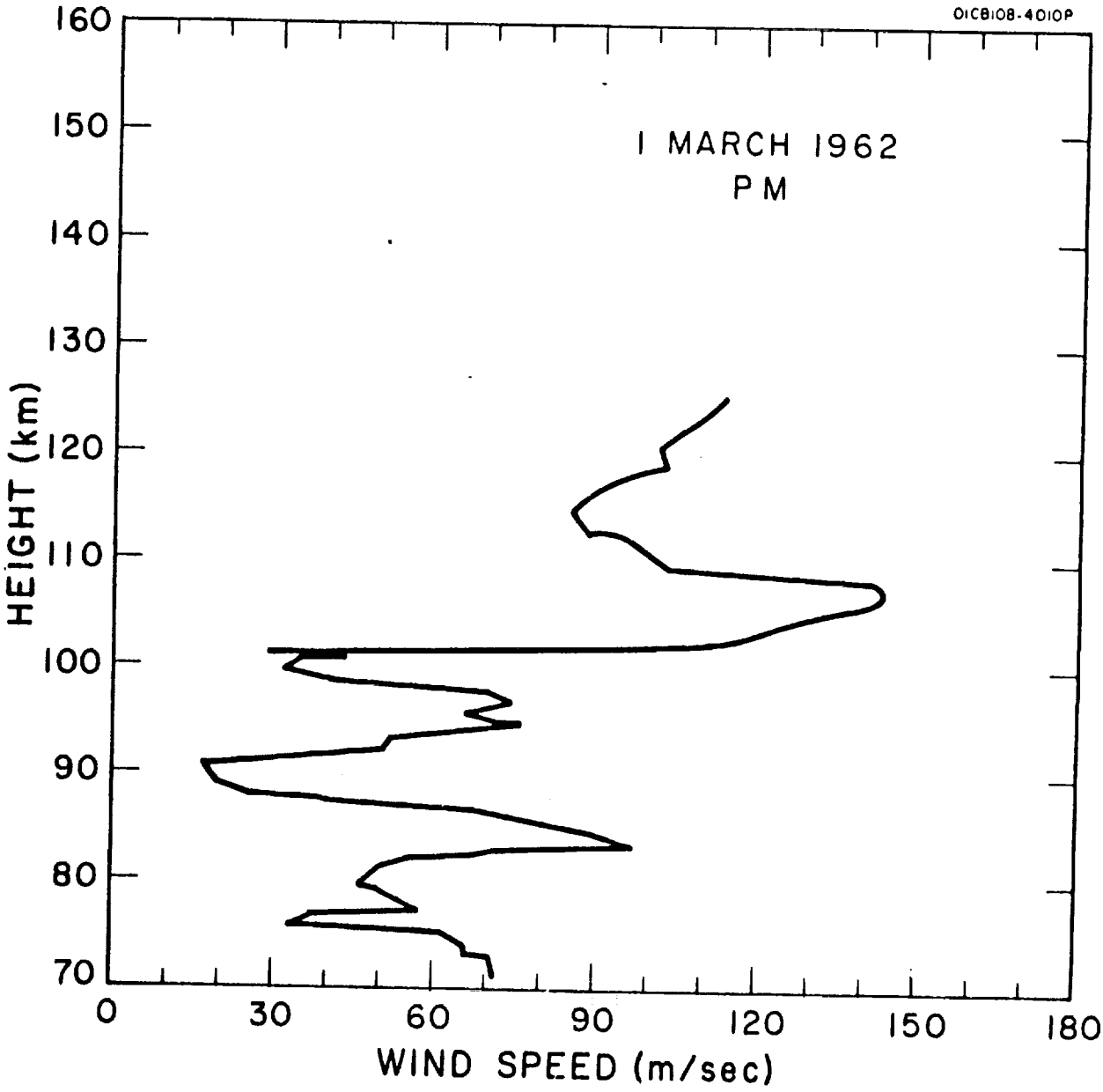

Figure A.12a. Wind speed as a function of height for evening twilight of 1 Marcy 1962.

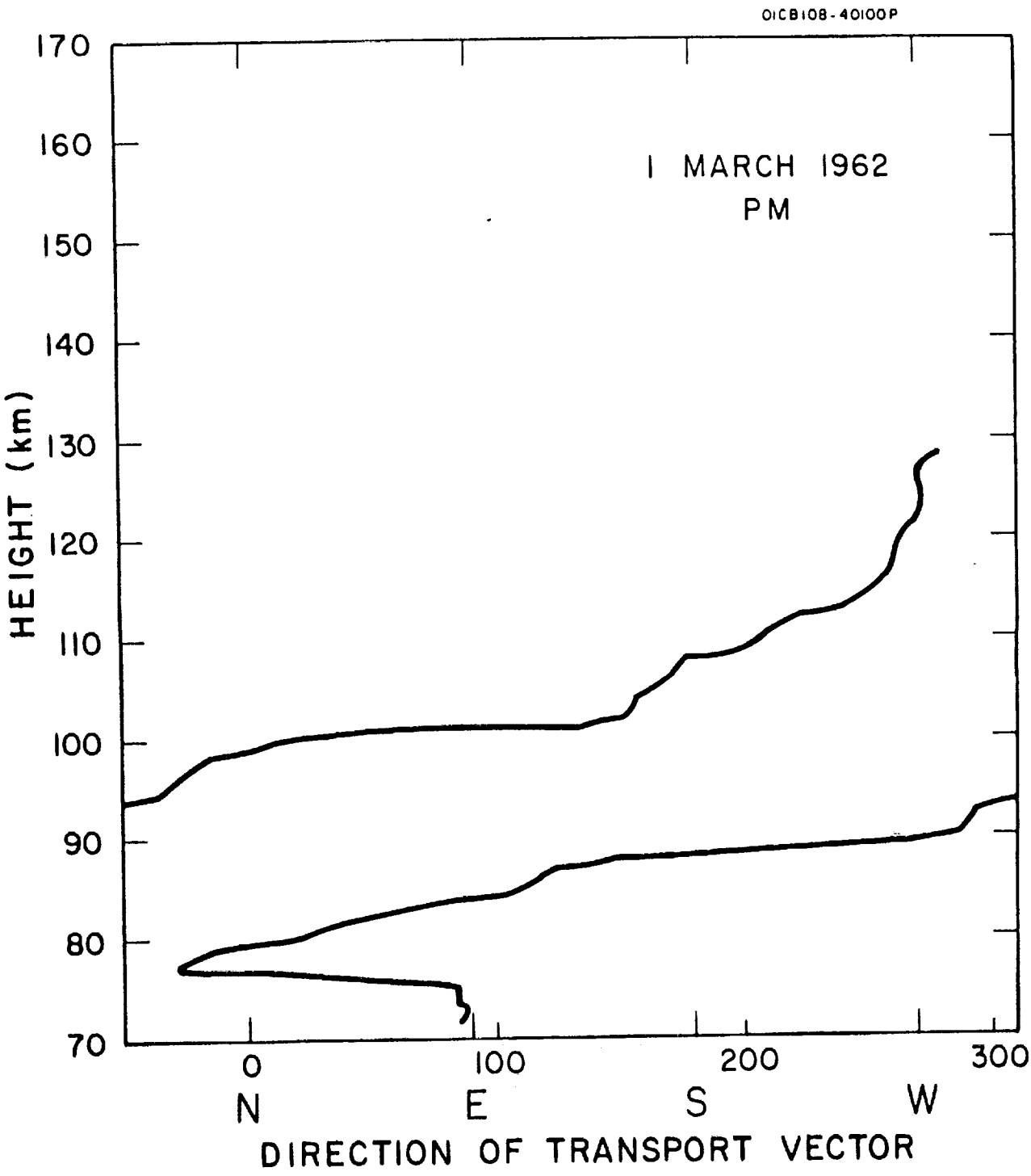

Figure A.12b. Direction of transport vector as a function of height for evening twilight of 1 March 1962.

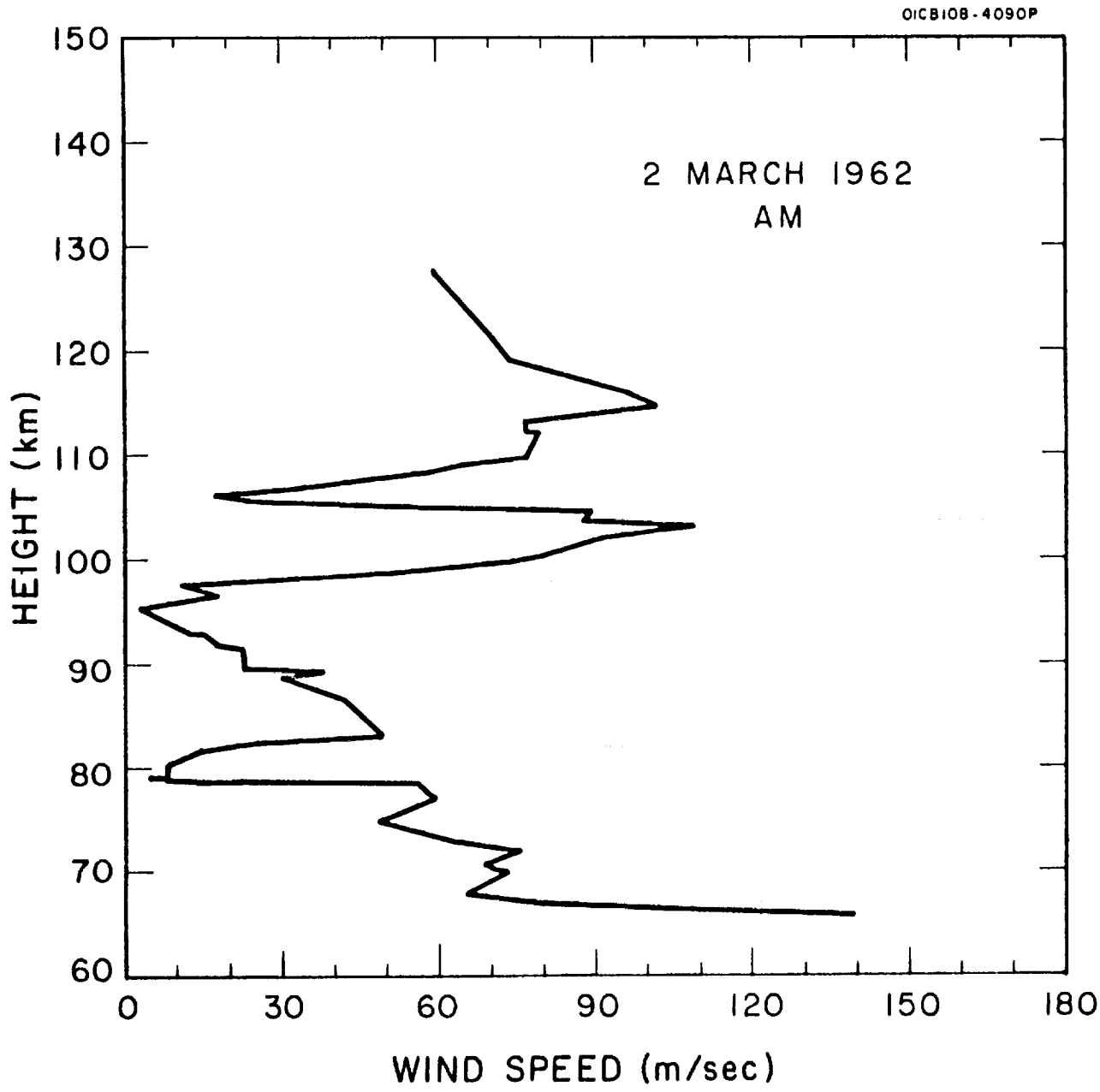

Figure A.13a. Wind speed as a function of height for morning twilight of 2 March 1962.

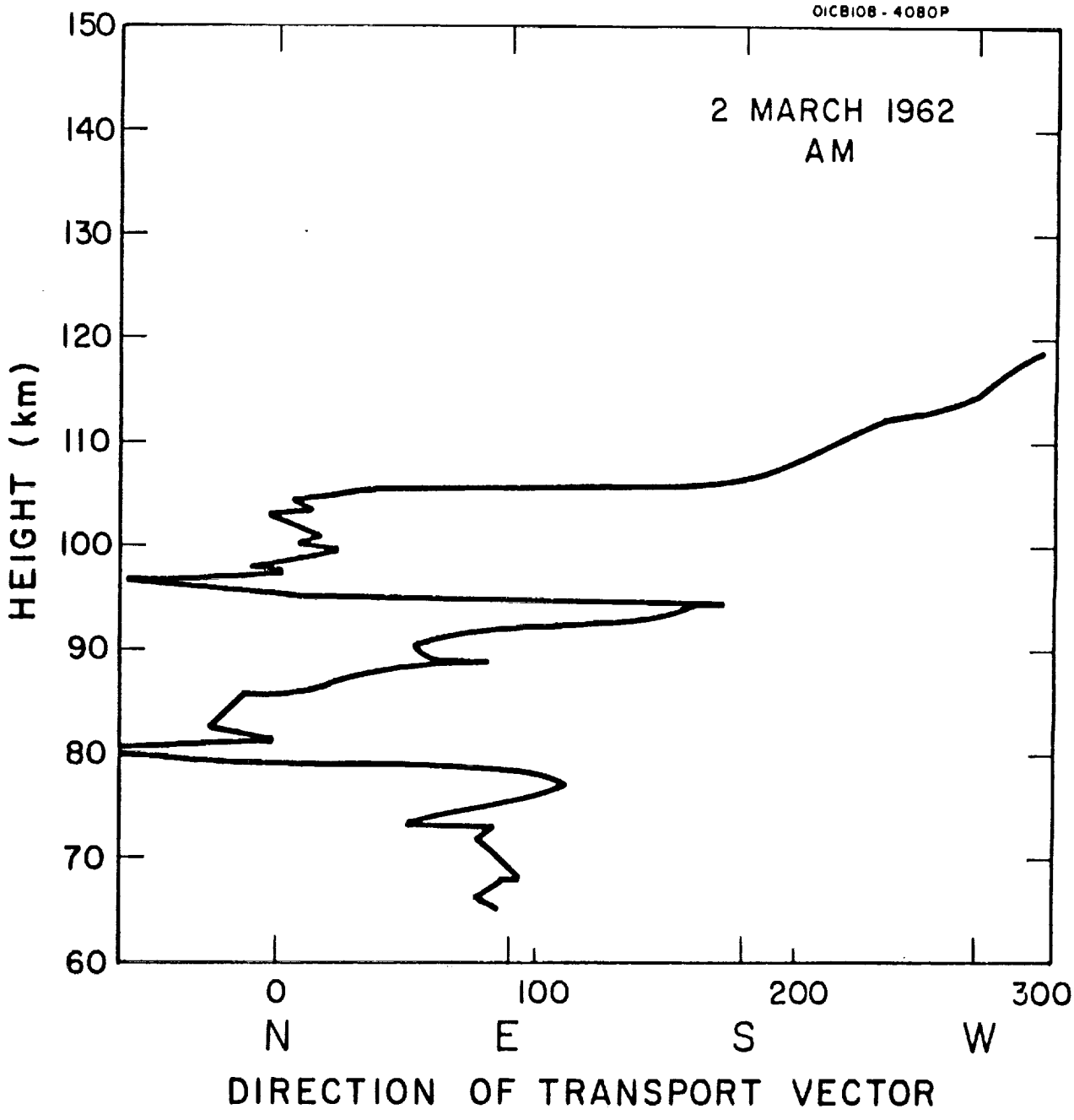

Figure A.13b. Direction of transport vector as a function of height for morning twilight of 2 March 1962.

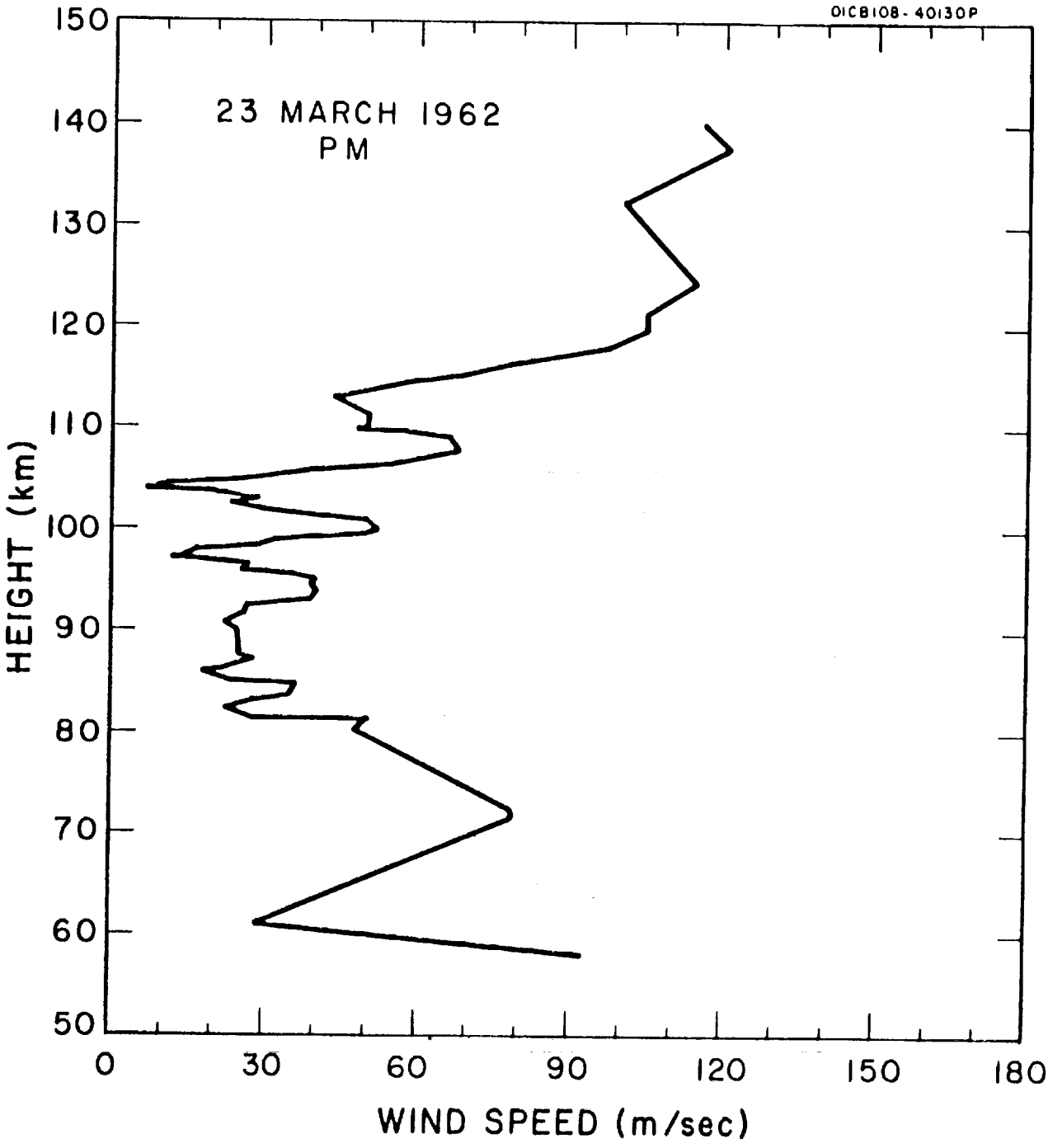

Figure A.14a. Wind speed as a function of height for evening twilight of 23 March 1962.

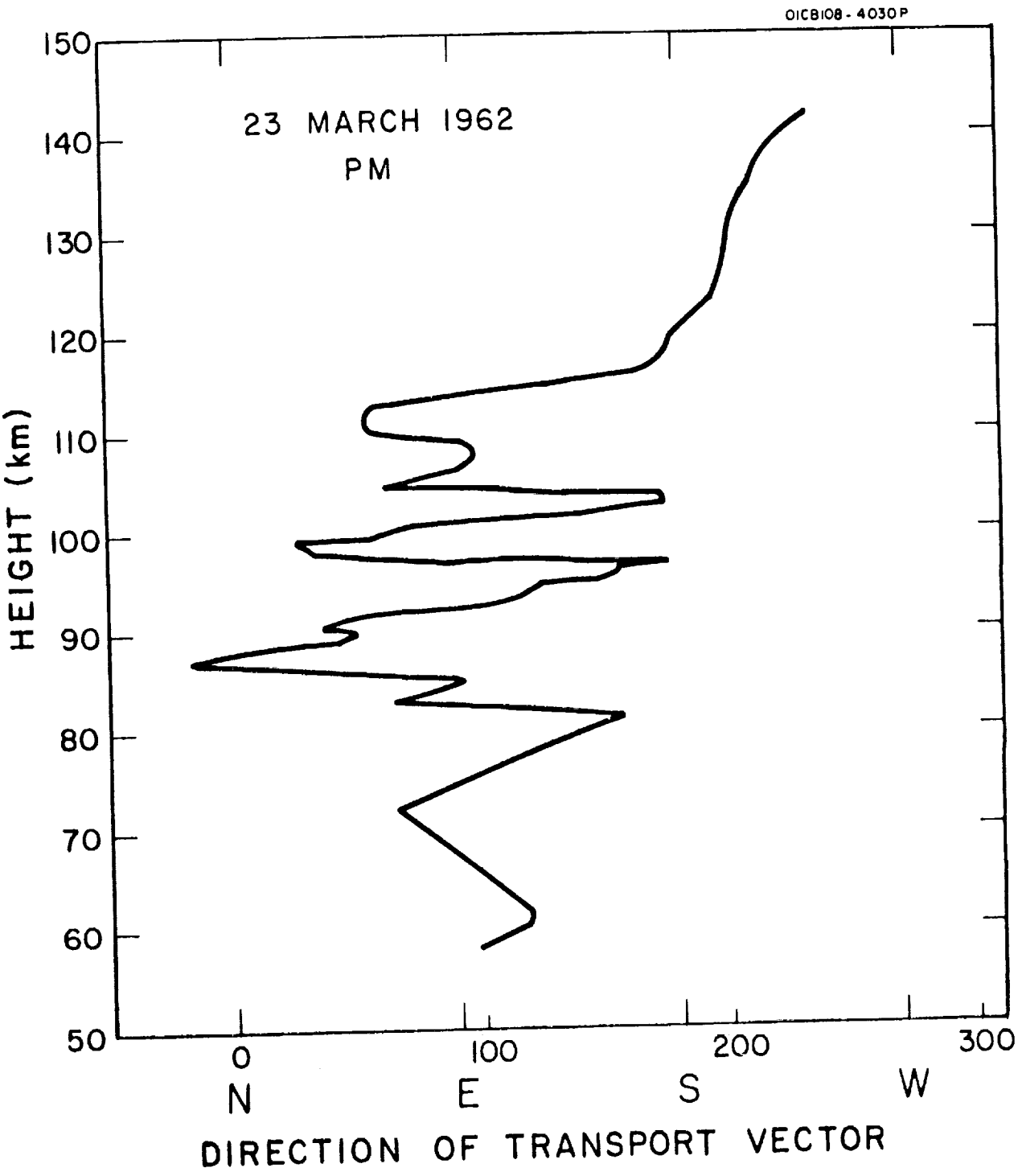

Figure A.14b. Direction of transport vector as a function of height for evening twilight of 23 March 1962.

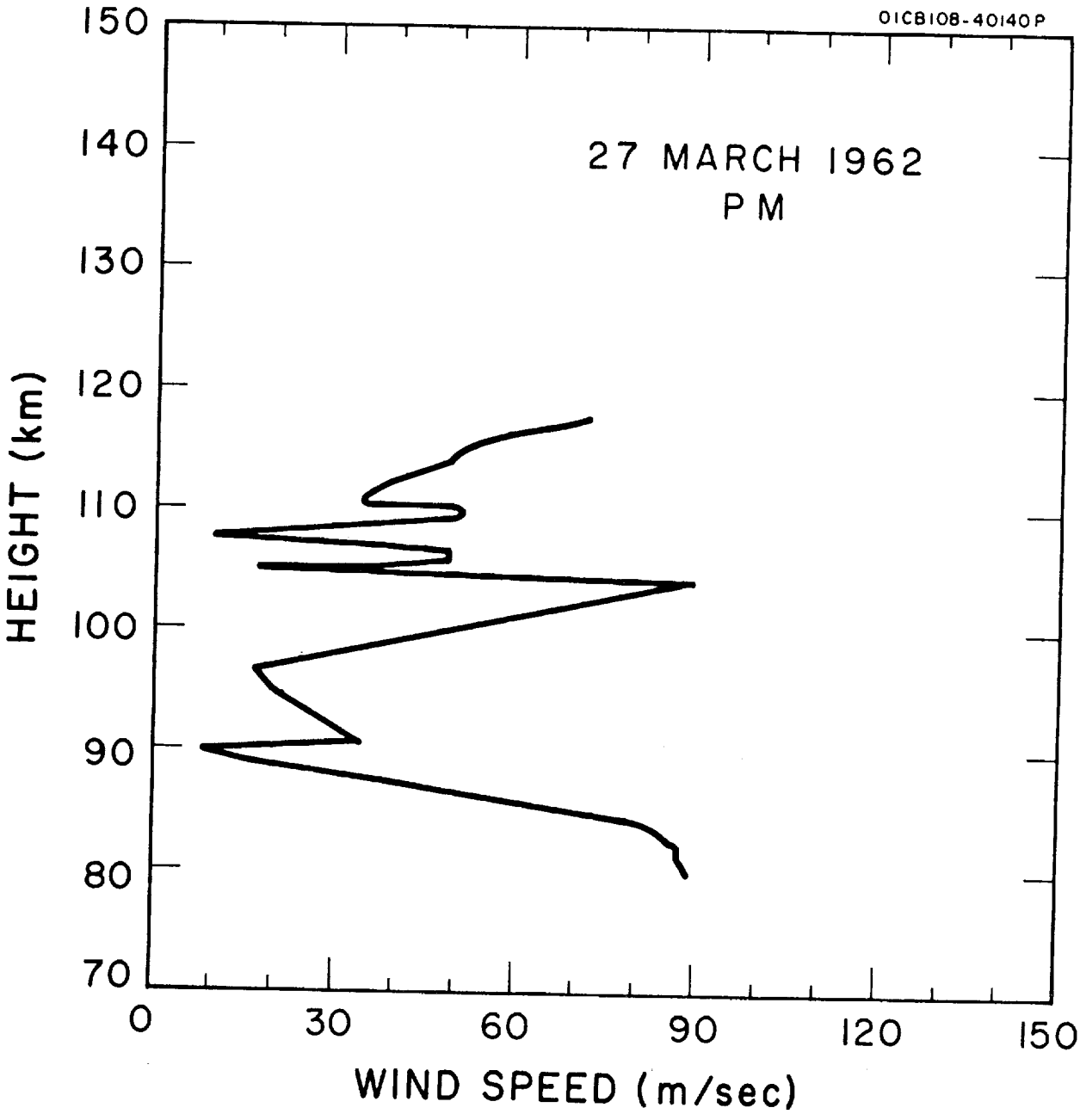

Figure A.15a. Wind speed as a function of height for evening twilight of 27 Marcy 1962.

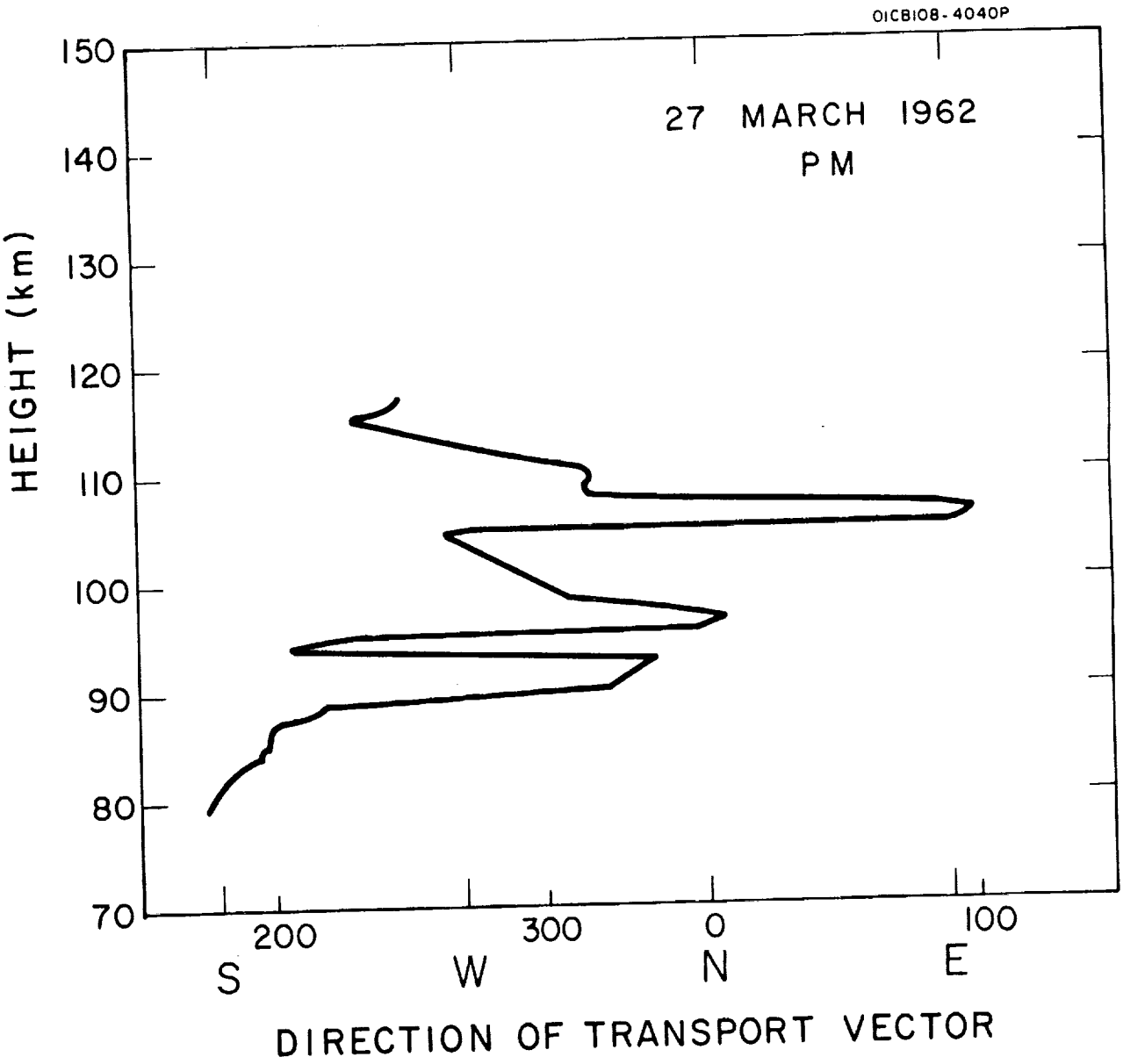

Figure A.15b. Direction of transport vector as a function of height for evening twilight of 27 March 1962.

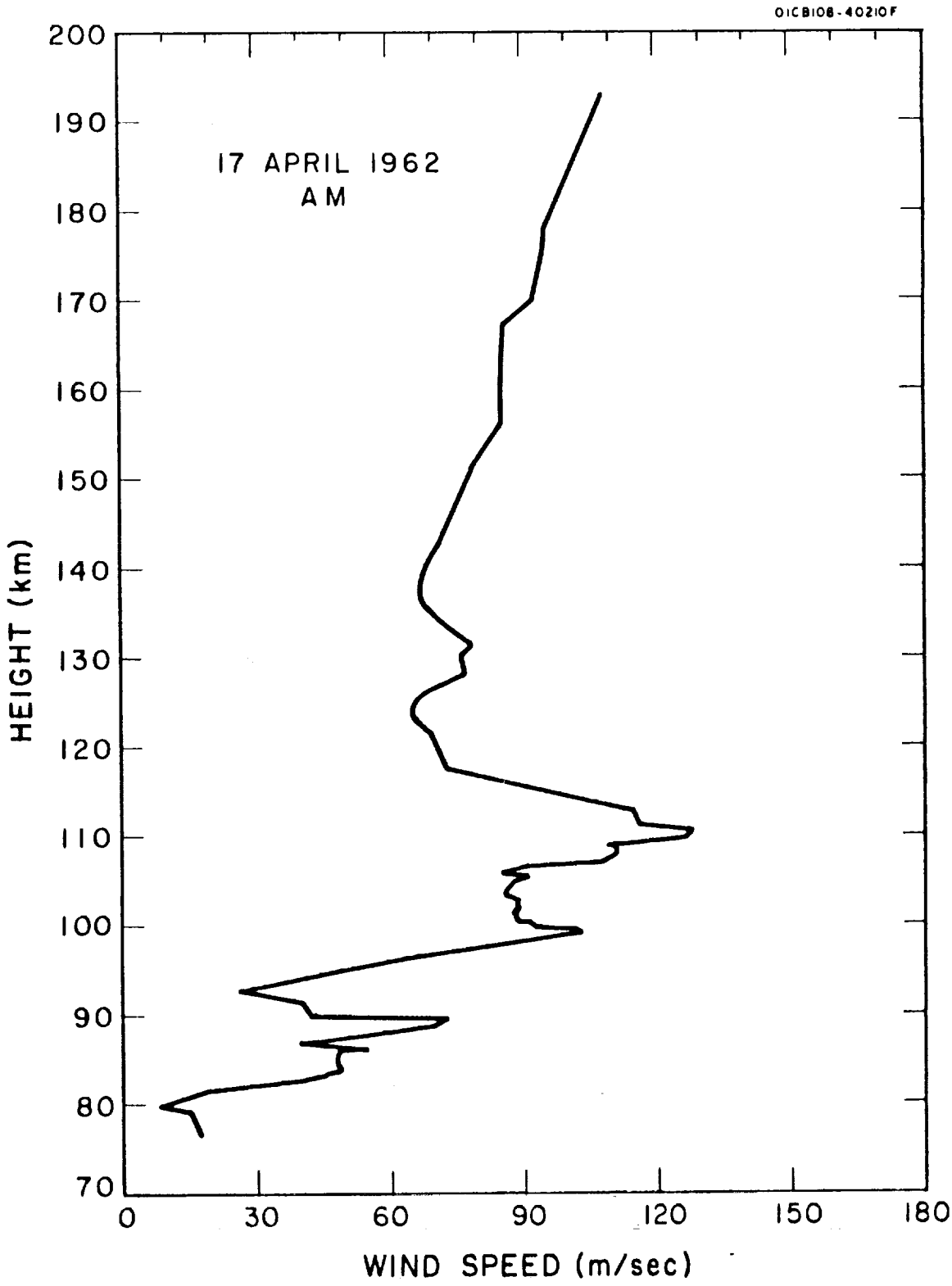

Figure A.16a. Wind speed as a function of height for morning twilight of 17 April 1962.

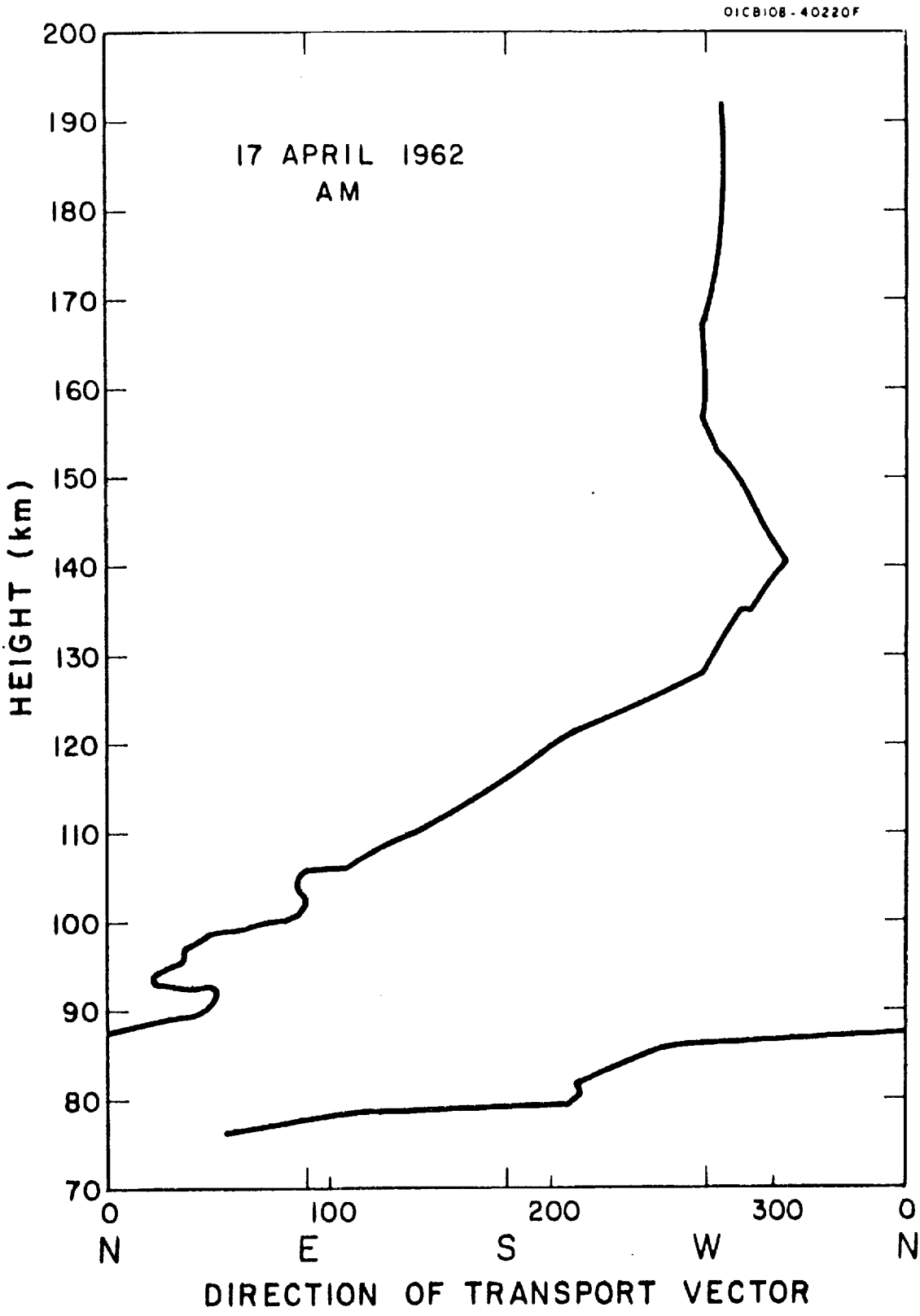

Figure A.16b. Direction of transport vector as a function of height for morning twilight of 17 April 1962.

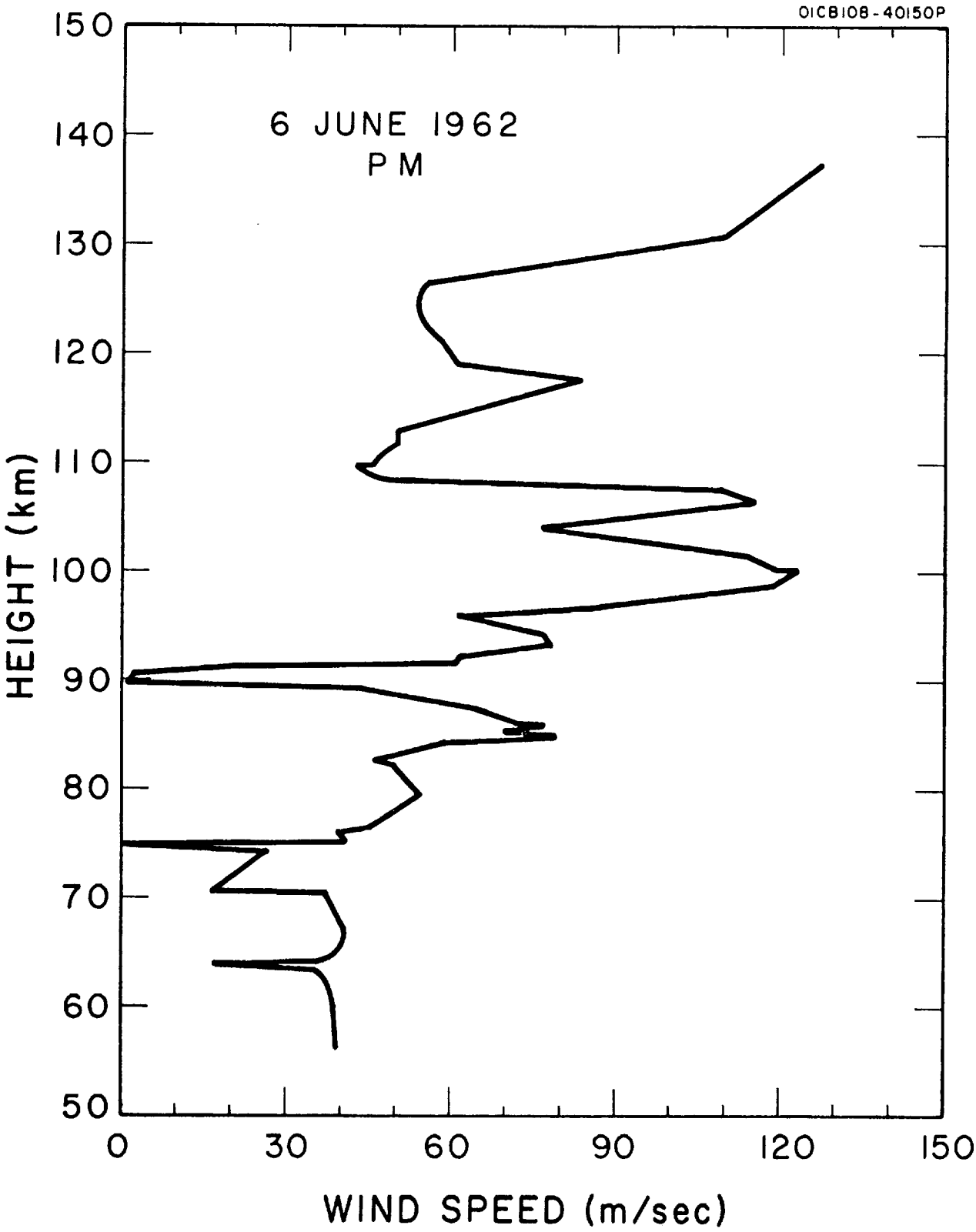

Figure A.17a. Wind speed as a function of height for evening twilight of 6 June 1962.

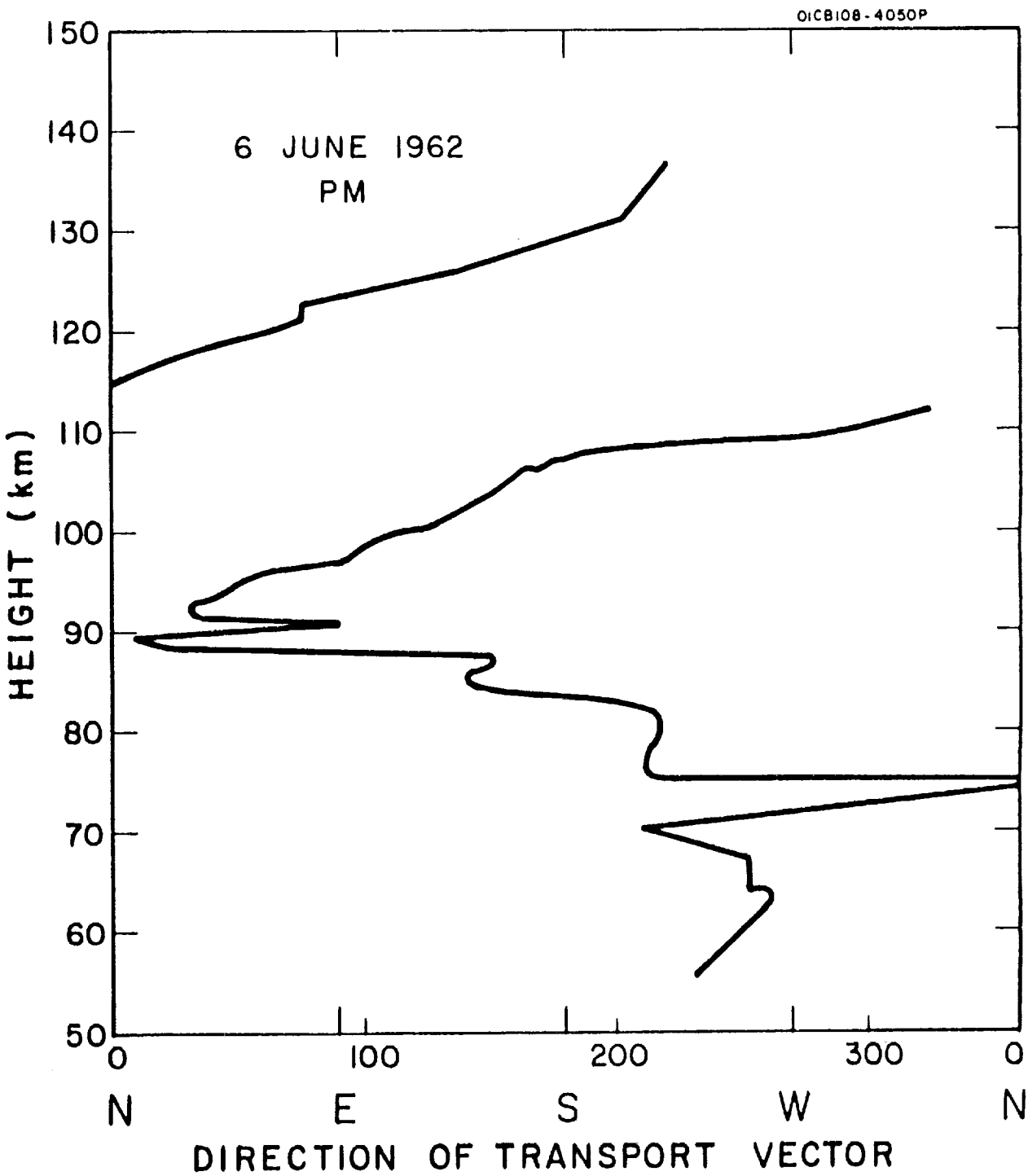

Figure A.17b. Direction of transport vector as a function of height for evening twilight of 6 June 1962.

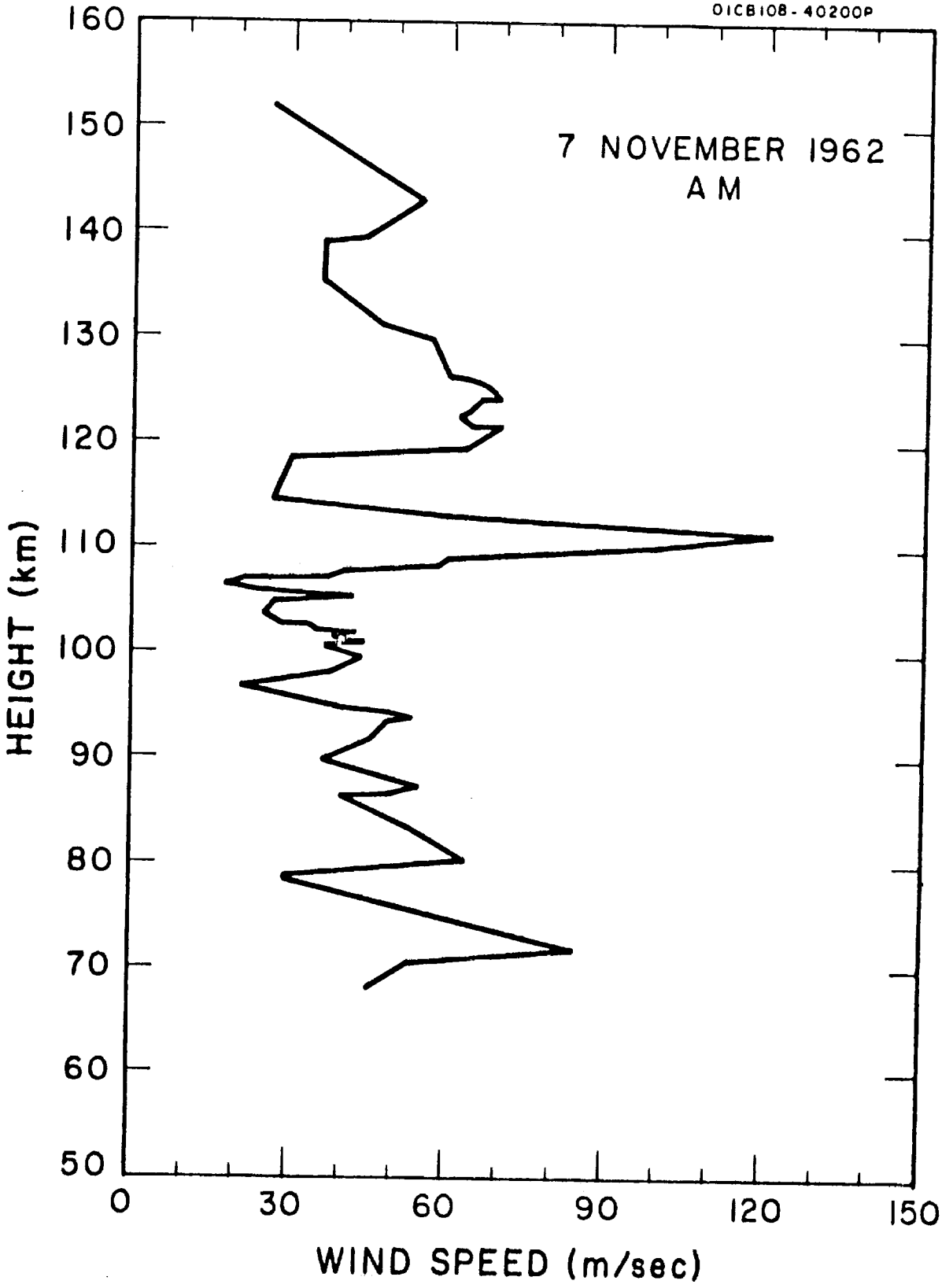

Figure A.18a. Wind speed as a function of height for morning twilight of 7 November 1962.

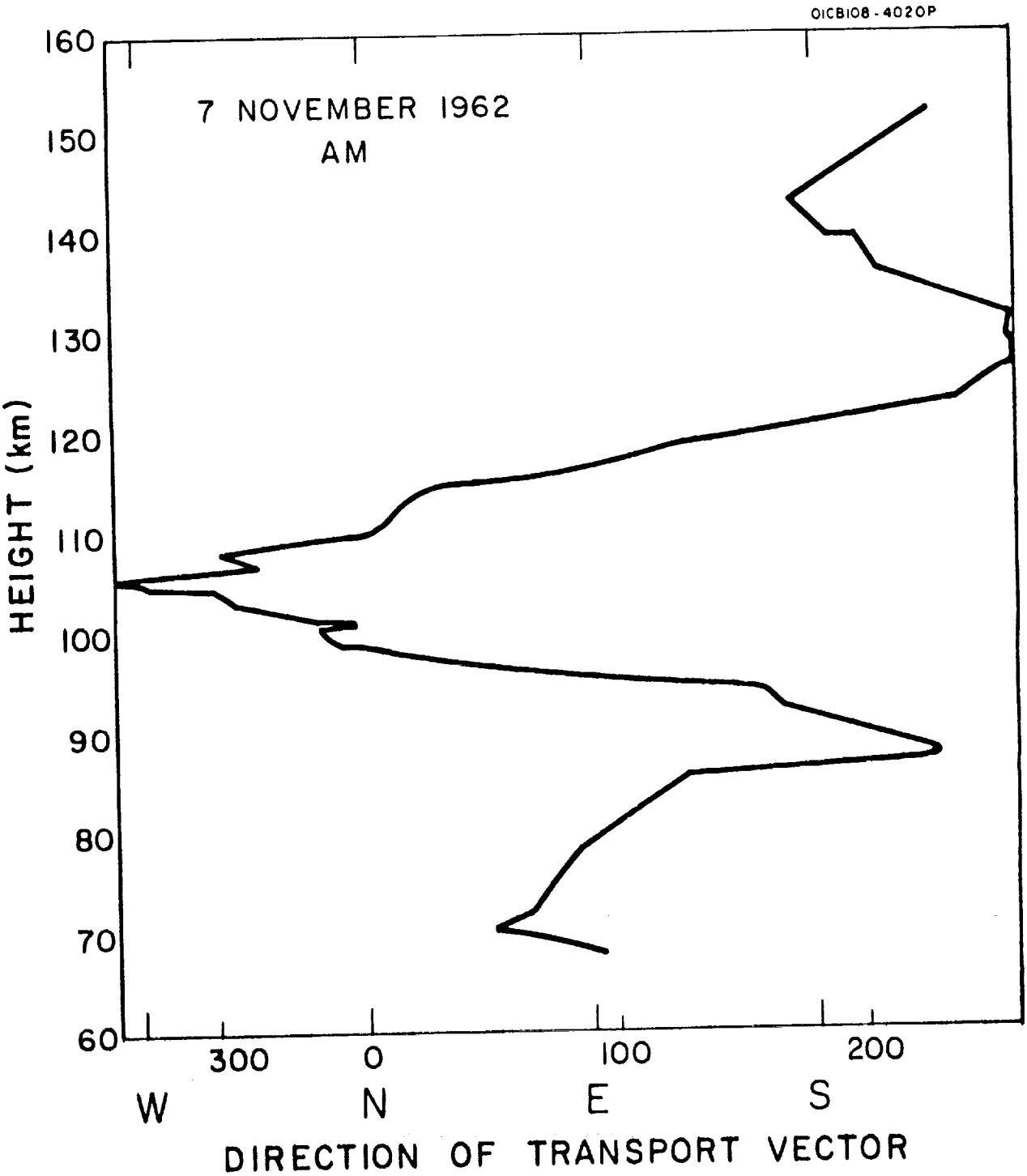

Figure A.18b. Direction of transport vector as a function of height for morning twilight of 7 November 1962.

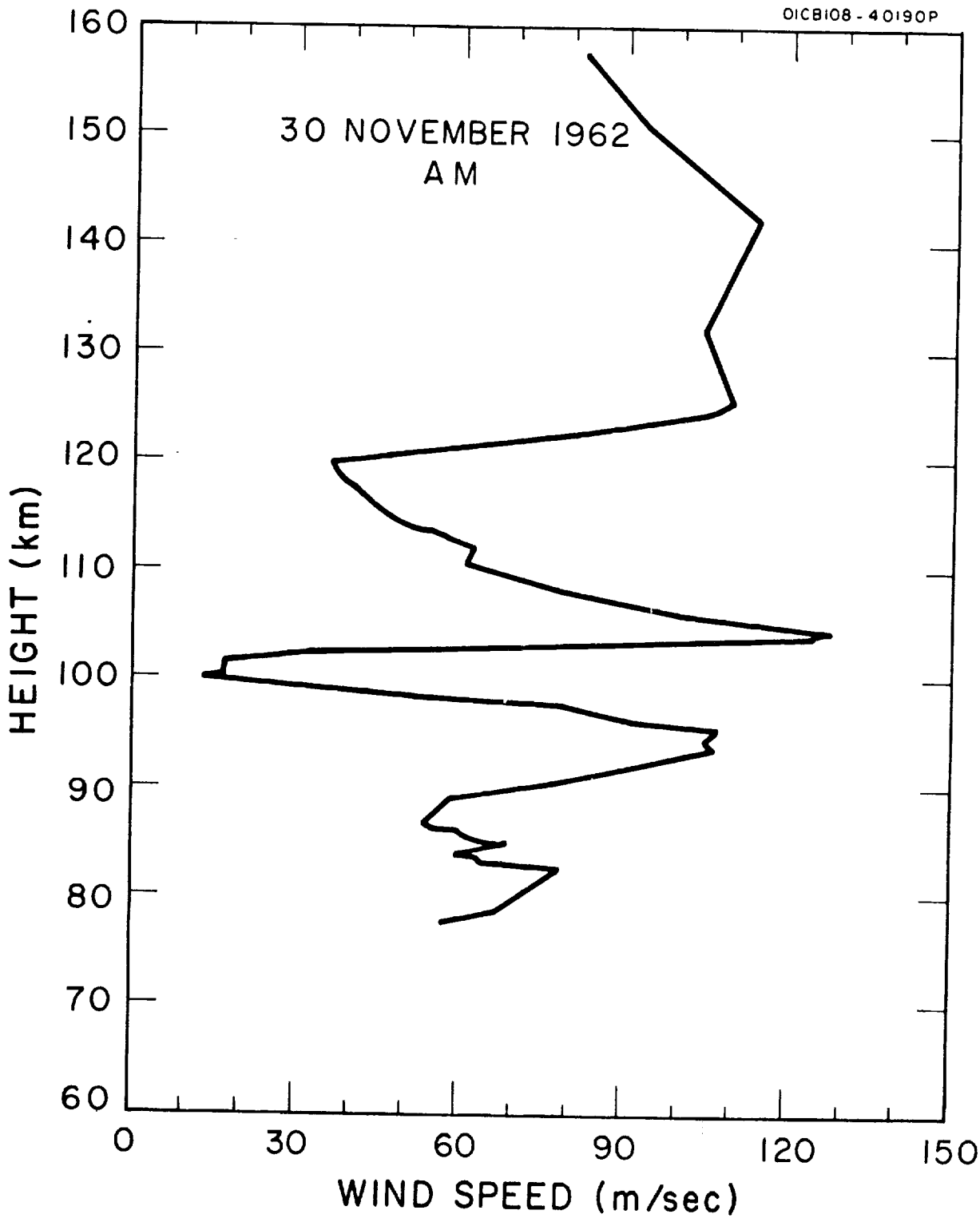

Figure A.19a. Wind speed as a function of height for morning twilight of 30 November 1962.

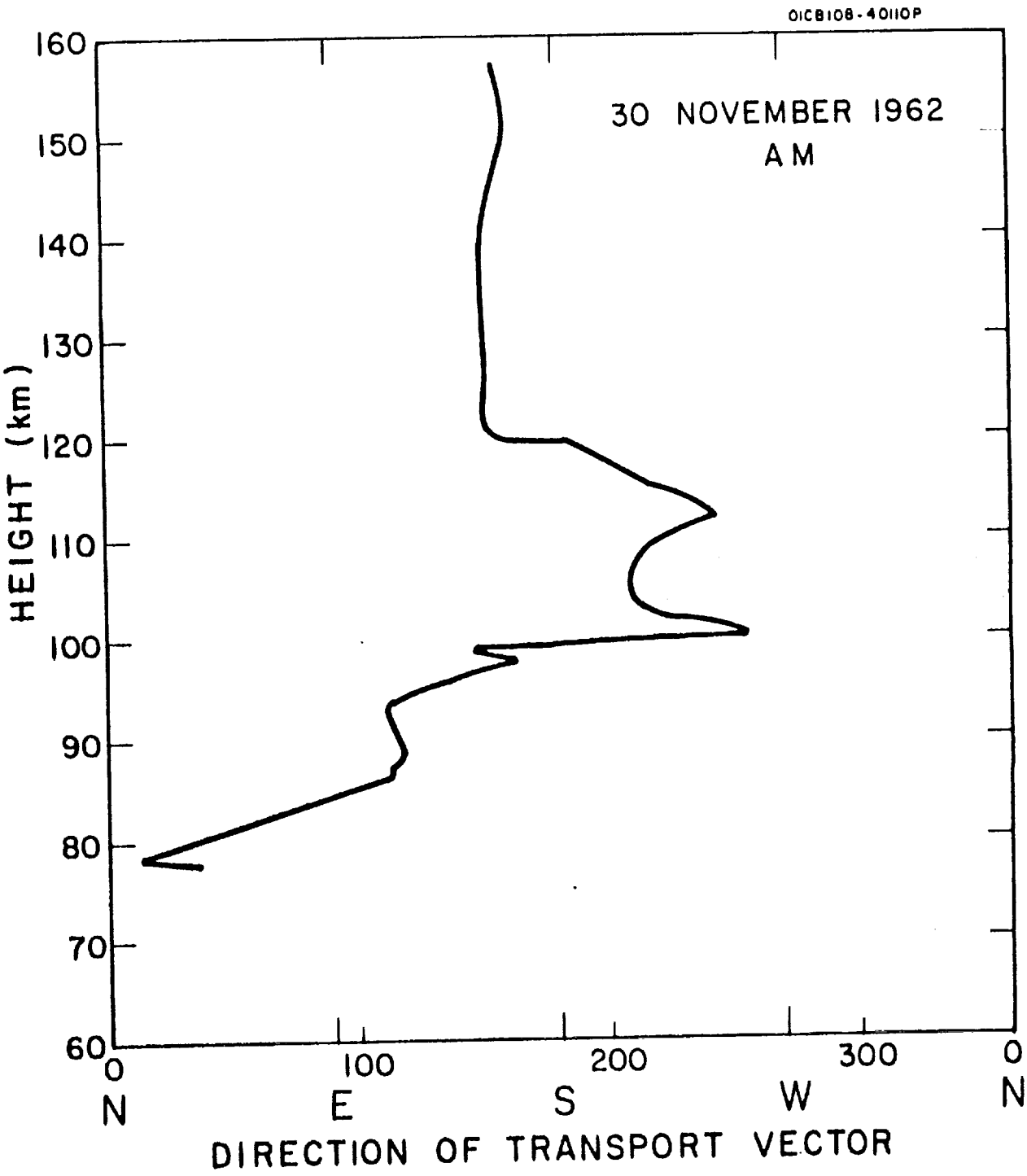

Figure A.19b. Direction of transport vector as a function of height for morning twilight of 30 November 1962.

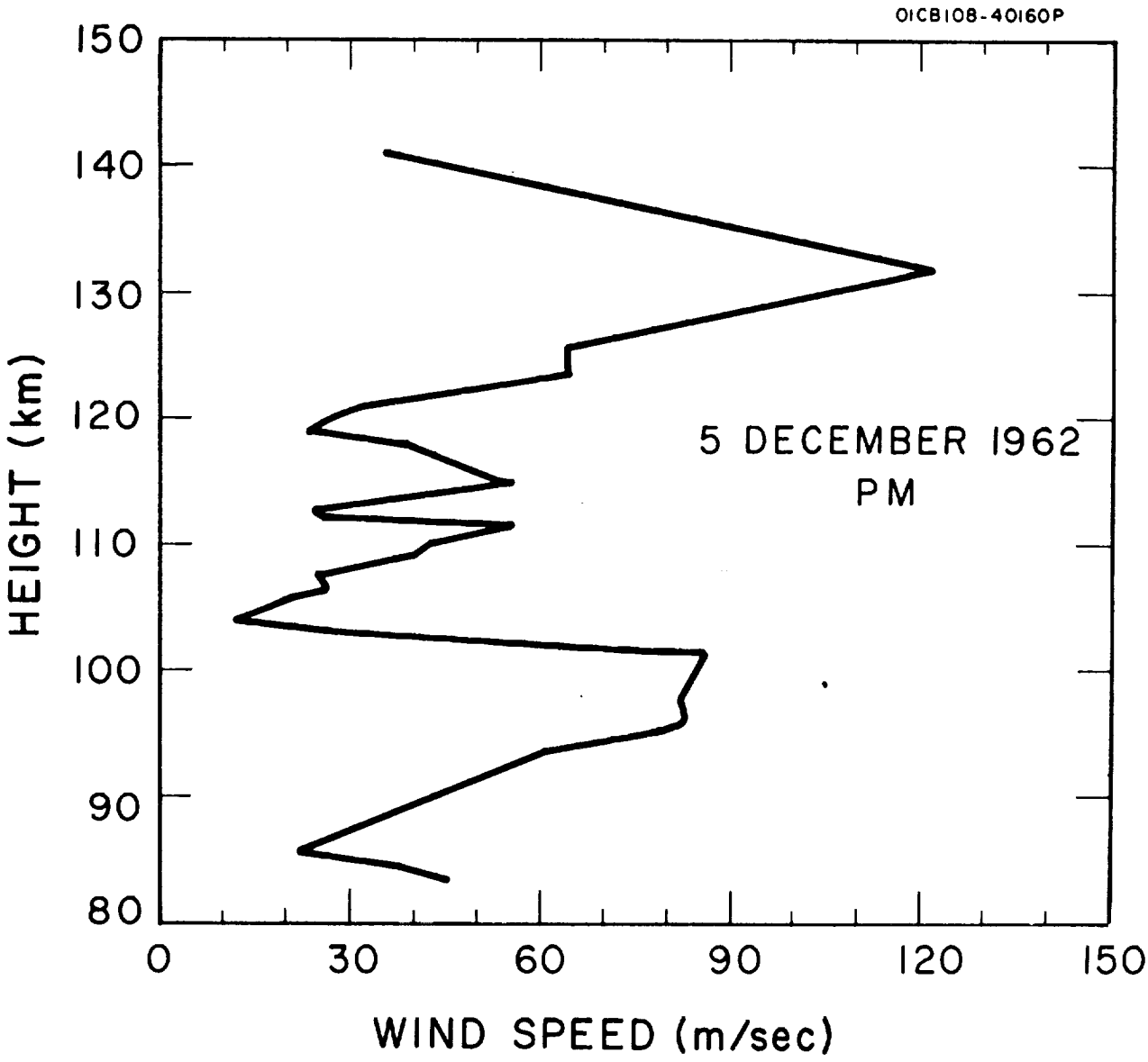

Figure A.20a. Wind speed as a function of height for evening twilight of 5 December 1962.

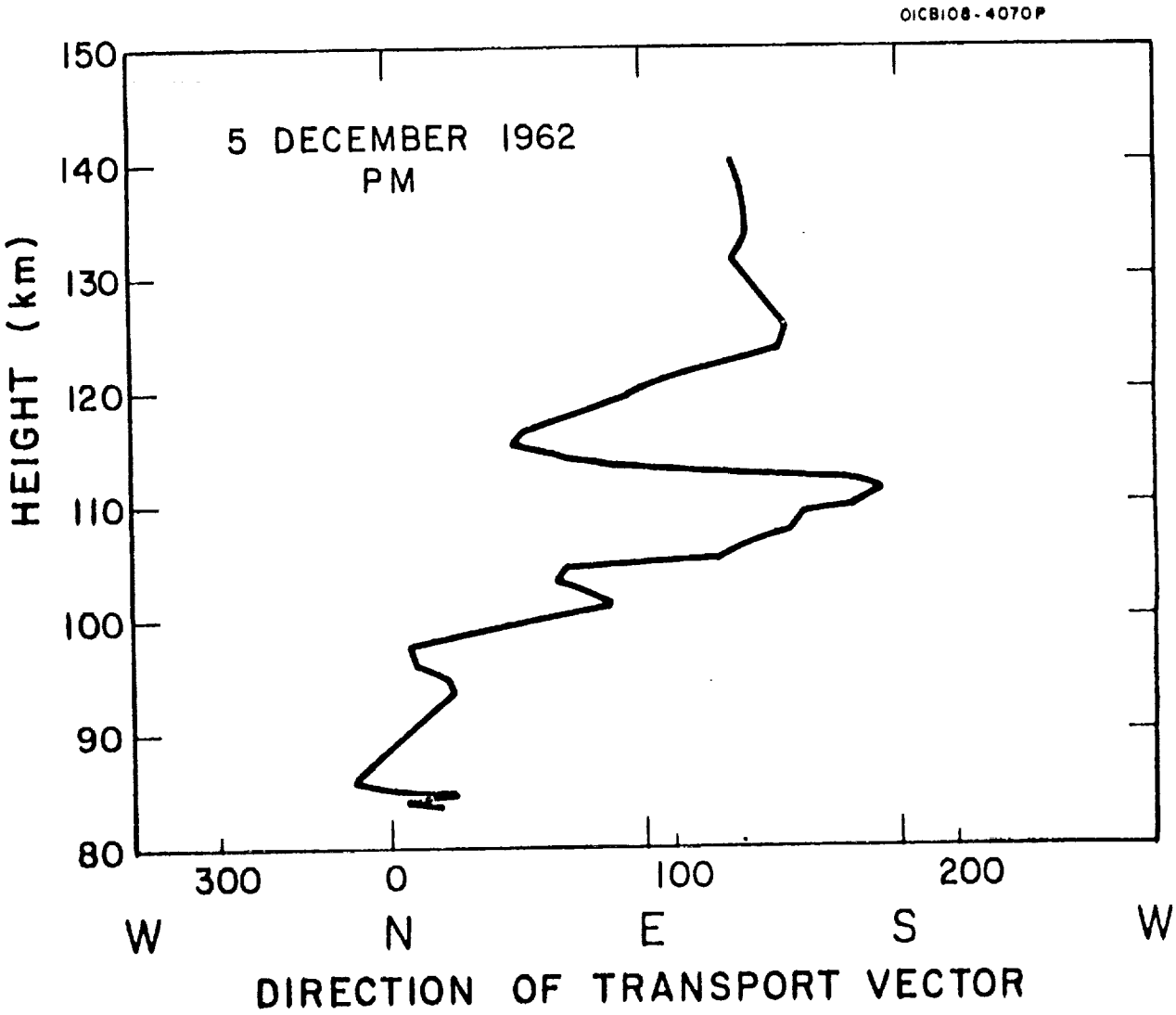

Figure A.20b. Direction of transport vector as a function of height for evening twilight of 5 December 1962.

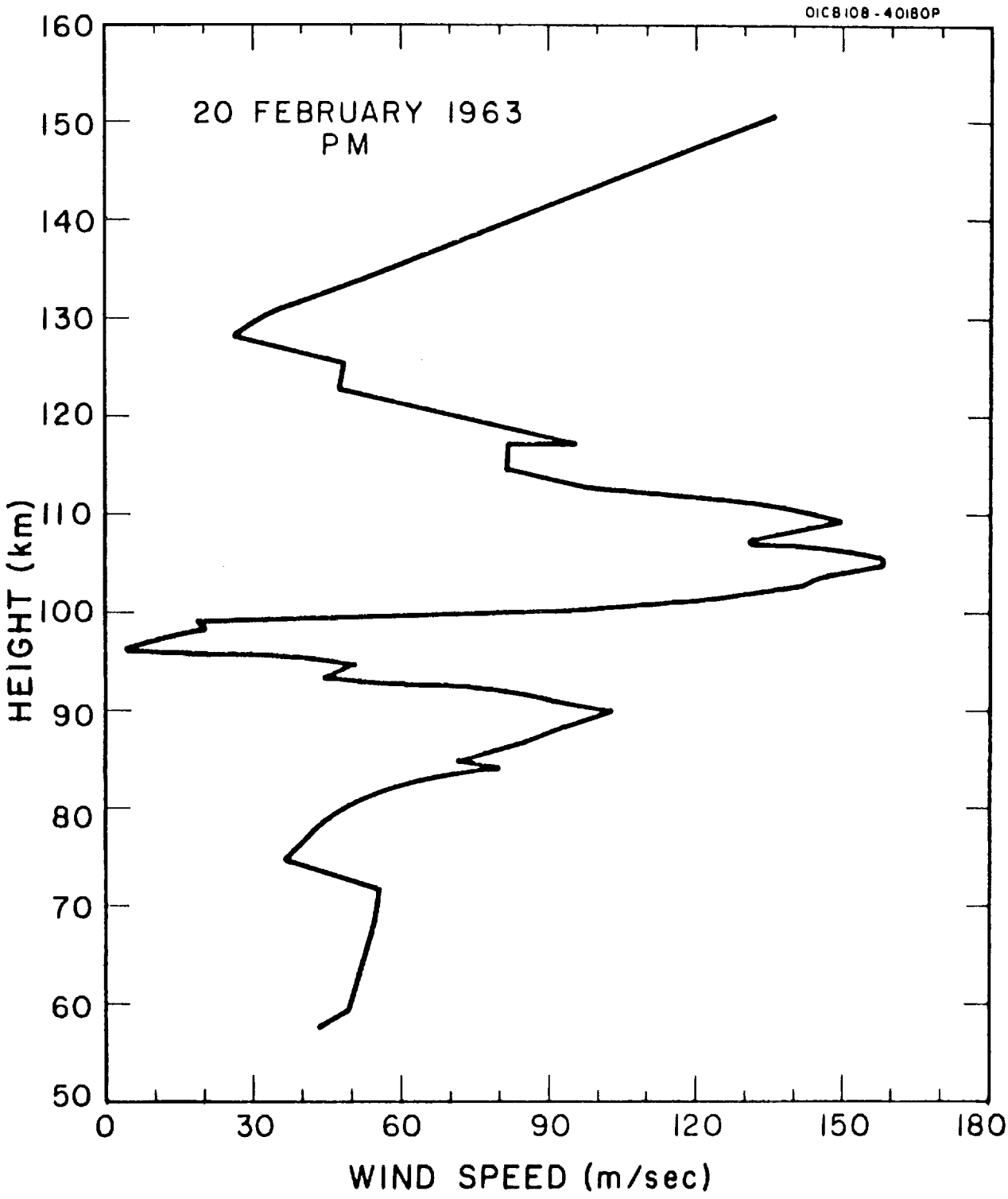

Figure A.21a. Wind speed as a function of height for evening twilight of 20 February 1963.

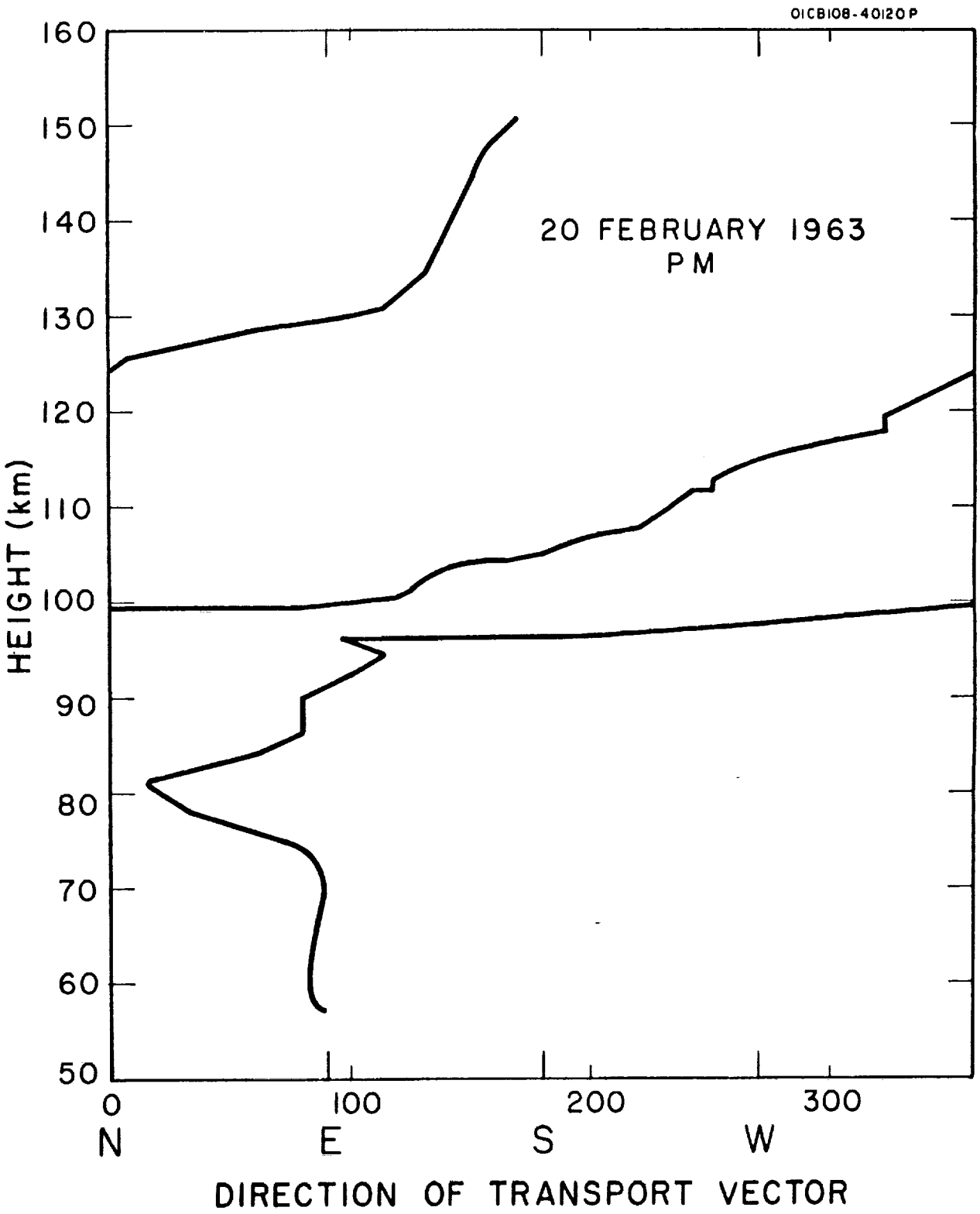

Figure A.21b. Direction of transport vector as a function of height for evening twilight of 20 February 1963.

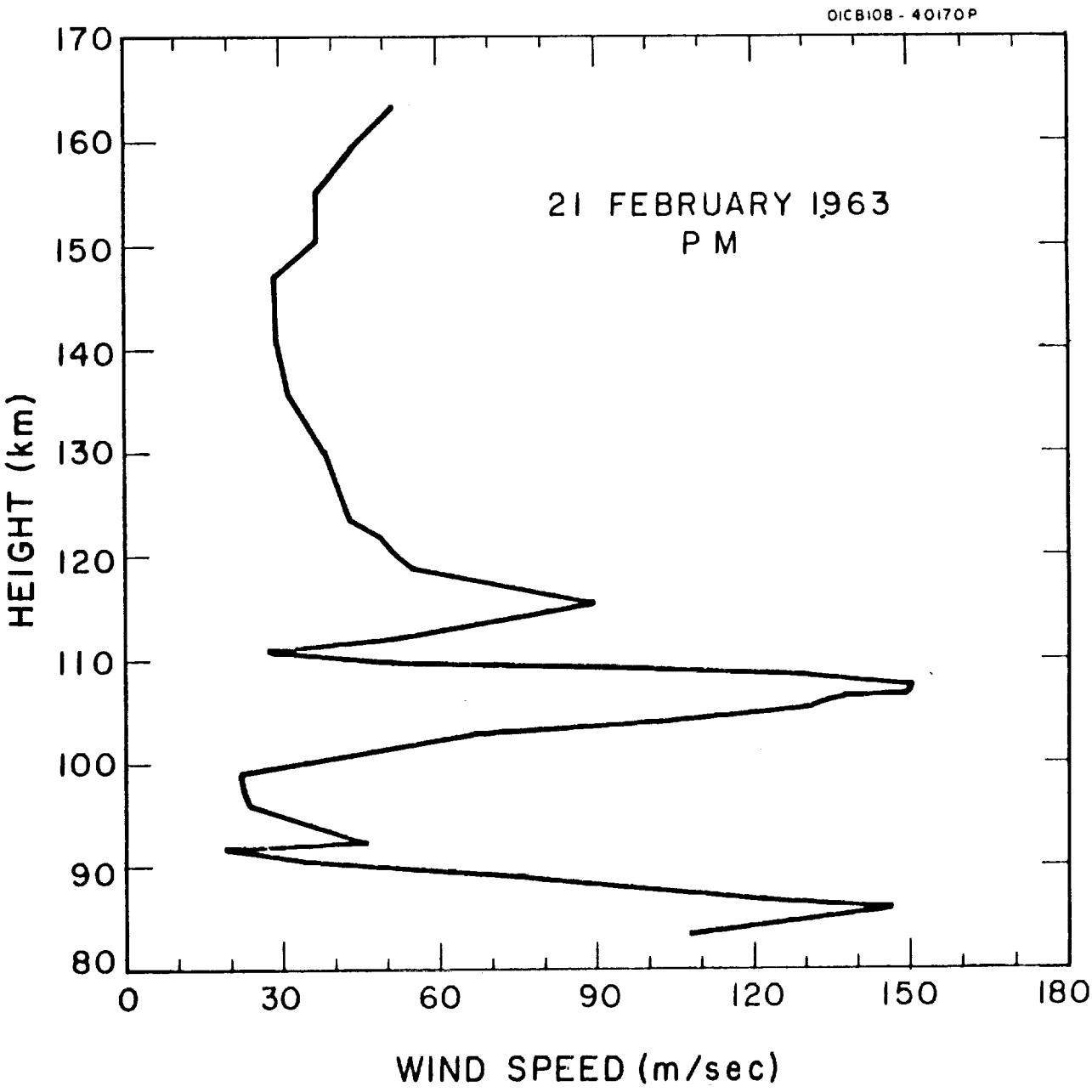

Figure A.22a. Wind speed as a function of height for evening twilight of 21 February 1963.

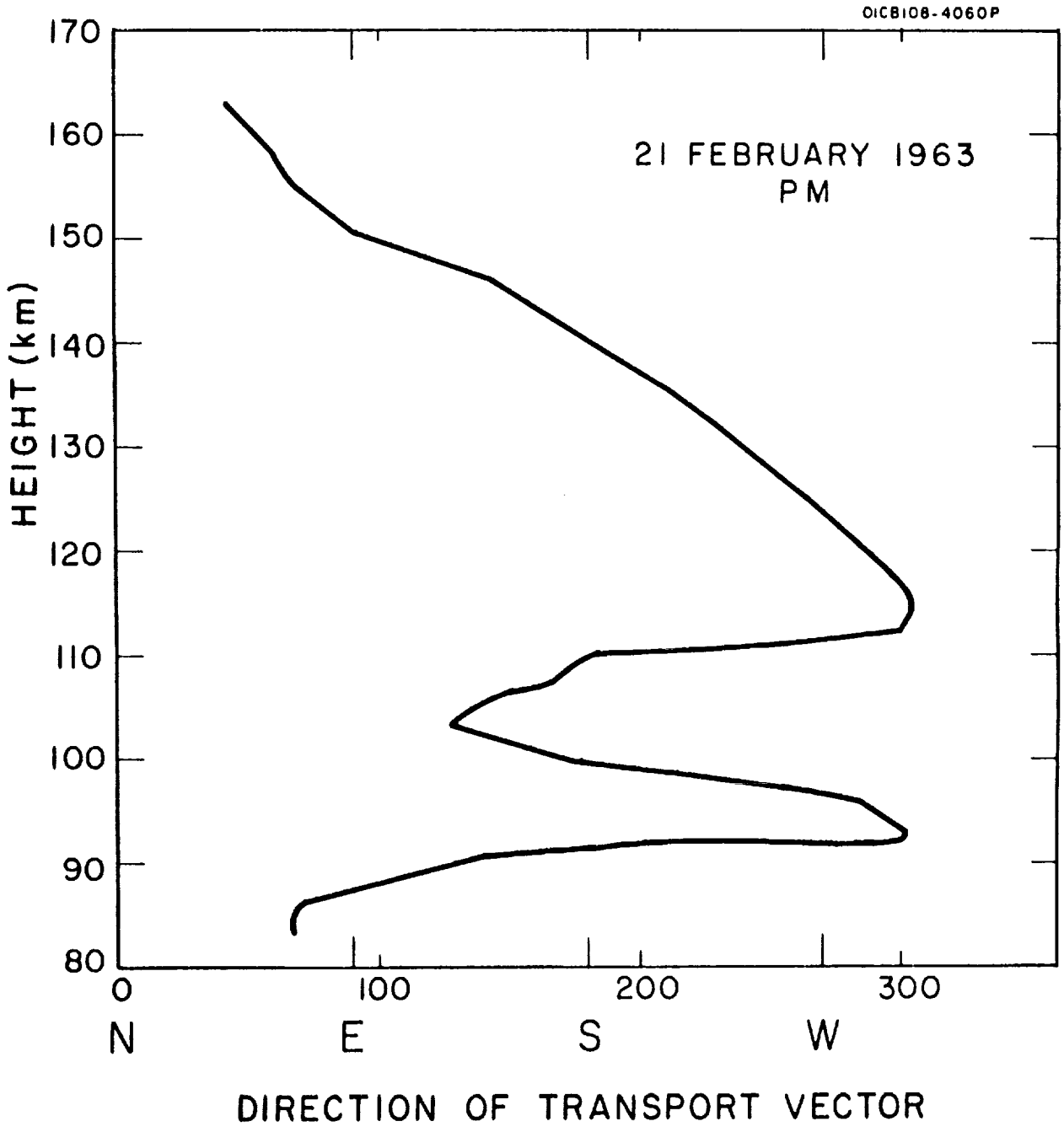

Figure A.22b. Direction of transport vector as a function of height for evening twilight of 21 February 1963.

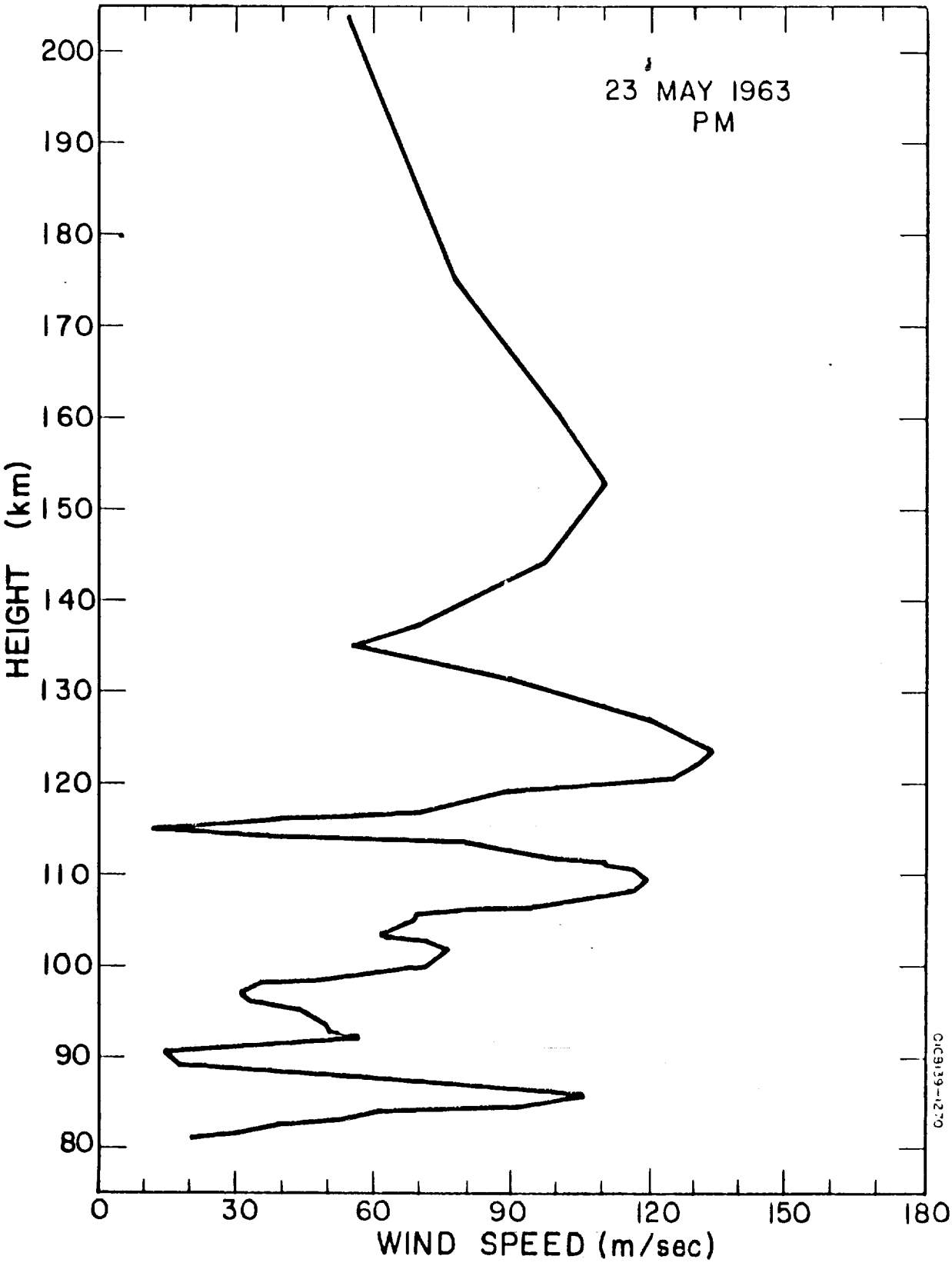

Figure A.23a. Wind speed as a function of height for evening twilight of 23 May 1963.

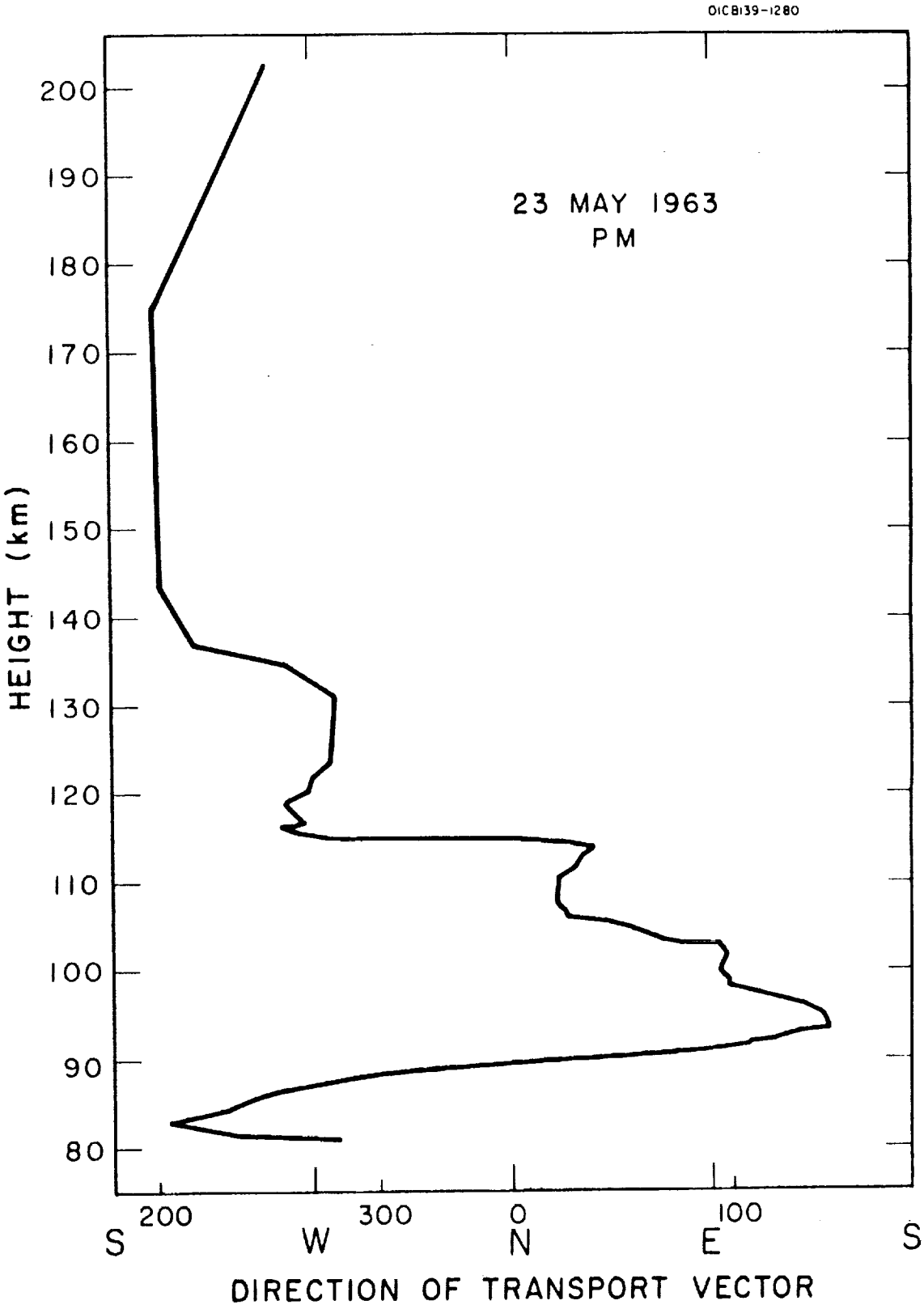

Figure A.23b. Direction of transport vector as a function of height for evening twilight of 23 May 1963.

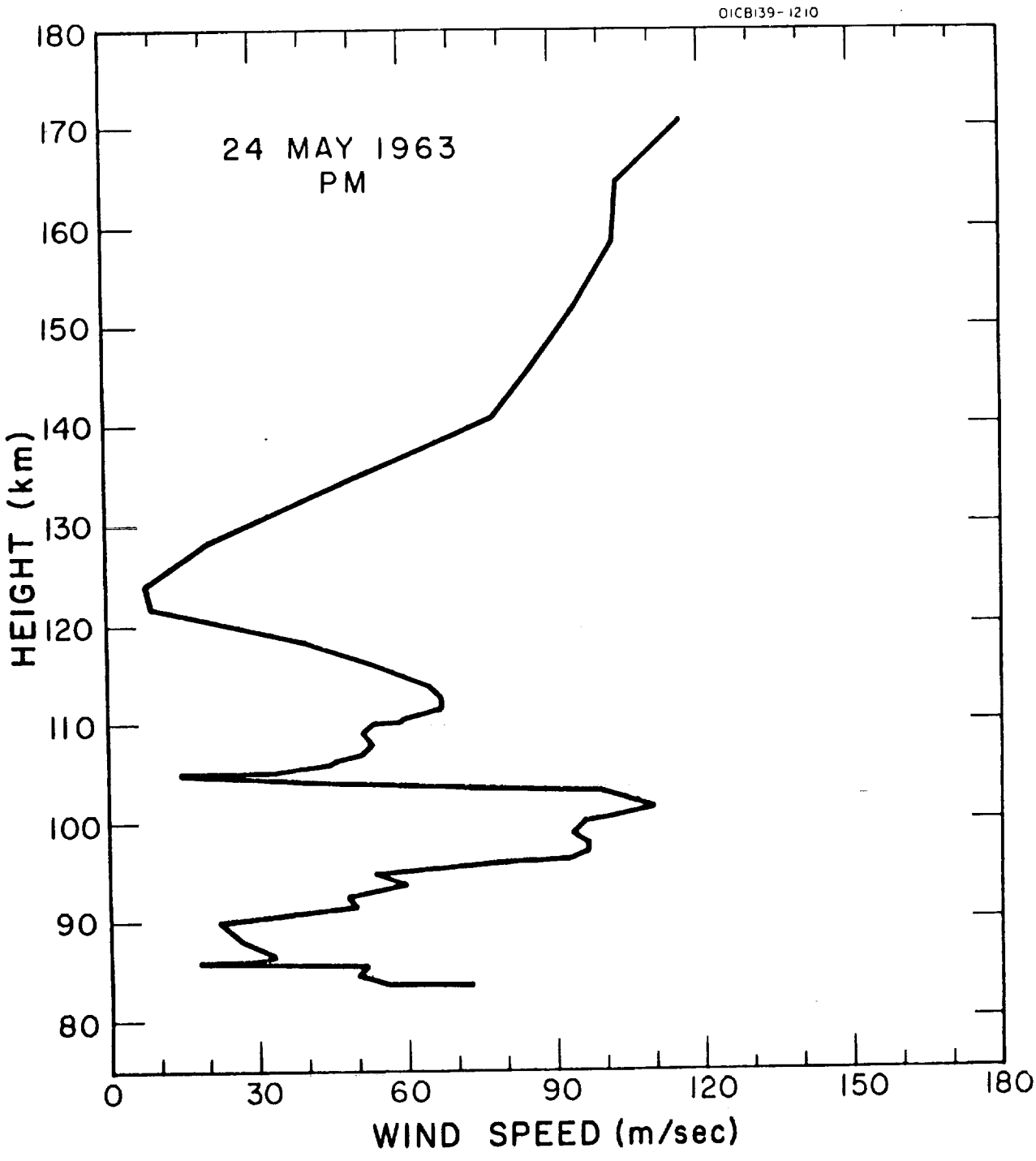

Figure A.24a. Wind speed as a function of height for evening twilight of 24 May 1963.

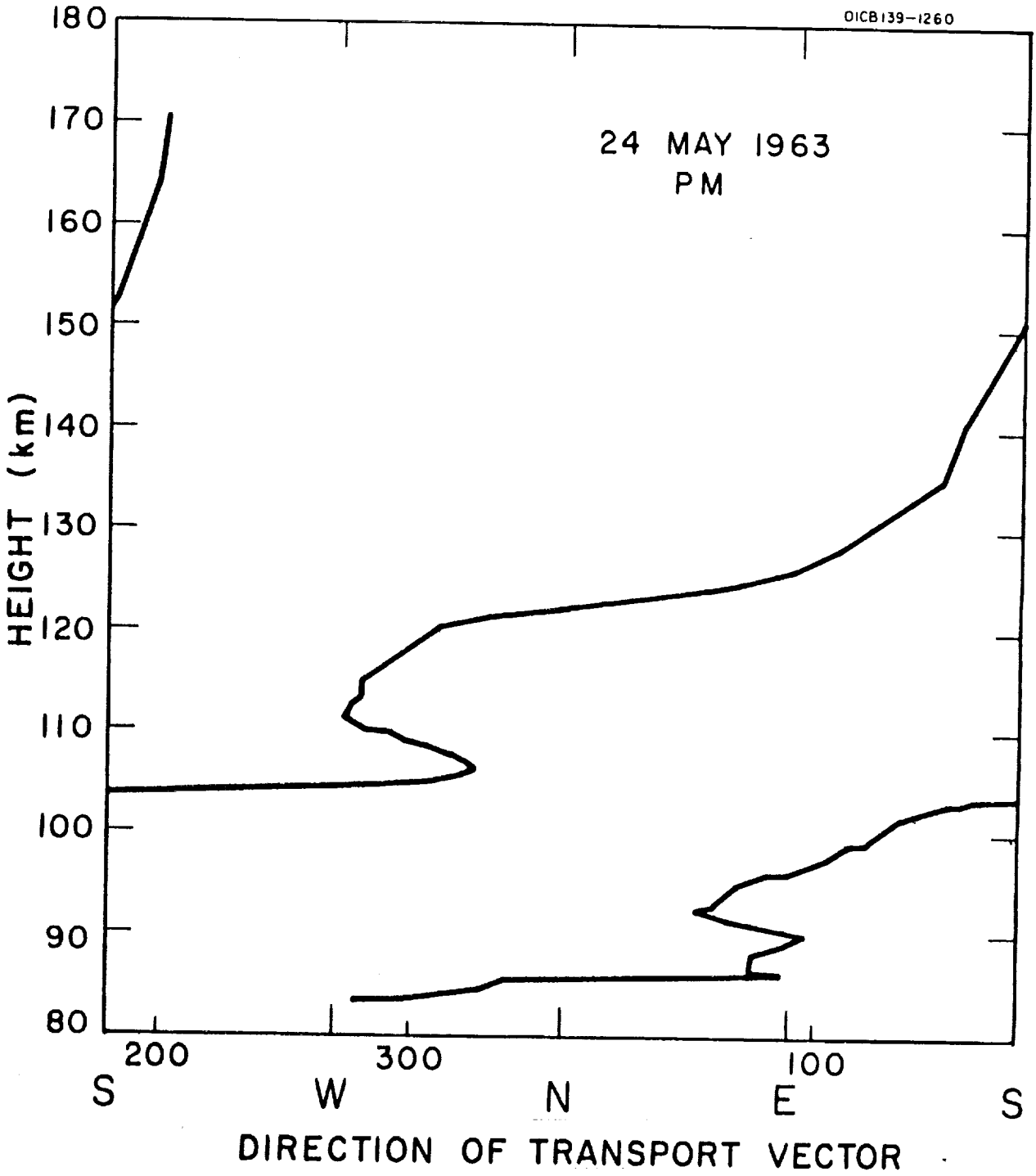

Figure A.24b. Direction of transport vector as a function of height for evening twilight of 24 May 1963.

NASA-Langley, 1964 CR-36